UNIVERSITY OF SOUTHERN QUEENSLAND

Development and Characterisation of a Chemical Film Actinometer with a Large Dynamic Range for Measurements of Solar Ultraviolet Exposure

A Dissertation Submitted by

R.A. Lester, BSc(Hons)

For the Award of

Master of Philosophy

2009

Declaration

The research contained in this dissertation is the full documentation of the research results that were published as

Lester, RA, Parisi, AV, Kimlin, MG, & Sabburg, J. 2003, 'Optical properties of poly(2,6-dimethyl-1,4-phenylene oxide) film and its potential for a long-term solar ultraviolet dosimeter', *Physics in Medicine and Biology*, vol. 48, pp. 3685-98.

I declare that this dissertation is comprised entirely of my own research (except where due acknowledgement is made), and no part of this dissertation has been written by another person. To the best of my knowledge, the work presented here is original and has not been published elsewhere other than in the reference stated above. This dissertation contains no material that to any substantial extent resembles work previously submitted for any other award at the University of Southern Queensland or any other educational or academic institution. All contributions to this dissertation and the research within are explicitly acknowledged.

Rick Lester

Signed .....

06/04/09

Acknowledgements

I wish to acknowledge the various contributions made to this project by a number of members of staff of the Faculty of Sciences at the University of Southern Queensland.

My Principle Supervisor, Dr Alfio Parisi (now Assoc Prof) initiated the concept for the project, provided supervision and training in a number of areas relating to ultraviolet physics, assisted with the assembly of experiments, and contributed substantially to the proof reading and editing of documents relating to this project.

Dr Jeff Sabburg made valuable contributions to experimental design and provided advice on error analysis, and also contributed to proof reading and editing. As an Associate Supervisor, Dr Michael Kimlin (now Assoc Prof) provided guidance for the casting aspect of the pilot study and also assisted in proof reading and editing during the early stages of the project. Prof John Mainstone, also an Associate Supervisor, contributed to project discussions and proof reading, and Dr Brad Carter took on the role of Associate Supervisor during the final stage of the project.

Dr Tania van den Ancker and Dr Ray Marshall provided essential workspace in the chemistry laboratory, assisted with the chemistry equipment required for the casting of chemical films, and also contributed to discussions relating to the photochemical nature of various actinometer materials.

Mr Graham Holmes provided technical assistance and provided a valuable support in equipment maintenance and repairs throughout the project, and also played a pivotal role in problem solving related to experimental logistics. Mr Pat McConnell also assisted with experimental apparatus.

Mr Oliver Kinder designed and constructed a number of precision mechanisms required for experimental work, and provided much needed technical assistance with these and other experimental devices, as well as repairs and maintenance. Although Mr Ken Mottram retired before the beginning of this project, I would like to thank him for the interesting discussions and moral support in the lead up to this project.

In addition, the Faculty of Sciences at the University of Southern Queensland financed the project by means of a research scholarship, and also provided the equipment and resources necessary for this project. I am grateful to, and thank all of those who have contributed and supported this research.

Abstract

Solar ultraviolet (UV) radiation arriving at the Earth's surface is a biological requirement for most forms of life, but also causes adverse responses in humans, animals and plants in cases of overexposure. Many of the adverse responses are cumulative in nature, and hence solar UV related environmental risk assessment requires quantification of long-term exposures and large UV doses.

Dosimetry methods for quantifying solar UV radiation exposure are extremely versatile and cost-effective compared to radiometric methods, and allow time integrated doses to be quantified efficiently. Biodosimetry often provides a large dynamic range, but is expensive, labour intensive and time consuming. Chemical actinometry is a cost and labour effective alternative to biodosimetry, but is disadvantaged for large-dose measurements by its relatively small dynamic range.

Poly(dimethyl phenylene oxide) (PPO) film was identified from the literature as a chemical actinometer material with the potential to reduce the labour and costs involved in the quantification of large solar radiation doses by means of a larger dynamic range. A fabrication technique for PPO film actinometers was established, and the optical properties of the actinometers were fully characterised.

The resulting actinometer provides an efficient method for quantifying either unweighted UVB dose or biologically effective dose. The spectral response resembles the erythemal action spectrum, and the solar erythemal calibration function is near linear. The PPO film actinometer is therefore very well suited to human exposure research, especially for evaluation of chronic responses, or cumulative acute responses in which large-dose measurements are required.

The PPO film actinometer now provides an additional tool in the quantification of solar UV radiation exposure. It has equal versatility, and similar costs, labour and equipment requirements to the most commonly employed actinometry methods. The larger dynamic range of PPO film however, reduces labour and costs associated with large-dose UV measurements.

Contents

List of Figures

List of Tables

Chapter 1

Introduction

1.1 Introduction

1.2 Definitions and Terminology

1.3 Project Objectives

1.4 Dissertation Overview

1.5 Summary

1.1 Introduction

Solar radiation is ubiquitous over the daytime side of Earth's surface. The energy imparted by solar ultraviolet (UV) radiation on incidence to terrestrial surfaces and biological systems is sufficient to alter the molecular or cellular structures of many of these materials. Such alterations may result in discolouration and degradation of polymers, and more importantly, disease in humans, animals and plants.

Substantial evidence has been presented in the literature suggesting that many organisms and ecosystems are perturbed by exposure to ambient levels of solar UV radiation (Häder *et al.* 1998). In addition to ambient radiation stress, organisms may also be exposed to increased levels of solar UV radiation, elevated by both natural and anthropogenic forces. These issues have been reinforced in recent years by the growing awareness of stratospheric ozone depletion due to industrial emissions of ozone-depleting gases into the atmosphere, and of the associated increase in solar UV radiation at Earth's surface (Appenzeller 1993; Herman *et al.* 1996; McKenzie, Connor & Bodeker 1999). Important environmental issues are therefore, the quantification of solar UV exposure and the assessment of its effects on organisms and ecosystems.

Many biological responses to UV radiation are cumulative in nature. Time-integrated exposure measurements are therefore required to assess the chronic effects of UV radiation on the biosphere. Radiometry is frequently employed to quantify solar UV radiation. The strength of this method is in the measurement accuracy afforded by sophisticated electronic detectors. Exposure calculations from instantaneous radiometric measurements however, require many measurements over the exposure period of interest, and the greater the variability of the UV radiation source, the greater the number of measurements required for integration such that a given level of accuracy is maintained. Since solar radiation continually varies at the Earth's surface due to complex atmospheric optics and geometrical factors, the time and labour involved in obtaining a sufficient number of instantaneous radiometric measurements for accurate integrations of large doses is often prohibitive. Although automated systems are becoming available, such instruments are expensive, bulky and cumbersome.

An alternative to radiometry is passive dosimetry, which is well suited to UV dose measurements since dosimeters naturally integrate over time and incorporate all variability into a measurement. The two main branches of dosimetry are biological dosimetry, or biodosimetry, and actinometry (also known as physical or chemical dosimetry).

Passive UV dosimeters must ultimately be calibrated against a radiometric instrument, and also incur imprecision related to the optical properties of the dosimeter. Dosimetry is therefore inherently less accurate than radiometry. Dosimetry methods however, have grown in popularity due to their low cost and versatility compared to radiometry, as well as their ability to provide direct measurements of time-integrated UV dose. The variability inherent in solar UV radiation that occurs over many time-scales is captured by the dosimeter in a single exposure measurement. This is particularly important where further UV radiation variability occurs due the motion of the subject under measurement (e.g. Milne *et al.* 1999; Cockell *et al.* 2001). Their small size also allows significant numbers of dosimeters to be deployed simultaneously, allowing spatially resolved UV data to be acquired over complex surfaces (e.g. Kimlin & Parisi 1999).

Biodosimetry is the leading technique in large-dose UV quantification, and provides the largest dynamic ranges available. Biodosimeters utilise UV sensitive organisms, or simple biological systems to gauge UV radiation dose, usually through UV induced DNA damage (Koussoulaki *et al.* 1997; Bérces, Gáspár & Rontó 1999, pp. 141-2; Rontó *et al.* 2000). The preparation of biodosimeters, and the post-exposure analytical procedures associated with this method however, are often complex and time-consuming. A measure of UV radiation dose by *Bacillus subtilis* dosimetry for example, is determined from the proteins synthesized after incubation and staining (Quintern *et al.* 1994).

Actinometry methods are available that simplify the preparation and analytical procedures, and hence reduce the labour and costs involved. These techniques utilise a change in optical absorbance of the actinometer material in response to UV radiation exposure. The absorbance change can often be quantified by means of standard photometric equipment.

The dose-capacity, or the maximum dose that can be registered by a single dosimeter, is substantially smaller for currently employed actinometer materials compared to biodosimetry materials. The resulting smaller dynamic range is a fundamental limitation of the actinometry methods in current use.

The most extensively employed actinometer material for solar UV radiation dosimetry is polysulphone (e.g. Knuschke & Barth 1996; Sydenham, Collins & Hirst 1996; Dunne 1999; Kimlin & Parisi 1999; Milne *et al.* 1999; Lester & Parisi 2002). Polysulphone actinometers have an operational life-span of about one day in summer at mid-latitudes, or a dose-capacity of about 12 kJ m^{-2} (CIE 1992). Many chronic UV induced biological responses are therefore difficult to quantify by actinometry since they occur over periods of years, provoked by the large-dose equivalent of many accumulated doses.

Large UV dose measurements employing polysulphone actinometry have been achieved by replacing actinometers on a daily basis, and calculating the cumulative exposure (Parisi *et al.* 2000). The disadvantages are however significant. A large number of actinometers are required, and the replacement procedure is time consuming and labour intensive. Time-integration errors are also introduced. Ideally, an actinometer material with a greater dynamic range should be employed for large-dose measurements.

An actinometer is required that has a larger dynamic range than is currently available to alleviate the labour, costs, and time associated with large-dose actinometry. The focus of the research is therefore on identifying an actinometer material with a greater dynamic range, and fully characterising the material's optical properties to provide a large-dose actinometer for solar UV exposure measurements. Manufacturing costs of such actinometers must be kept to a minimum such that the advantages of a larger dynamic range are not outweighed by fabrication costs.

1.2 Definitions and Terminology

Electromagnetic radiation (EMR) is a form of energy that propagates through space by means of electric and magnetic fields oscillating perpendicular to each other. The amount of energy carried by EMR depends on the wavelength of the oscillating

fields. The nature and propagation of EMR through space is described by Maxwell's equations (Halliday, Resnick & Walker 1997, p. 803).

The International Commission on Illumination (CIE) is an international authority of lighting and radiation. The CIE definitions and terminology recommendations have been adopted in this dissertation. The UV radiation waveband is defined by the CIE as the region of the EMR spectrum that lies between the ionising-nonionising boundary (100 nm) and the visible boundary (400 nm). The CIE also recognises the ultraviolet-C (UVC), ultraviolet-B (UVB) and the ultraviolet-A (UVA) wavebands as biological subdivisions of the UV waveband. These subdivisions constitute the respective wavebands of 100 nm to 280 nm, 280 nm to 315 nm and 315 nm to 400 nm (CIE 1987).

Electromagnetic radiation in the UV waveband is most often quantified radiometrically in terms of various radiance units. Irradiance is defined as the radiant power per unit area incident upon a surface at all wavelengths, while spectral irradiance is the radiant power distribution expressed as irradiance per unit frequency. The SI unit for irradiance is W m^{-2} and that for spectral irradiance is W m^{-2} Hz^{-1}. The unit of W m^{-2} nm^{-1} is often used for irradiance quantification in the UV waveband, and is the only deviation from SI units in this dissertation. Exposure is wavelength- and time-integrated irradiance and its measurement is dose with units of J m^{-2}. Biologically effective UV irradiance is the spectrally determined irradiance component of the UV waveband that causes a given biological response. Biologically effective dose is defined as the wavelength- and time-integrated irradiance, where the spectral irradiance is weighted by the biological response of interest.

1.3 Project Objectives

The principal objective of this research is to reduce the labour and costs involved in the dosimetry of large solar UV radiation doses by developing an actinometer with a larger dynamic range than is currently available.

The steps required to meet this objective are as follows:

- To identify a chemical with physical and optical properties that are suitable for use in the dosimetry of large doses of solar UV radiation.
- To develop an efficient method for the fabrication of actinometers that utilise the material identified above.
- To characterise the identified material by experimentally investigating and quantifying its optical properties that are relevant to the quantification of solar UV radiation.
- To calibrate the response of the fully characterised actinometer for UV radiation dose measurements against a suitable radiometer, and to evaluate the potential of the actinometer for quantification of UV exposure within specific wavebands and for biologically effective exposure.

These objectives in detail are as follows:

1.3.1 Literature Search for a Suitable Dosimeter Material

The literature was extensively searched for chemicals that are photosensitive in the UV radiation waveband. Information concerning the optical properties of these chemicals was compiled and studied in order to identify one that would provide the optimum properties for large-dose solar UV dosimetry. The factor of priority in this search was the dynamic range, which led to further investigations of poly(2,6-dimethyl-1,4-phenylene oxide) (PPO).

1.3.2 Fabrication of PPO Film

The literature indicates that the most cost effective and versatile methods of actinometry employ photosensitive materials in the form of a chemical film. A cost effective method of casting PPO into thin film was therefore required. Casting experiments were conducted to assess the feasibility of fabricating PPO film actinometers employing currently available equipment.

1.3.3 Investigation of PPO Film Thickness and Dose-Response

In addition to resistance to damage from normal handling, a dosimeter film for large-dose solar UV radiation measurements must be sufficiently durable to withstand the outdoor environmental forces over long periods of time. The film thickness that provides sufficient durability must also have a useful dose-response. It was therefore necessary to investigate the dose-response of PPO film as a function of film thickness.

1.3.4 Quantification of the Optical Properties of PPO Film Actinometers

The characteristics of a dosimeter are determined by its optical properties, and it is these characteristics along with the calibration that determine the accuracy with which a dosimeter measures dose. The quantification of the optical properties of PPO film was therefore necessary to establish the accuracy of dose measurements and to optimise the use of PPO film for solar UV actinometry. The dose-response, spectral response, angular response, reciprocity, temperature effects, dark reaction, and reproducibility were experimentally quantified.

1.3.5 UV Radiation Calibrations

PPO film actinometers were calibrated against a spectroradiometer and a broadband solar erythemal radiometer. These calibrations were extended over the entire dynamic range of the actinometer to determine the largest biologically effective UV dose measurable by a single PPO film actinometer.

1.4 Dissertation Overview

The approach of the research presented in this dissertation is outlined as follows:

- Chapter 2 provides an account of the biological effects of solar UV radiation on humans, animals and plants, which emphasises the need to develop efficient and cost effective methods for quantifying solar UV radiation.

- Due to the energetic nature of the UV waveband and the constantly changing UV radiation field at the surface of the Earth, solar UV radiation is technically difficult to quantify. The atmospheric and geometrical parameters that modulate solar UV are discussed in chapter 3.

- The optical properties and theory relevant to solar UV actinometry are reviewed in chapter 4, while the optical properties of currently available photosensitive materials that may be employed in passive UV actinometry are reviewed in chapter 5. The relevant optical properties are discussed in detail, and the most suitable materials for large-dose UV radiation measurements are evaluated.

- The experimental research conducted in the development and characterisation of the PPO film actinometer is presented in chapter 6. The experimentally determined optical properties are analysed and discussed in the context of their utility for high-dose measurements of solar UV radiation. The research findings are discussed and the project is concluded in chapter 7.

1.5 Summary

Ambient levels of solar UV radiation are detrimental to many organisms including humans. Environmental and sociological risk factors are therefore associated with UV radiation exposure, and are enhanced by stratospheric ozone depletion. Monitoring systems are therefore required to assess UV radiation exposure risks. Passive UV radiation actinometry provides a cost-effective method for such monitoring, but is limited to the measurement of relatively small doses. Large-dose quantification can be achieved by replacement of actinometers, but introduces error and is time and labour intensive.

The research presented in this dissertation provides a cost-effective method for quantifying larger doses of solar UV radiation than has been possible with a single actinometer. This allows the labour, costs, and integration errors in large-dose measurements to be minimised, while preserving the versatility of the actinometric methods. This is achieved by utilising PPO as an actinometer material, since this research has confirmed PPO film to have a larger dynamic than currently utilised

actinometer materials. The manufacturing procedures for the PPO film actinometer are developed and the physical properties and optical characteristics of the actinometer are determined. Finally, the actinometer is calibrated for measurements of biologically effective UV radiation.

Chapter 2

Responses of Biological Systems to Solar UV Radiation

2.1 Introduction

Sunlight is a requirement for almost all animals and plants. Solar UV exposure provides a catalyst for the production of vitamin-D in mammals and plants, and plants require photosynthetically active radiation (PAR) for photosynthesis. As a result of required sunlight exposure, the dermal tissue of plants and animals are exposed by necessity to solar UV radiation. The ocular tissue of sighted diurnal animals is also exposed. In many cases, the UV radiation dose necessary for biological function is much smaller than that imposed by the Sun. For example, solar UV doses are routinely measured at subtropical latitudes that are greater by an order of magnitude or more than the dose required to produce sufficient vitamin-D in humans (Holick 2004; Seckmeyer *et al.* 2008). Inadvertent or involuntary overexposure to UV radiation is therefore a frequent occurrence. Such overexposures result in a myriad of well known adverse biological responses in humans, animals and plants.

Biological responses may occur at the molecular level, or at the macroscopic level where large portions of tissue, or the organism as a whole is affected. Responses may also be acute or chronic. These factors depend on the duration, flux, and spectral distribution of the exposure, and the type of tissue exposed. In general, the magnitude of an acute response is directly related to the UV dose, while chronic responses are often proportional to cumulative UV dose. The accumulation of many intermittent small doses can therefore lead to chronic responses, even when the small doses are in themselves too small to trigger an acute response. Chronic responses tend to continue long after the initial offending exposure has ceased, and may result from prolonged or cumulative exposure to UVA and/or UVB radiation.

The chronic nature of many UV induced responses emphasises the need for both long-term and cumulative solar UV dose measurements. This chapter describes the biological responses induced by UV radiation, and provides an understanding of the importance of quantifying this waveband.

2.2 Molecular and Cellular Level Responses in Humans

2.2.1 DNA and Cellular Damage

Isolated biomolecular bonds absorb UV radiation at wavelengths shorter than about 200 nm. The peak absorption of biomolecules moves toward longer wavelengths with increasing number of conjugated single and double bonds. Purine and pyrimidine bases of DNA contain conjugated chains or rings of such bonds (de Gruijl 2000). DNA molecules are therefore major targets for the absorption of UV radiation. Coohill (2001, p. 93) presents the absorption spectrum of DNA and typical proteins, showing absorption peaks of 260 nm and 280 nm for these molecules respectively. DNA absorption increases rapidly with decreasing wavelength between about 300 nm and 260 nm. A similar increase in absorption occurs for proteins as wavelengths decrease from 300 nm to 280 nm. Therefore, in the solar UV radiation waveband the maximum absorption by both DNA and proteins occurs at 280 nm.

Under most circumstances absorbed UV energy is dissipated innocuously along the DNA structure as heat. On occasion however, new chemical bonds known as photolesions are formed within the DNA molecule. The most prevalent forms of DNA photolesions are the pyrimidine dimers (Petersen & Small 2001), which constitute 98% of DNA damage. The remaining 2% occur in the form of DNA-protein cross-linkages and DNA single-strand and double strand breaks. Of the pyrimidine dimers, about 75% are cyclobutane pyrimidine dimers (CPDs) and 25% are pyrimidine(6-4)pyrimidone dimers (6-4PP) (Tobin 2002, p. 186).

2.2.2 DNA Repair Mechanisms

Cells have evolved a number of efficient repair mechanisms to cope with the various types of DNA lesions that result from UV radiation exposure. DNA lesions may be repaired by excision-repair, photo-reactivation, recombination repair or apoptosis mechanisms. In response to moderate DNA damage, the excision-repair mechanism is thought to employ cell-cycle-arrest followed by DNA repair. In this process photolesions are replaced by the correct chemical bonds by using the undamaged

DNA strand as a template. This repair mechanism appears to be activated by CPD lesions (Lo *et al.* 2005). If both DNA strands contain photolesions, then there is no suitable template available and the repair mechanism fails leaving the photolesions intact. Photo-reactivation involves the reduction of pyrimidine dimers by enzymatic action, which occurs only in the presence of UVA radiation (Roza *et al.* 1991). Like excision-repair, photo-repair is not 100% efficient and not all UV damaged cells are repaired (Coohill 2001, pp. 99-104; Petersen & Small 2001). In the case of extensive DNA damage, apoptosis (programmed cell death) may be induced, and is initiated mainly by 6-4PP lesions (Crespo-Hernádez, Cohen & Kohler 2005). Recombination repair responds to double strand breaks. A reciprocal exchange and subsequent rejoining of the parent DNA strands occur to repair this type of lesion (Sherbet 2003, p. 8). Thacker (2001, pp. 419-23) provides comprehensive details of recombination repair. Photolesions that are not removed by a repair mechanism or by apoptosis inhibit the ability of DNA to replicate correctly, leading to genetic mutations that give rise to organism level inflictions including different types of skin cancers, and various eye diseases (Crespo-Hernádez, Cohen & Kohler 2005).

2.2.3 Mutation of the *p53* Tumour Suppressor Gene

The immune system employs a number of tumour suppression genes that under normal circumstances use cell cycle arrest, DNA repair, and apoptosis to prevent cancerous cells from replicating (Ho & Li 2005). The gene known as *p53* is a tumour suppressor gene that plays a significant role in responding to cell damage caused by UV radiation. The *p53* gene is critical for inducing apoptosis and regulating cell division (Gross *et al.* 2005, p. 576). Research has shown that the *p53* gene is itself the most commonly mutated gene in humans by UV radiation (Pacifico & Leone 2007). As *p53* damage accumulates with increasing exposure, increasing numbers of abnormal cells are able to proliferate (Ackerman & Mones 2006). The *p53* tumour suppression gene is frequently found in mutated form at sites of actinic keratosis (Einspahr *et al.* 1997), basal cell carcinoma (D'Errico *et al.* 1997), squamous cell carcinomas (Einspahr *et al.* 1997; Pacifico & Leone 2007) and malignant melanoma (Yang, Rajadurai & Tsao 2005).

2.3 Organism Level Responses in Humans

2.3.1 Dermal Responses

Vitamin D Synthesis

Typically, over 90% of the human vitamin D requirement is synthesised in the skin through exposure to solar UV radiation. Evidence of the beneficial effects of vitamin D has been reviewed by several authors. The results of Garland *et al.* (2006) and van der Rhee, de Vries and Coebergh (2006) show convincing evidence of sufficient vitamin D status as a defence against a number of internal cancers including colon, breast, prostate and ovarian tumours (Norval *et al.* 2007). Vitamin D status has also been implicated as a defence against autoimmune diseases including type II diabetes, multiple sclerosis, rheumatoid arthritis, and inflammatory bowel diseases (Norval *et al.* 2007). The importance of small (suberythemal) regular doses of sunlight therefore cannot be underestimated, and is required for general well being.

Current guidelines suggest that daily exposures of 40% of the body to 0.25 minimum erythemal dose[1] (MED) is adequate to produce a sufficient level of vitamin D for optimum health. At mid-latitudes during summer, this translates to about 4 to 10 minutes of midday exposure to solar radiation for the fair skin population, and about 60 to 80 minutes for those with dark skin colour (Grant & Holick 2005). Since these periods are often exceeded through outdoor occupational or recreational solar exposure, overexposure frequently occurs.

Erythema and Sunburn

Erythema and sun-tanning are the skin's initial responses to UV overexposure. Erythema is an acute inflammatory response to UVB radiation that causes reddening of the skin marking the onset of sunburn, and subsides rapidly after exposure has ceased. UVB radiation exposure beyond erythema results in sunburn. Another more severe type of erythema is associated with sunburn and occurs as a delayed reaction usually several hours after the exposure. The injury resulting from sunburn is acute

[1] The MED is the approximate mean minimum UV dose that induces erythema in previously unexposed type I (sun-sensitive) skin within 24 hours of exposure, and is defined here as 200 J m^{-2}.

and reversible as damaged skin cells are removed in the process of peeling (Swanson 2006, pp. 624-5).

Sun-Tanning

Sun-tanning is a protective response of human skin to UV radiation. UVA radiation stimulates the secretion of pre-existing melanin from the melanocytes resulting in acute sun-tanning. The melanocytes are stimulated by UVB radiation to create and secrete new melanin, resulting in a chronic form of sun-tanning (Ballotti & Ortonne 2002, p. 2-4). Melanin has photochemical properties that allow the efficient conversion of absorbed UV radiation into non-radiative forms of energy that is harmlessly absorbed by the skin cells (Meredith & Riesz 2004). The protective effects of sun-tanning are however limited. Melanin is capable of absorbing only 50% to 75% of incident UV radiation (Brenner & Hearing 2008), leaving the remainder in a potentially damaging form. Furthermore, photolysis of melanin has been implicated as a cytotoxin involved in the development of cutaneous malignant melanoma (Wood *et al.* 2006; Brenner & Hearing 2008). The large cumulative UV radiation exposures involved in maintaining a suntan for cosmetic purposes may lead to any type of skin cancer (Jones, Moseley & Mackie 1987). Sunbathing and the use of tanning beds are therefore high-risk activities.

Skin Cancer

Genetically injured skin cells that escape repair are able to replicate to form tumours of the epidermis resulting in skin cancers. UV radiation in large doses is therefore a powerful carcinogen. Skin cancers in humans occur in three main types depending on the cells that are affected. Basal cell carcinomas (BCC) and cutaneous squamous cell carcinomas (SCC) are nonmelanoma skin cancers (NMSC) that do not involve the melanocytes. The vast majority (about 97%) of skin cancers are NMSC. Of these, around 80% are BCC and 20% are SCC (Alam & Ratner 2001). BCC involves the formation of tumours within the basal cell layer at the base of the epidermis. The mortality rate due to BCC is low as these tumours metastasise infrequently and are therefore not usually serious, but medical treatment is required in order to avoid disfigurement, which may arise in advanced cases. An estimated 50% to 90% of the

BCC incidence and mortality are attributable to UV radiation exposure (Lucas *et al.* 2006 p. 35), and from 50% to 70% of the total SCC burden is caused by UV exposure (Lucas *et al.* 2006 p. 28).

The less common SCC are more serious than BCC as they are often more invasive and metastasise more frequently at a rate of about 3% (AOCD n.d.). Cutaneous squamous cell tumours arise in the keratinocytes of the epidermis. They often begin as pre-malignant lesions called actinic keratosis, which themselves form in skin areas that have been damaged by UV radiation (Bogle 2006, p. 143). Between 10% and 15% of actinic keratosis evolve into SCC. The presence of actinic keratosis also indicates the existence of UV induced skin damage, and is therefore a significant risk factor for any type of skin cancer (AOCD n.d.).

The most dangerous type of skin cancer is the cutaneous malignant melanoma (CMM), which occurs in about 3% of all skin cancer cases. CMM originate in melanocytes; the pigment producing cells within the basal layer at the base of the epidermis. CMM have a high rate of metastasis. Non-cutaneous tumours resulting from metastasis of the original CMM to other organs including the lungs, liver and brain occurs frequently, in which case the disease most often becomes life threatening. The estimated upper and lower limits of the burden of CMM caused directly by UV radiation exposure are 50% to 90% respectively (Lucas *et al.* 2006, pp. 20-1).

The risk of skin cancer depends on a number of factors including age, skin pigmentation, chemical exposure, and genetic predisposition. The primary aetiological factor for all types of skin cancer however, is UV radiation exposure (D'Errico *et al.* 1997; Lens & Dawes 2004; Breitbart, Greinert & Volkmer 2006). The incidence of all types of skin cancer and the mortality rate from melanoma are significantly greater in the Caucasian population compared to the dark-skin population, and has grown substantially since the late 1970s. The global incidence of BCC is estimated to have increased some 10% annually (Wong, Strange & Lear 2003), while the incidence of malignant melanoma has increased faster than any other type of cancer (Lluria-Prevatt & Alberts 2005, pp. 239-40). Figure 2.1 shows the incidence of malignant melanoma in Australia, UK, and USA.

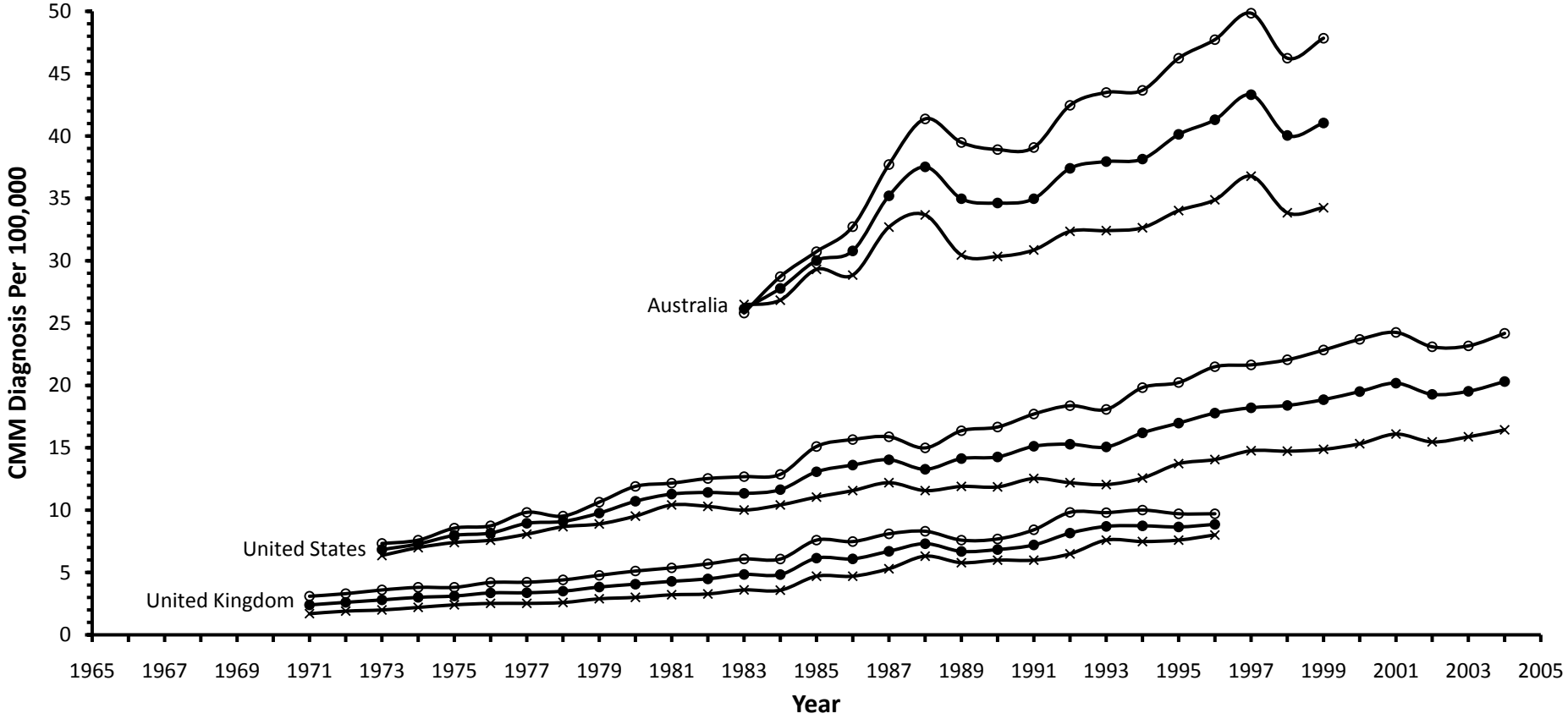

Figure 2.1: Incidence rates of cutaneous malignant melanoma for Australia, the United States and the United Kingdom diagnosed in males (○), females (×), and both males and females (●). The data for this chart were obtained from the National Statistics Clearing House (nschdata.org), the Australian Institute of Health and Welfare (aihw.gov.au), and the Surveillance, Epidemiology, and End Results Database (seer.cancer.gov).

The increases in the incidence of skin cancer are due to several factors. These include an increase in exposure of populations to solar UV radiation, through both ozone depletion (Orellana 2002) and changes in sociological behaviour (including the use of tanning beds) (Stulberg, Crandell & Fawcett 2004), and more frequent diagnosis due to increased public awareness of Sun exposure and skin cancer.

2.3.2 Ocular Responses

By necessity for outdoor vision, mammalian eyes are exposed to solar UV radiation. In humans, UV radiation is absorbed by the cornea and lens of the eye, but is not utilised in vision. Excessive ocular exposure to UV radiation is the cause of several different types of serious eye injury and disease. Photokeratitis and photoconjunctivitis are temporary inflammations of the cornea and conjunctiva respectively that result from ocular exposure. These afflictions can present severe pain, temporary chromatic visual disturbances and temporary loss of vision. The damage is usually reversed within about 48 hours after exposure has ceased and permanent eye damage is rare (McCarty & Taylor 2001; WHO n.d.). Due to the cumulative effects of UV radiation however, repeated episodes of photokeratitis and/or photoconjunctivitis are a risk factor in the development of chronic responses including pterygium, cortical cataracts and ocular carcinomas. Cortical cataracts form when a small region of the eye's lens tissue becomes opaque, and are a leading cause of visual impairment and blindness worldwide (Thylefors *et al.* 1995; McCarty & Taylor 2001). Cumulative ocular exposure to broadband or UVB radiation has been implicated as the primary environmental risk factor in the development of cortical cataracts (McCarty & Taylor 2001; Oriowo, Cullen & Sivak 2002). Lucas *et al.* (2006 p. 50) estimate that 20% of the total incidence of cortical cataract, and 5% of all cataract related disease is the result of UV exposure. Pterygium forms as a triangular network of fleshy tissue that grows over the cornea of the eye. Pterygium are believed to result from eye infections, chronic eye irritation from exposure to dust, and exposure to UV radiation. 42% to 74% of the total incidence of pterygium is estimated to be attributable to UV exposure (Lucas *et al.* 2006 p. 55).

2.3.3 Immunosuppression

Human skin contains a number of cells that form part of the immune system. These cells identify and destroy foreign agents that enter the body such as cells that have been mutated by viral infection or radiation exposure. The destruction of such cells results in inflammation. With the introduction of a large number of damaged cells, as in the case of overexposure to UV radiation, the resulting inflammatory response may interfere with other necessary functions of the skin. The body's natural defence mechanism therefore suppresses the immune response to allow normal function of the skin (Longstreth *et al.* 1998). Such UV induced immunosuppression has been related to an increased growth rate of cancer cells (Damian *et al.* 2008).

2.4 Responses in Animals

UV induced diseases of dermal and ocular tissue inflict a number of animals as well as humans. Little clinical data is available that clearly demonstrates the role of UV exposure in these animal diseases, but some research and veterinary records indicate that the risk factors relating to UV exposure for some diseases resemble those for humans.

Many domestic animals including horses, livestock, and cats and dogs suffer from skin cancers (Elwood 2004, p. 3). As for humans, UV exposure is a factor in the aetiology of actinic keratosis in dogs and cats, and canine and feline SCC are commonly associated with sites of actinic keratosis (Gross *et al.* 2005, p. 576). SCC in animals occur most frequently at anatomical sites that have fair coloured pigmentation, or at sites that are not protected from Sun exposure by fur (Rabo, Usman & Kolo 2000). These sites include the eyes, eyelids, ears, teats and mucocutaneous margins (Sherman 2002, p. 216). Equine SCC is the second most common cancer in horses (Habegger 1999). The incidence of ocular SSC in Appaloosa and draft horses is greater closer to the equator and at higher altitude locations, implicating solar UV exposure as an aetiological factor. Cattle are also susceptible to SCC. In some parts of Australia, up to 6% of Hereford cattle are inflicted with bovine ocular SCC, which has a significant economic impact on the beef industry (Sherman 2002, pp. 216-7). Furthermore, solar UV exposure is a well-

known precursor to infectious bovine keratoconjunctivitis (pinkeye) in cattle. Infection is often subsequent to inflammation of the conjunctiva and cornea of the eye due to solar UV exposure, especially in cattle lacking pigmentation of the eyelids (Kirkpatrick & Lalman n.d.).

Melanoma is common but benign in cattle and rarely occurs in sheep. Equine melanoma is usually less aggressive and metastasises less frequently compared to melanoma in other animals. However, the cost of equine melanoma is high in lightly coloured horses, with up to 80% of mature grey and white Lipizzaner, Arabian and Percheron breeds affected. Canine melanomas account for about 7% of malignant tumours in dogs. The prognoses for dogs, and most other animals diagnosed with melanoma are generally grim. The incidence profile of equine melanoma (Smith, Goldschmidt & McManus 2002), and the latitudinal incidence distribution of melanoma diagnosed in Angora goats (Sherman 2002, pp. 216-7) suggests a likely connection between melanoma in animals and UV exposure.

2.5 Responses in Plants

As photosynthetic organisms, plants are inevitably exposed to solar UV radiation, which has well known detrimental effects on many susceptible species. These effects are primarily related to genomic damage and damage of the photosynthetic system (Fiscus & Booker 1995). The types of DNA lesions that occur in mammals occur also in plant cells. Like mammals, plants have also evolved protective mechanisms such as UV absorbing flavonoids (Madan & Sengupta 2000), and DNA repair including photoreactivation and excision repair (Kimura *et al.* 2004). Despite these protective mechanisms, solar UVB radiation has been observed to cause measurable DNA damage in barley (Mazza *et al.* 1999) and in temperate rainforest species of South America (Rousseaux *et al.* 1999).

In addition to genetic damage, the photosynthetic apparatus of plants may be damaged by UV radiation. Significant reductions in photosystem II (PSII) photosynthesis has been observed in the leaves of a number of higher plant species, including sweet potato (Kim *et al.* 2007), *Chenopodium album* (van Rensen,

Vredenberg & Rodrigues 2007), bean plants (Cen & Bornman 1990), cucumbers (Battaglia & Brennan 2000), and many others.

The consequence of DNA damage and photosynthetic inhibition due to solar UV radiation may be a reduction in plant biomass. Examples of growth retardation due to UVB exposure have been observed in wheat seedlings (Tian & Lei 2007) and soybeans (Guruprasad *et al.* 2007).

2.6 Biologically Effective Radiation

The tissues of humans, animals and plants are complex biological structures with spectral absorption properties that differ significantly from one tissue type to another. The magnitude of a biological response depends therefore on both irradiance and the wavelength of induction. In order to find a correspondence between UV irradiance in physical units and a given biological response, a spectral weighting function known as a biological action spectrum is required. An action spectrum for a given biological response is derived from the relative efficiency of spectral UV irradiance in inducing that response as a function of wavelength. If λ_0 is the wavelength of maximum efficiency, then the action spectrum for the response is given by

$$A(\lambda) = \frac{H(\lambda_0, t)}{H(\lambda, t)} \tag{2.1}$$

(de Gruijl 2000) where $A(\lambda)$ is the spectral weighting function (or action spectrum), $H(\lambda_0,t)$ is the monochromatic dose administered at the wavelength of peak efficiency for a time period of t, and $H(\lambda,t)$ is a dose administered for the same time period but at any wavelength λ of interest. If $A(\lambda)$ is independent of dose, then equation 2.1 indicates that the quantity $A(\lambda)H(\lambda,t)$ is the equivalent of the dose $H(\lambda,t)$ at the monochromatic wavelength of λ_0 (de Gruijl 2000). Biologically effective irradiance (I_{BE}) is therefore the wavelength-integrated product of spectral irradiance of the source and the action spectrum of interest, given by

$$I_{BE} = \int_{\lambda_1}^{\lambda_2} I(\lambda) A(\lambda)\, d\lambda \ (\mathrm{W\ m^{-2}}) \tag{2.2}$$

where $I(\lambda)$ is the spectral irradiance of the source, $A(\lambda)$ is the action spectrum, and λ_1 and λ_2 are the upper and lower bounds of the waveband of interest (Diffey 1989, pp. 139-40; CIE 1992).

The product of solar spectral irradiance and the erythemal action spectrum is shown in figure 2.2, and action spectra for a number of biological responses are shown in figure 2.3. Biologically effective dose is then calculated as the time-integrated biologically effective irradiance, or

$$H_{BE} = \int_0^T I_{BE} dt = \int_0^T \int_{\lambda_1}^{\lambda_2} I(\lambda) A(\lambda) d\lambda dt \text{ (J m}^{-2}\text{)} \qquad (2.3)$$

where T is the total duration of the exposure.

The minimum erythemal dose (MED) is frequently used unit for quantifying UV radiation dose that is weighted against the erythemal action spectrum. The MED quantifies the approximate mean minimum dose required to induce the erythemal response in previously unexposed human skin within 24 hours of exposure. The dose required to induce erythema depends strongly on skin type; the fairer the skin, the lower the required dose. The MED must therefore be defined for a given skin type. Most commonly (and for the purpose of this research), the MED is defined for type I skin which sunburns easily and never tans. For type I skin, the MED is defined as a dose of 200 J m^{-2}.

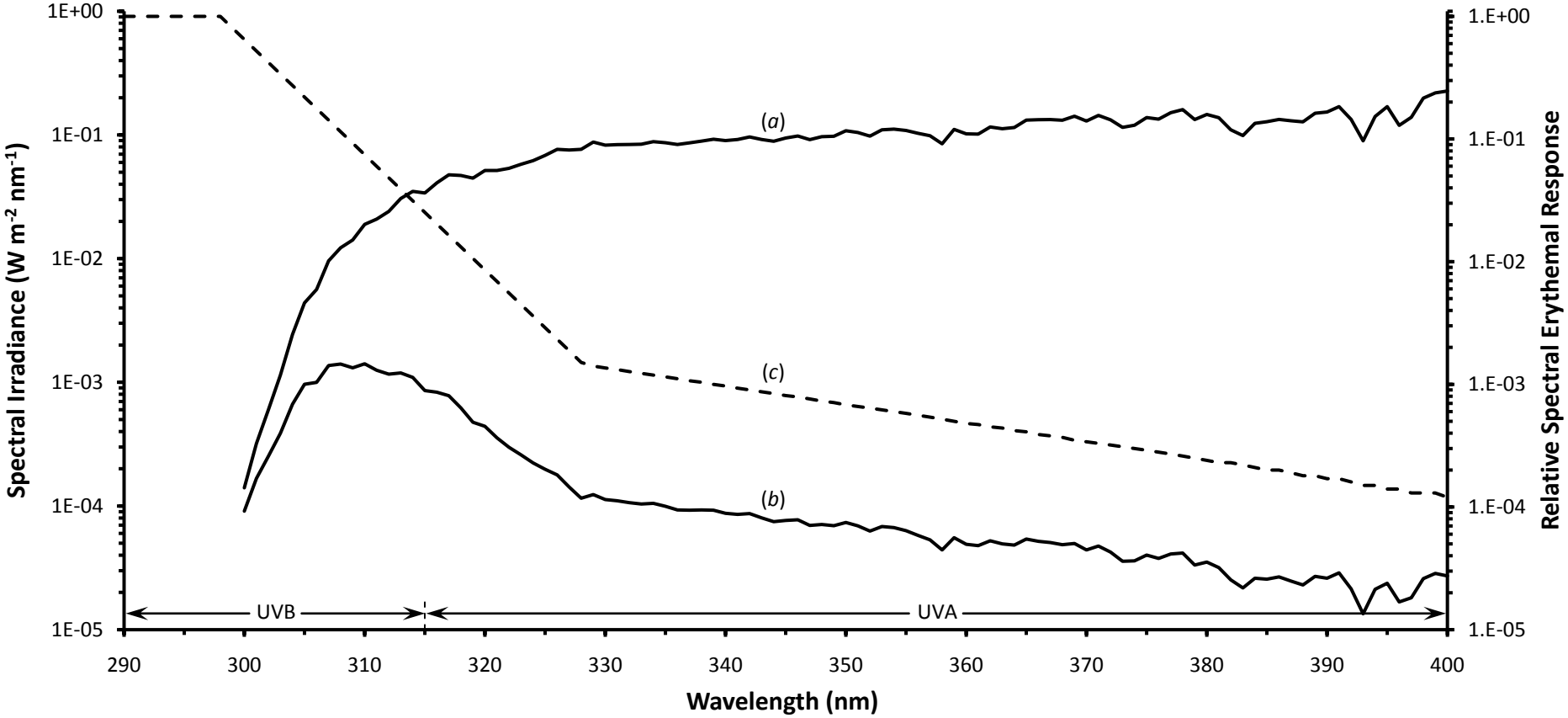

Figure 2.2: Solar spectral UV irradiance (*a*) (left axis) and erythemal spectral irradiance (*b*) (left axis) on a horizontal plane. The solar irradiance was measured in Toowoomba at a solar zenith angle of 44°. The erythemal spectral irradiance is calculated from the product of the solar spectral irradiance and the CIE erythemal action spectrum (CIE 1987) (*c*) (right axis).

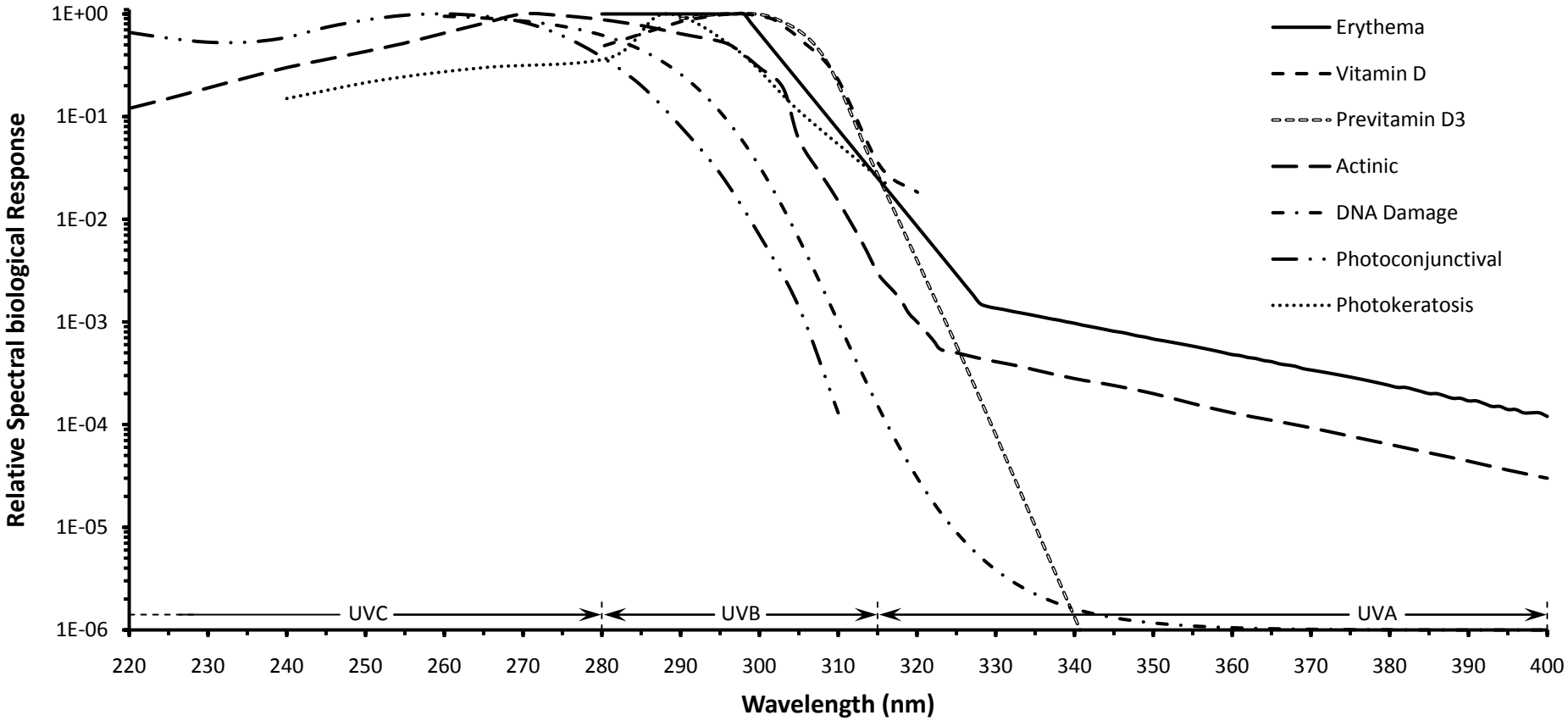

Figure 2.3: Action spectra for biological responses including human erythema (CIE 1987), vitamin D synthesis (MacLaughlin, Anderson, & Holick 1982), previtamin D3 synthesis (CIE 2006), actinic response (IRPA 1989), DNA damage (Setlow 1974), photoconjunctivitis (CIE 1986a), and photokeratitis (CIE 1986b).

In the case that the spectral sensitivity of a broadband detector corresponds to a given biological action spectrum, the detector may be used to provide direct measurements of biologically effective dose without the need for spectral measurements. Therefore, although equations 2.2 and 2.3 depend on spectral irradiance, action spectra are also an important aspect of broadband radiometry and dosimetry.

2.7 Summary and Conclusions

UV radiation is required by animals and plants for biological function, but due to the significant intensity of this waveband at the Earth's surface, UV overdose is a common occurrence that leads to a number of adverse biological responses. In both humans and animals, these responses include erythema and sunburn, ocular diseases, skin cancer, and damage to DNA and the immune system. Humans are frequently exposed both occupationally and recreationally to UV radiation. The synergy of DNA damage, *p53* mutation, and immunosuppression is most likely a contributing factor to the high incidence of skin cancer in Australia and other countries. Solar UV radiation is also strongly implicated as the primary aetiological factor in the development of skin cancer in domestic pets and livestock, and is known to impede the growth of a number of plant species, many of which are commercially important.

Due to the biological requirement of UV exposure and the potential for overdose, the quantification of this waveband at the Earth's surface must be a priority in the assessment of environmental health and safety. The array of chronic effects induced by large or cumulative doses warrants the development of cost effective methods for large-dose quantification. The measurement of UV irradiance or dose provides limited information with regard to biological responses due to the dependence of these responses on the spectral distribution. However, the availability of a number of biological action spectra provides a means of quantifying biologically effective radiation such that the effects of solar UV radiation on the biosphere can be fully assessed.

The effects of UV radiation overdose are of primary concern to human health. Due to the impacts of UV exposure on animals and plants however, veterinary sciences

and agricultural sciences also benefit from the quantification of biologically effective solar UV radiation.

Chapter 3

Variability and Distribution of Solar UV Radiation

3.1 Introduction

Solar radiation emanates from the Sun and irradiates the daytime side of Earth's surface via Earth's atmosphere. Solar irradiance at the Earth's atmospheric perimeter varies cyclically on a global scale with diurnal and annual periods due to the Earth's motion and the geometry of the Earth-Sun system. Atmospheric absorption and scattering processes result in random and seasonal fluctuations of both solar UV irradiance and spectral UV irradiance at the Earth's surface at micro- to synoptic-scales. Ground level irradiance variations are therefore the net effect of the cyclical variations at the atmospheric perimeter and sporadic effects that occur within the atmosphere. The spatial distribution of solar UV irradiance also depends on these geometrical and atmospheric factors. Stratospheric ozone depletion has additionally caused an unnatural disturbance in both the latitudinal and spectral distributions of solar UV irradiance.

The variability of solar radiation results in a complex and continually changing UV radiation field at the Earth's surface. This complexity imposes difficulties and limitations in estimating UV exposures in the absence of direct measurements. The performance and accuracy of solar UV detectors involved in direct measurements however, are themselves influenced by the nature and variability of the UV radiation field. It is therefore important to consider variability factors in the radiation field in which a detector is to operate.

3.2 Astronomical and Geometrical Factors

For any fixed terrestrial coordinate, solar irradiance waxes and wanes at the Earth's surface through the course of a solar day due the axial rotation of the Earth. This diurnal irradiance cycle peaks at solar noon as the Sun reaches its highest point in the sky, and then declines to effectively zero after sunset. The Earth's axis of rotation is inclined at an angle of 23.5° to the normal to the plane of the ecliptic and effectively retains its orientation in space as the Earth orbits the Sun. As a result, for one half of the Earth's orbit one hemisphere is tilted toward the Sun while the other is tilted away. The hemisphere tilted toward the Sun experiences spring followed by summer, while the opposite hemisphere experiences autumn followed by winter. At non-

equatorial locations, the period of daylight is therefore greater in the spring/summer hemisphere, resulting in larger solar radiation exposures of this hemisphere compared to the autumn/winter hemisphere. During the second half of the orbit the situation reverses. The Earth's axis slowly tilts what was previously the spring/summer hemisphere away from the Sun to become the autumn/winter hemisphere and vice versa. An annual solar UV irradiance cycle therefore occurs at non-equatorial coordinates due to the Earth's orbital motion around the Sun. The peak irradiance due to this cycle occurs at the summer solstice (~ June 22) in the northern hemisphere, and at the winter solstice (~ December 22) in the southern hemisphere.

Direct solar UV radiation arriving undeviated from the direction of the Sun is reduced at the Earth's surface by the cosine of the angle of incidence of the radiation (Sturman & Tapper 1996, pp. 32-3). The angle of incidence *i* is related to solar zenith angle (SZA) by $i = 90° - \mathrm{SZA}$ and is therefore a function of time-of-day, season and latitude. Hence this cosine weighting contributes to the diurnal and annual UV irradiance cycles.

3.3 Atmospheric Processes

3.3.1 Atmospheric Absorption and Scattering

The Earth's surface is shielded from high-energy solar radiation by ionospheric gas atoms that become ionised by the absorption of wavelengths shorter than about 100 nm. Radiation in the UV waveband is nonionising, and is therefore unimpeded by the ionosphere and passes into the lower layers of Earth's atmosphere. The interaction of solar UV radiation with gas molecules and aerosols in these layers results in spectral attenuation through scattering and absorption interactions. The degree of interaction is determined by the spectrally dependent complex refractive index,

$$N(\lambda) = n(\lambda) + ik(\lambda) \tag{3.1}$$

of the interacting atmospheric constituent. The real component $n(\lambda)$ is defined as the ratio of the speed of light in a vacuum to the speed of light in a medium, and

corresponds to scattering. The loss of electromagnetic energy, or absorption, is derived from the imaginary component, $k(\lambda)$ (Marley *et al.* 2001; Tardif 2001).

Equation 3.1 depends on the chemical compositions of the atmospheric constituents and the wavelength of the radiation with which they interact. Gas molecules in the lower mesosphere and the stratosphere undergo photodissociation on absorption of shortwave UV radiation. This process is dominated by molecular oxygen, which absorbs efficiently in the UVC waveband at wavelengths shorter than 240 nm (de Gruijl & van der Leun 2000). The resulting atomic oxygen reacts with molecular oxygen to form ozone (O_3) (McConnell & Jin 2008), which absorbs predominantly in the Hartley waveband (200 nm to 320 nm) with the peak absorption centred around 250 nm (Pickett 1994; de Gruijl & van der Leun 2000). Ozone concentration peaks in the lower stratosphere at an altitude of about 20 km forming the ozone layer. As a result of oxygen and ozone absorption, no UVC reaches Earth's surface, and wavelengths in the UVB waveband up to about 290 nm are completely attenuated. The efficiency of ozone absorption increases with decreasing wavelength in the UVB waveband. The solar UV radiation waveband that arrives at Earth's surface therefore extends from about 290 nm to 400 nm.

Small amounts of ozone are produced naturally in the troposphere and contribute to the absorption of solar UVB radiation. Anthropogenic emissions of nitrogen oxides, carbon monoxide, and other volatile organic compounds react in the presence of UV radiation to form ozone. This ozone pollution also contributes to the reduction of UV irradiance at the Earth's surface (Sabziparvar, de F. Forster & Shine 1998).

In addition to absorption, atmospheric constituents redistribute solar energy in various elastic scattering processes, in which the energy of the interacting photon remains unchanged after the interaction. Rayleigh scattering occurs when the diameter of the scattering element is small compared to the wavelength of the interacting photon. The Rayleigh scattering intensity I_R of unpolarised radiation from molecules is given by

$$I_R = I_0 \frac{8\pi^4 N\alpha^2}{\lambda^4 R^2}\left(1+\cos^2\theta\right) \tag{3.2}$$

where I_0 is the initial intensity, N is the number of isotropic and randomly distributed scattering elements, α is the polarisability of the molecule, R is the distance from the scatterer, and θ is the scattering angle (HyperPhysics.com n.d.). Equation 3.2 indicates that Rayleigh scattering intensity varies inversely with the fourth power of wavelength. Since the angular intensity distribution is determined by $\left(1+\cos^2\theta\right)$, the back-scattering and forward-scattering intensities are equal, while the scattering intensity in directions perpendicular to the direction of the incident photon is half that of the scattering intensity in parallel directions (Jeske 1988, p. 265). The main scattering elements in Earth's atmosphere are gas molecules, which are sufficiently small to induce Rayleigh scattering in the UV waveband. Rayleigh scattering is therefore the dominant process for the redistribution of solar UV radiation.

Mie scattering becomes increasingly important in the troposphere where aerosols such as dust, pollen, smoke particles and cloud droplets are abundant. Aerosols are typically large in diameter compared to the wavelengths of the UV radiation waveband and result in a scattering distribution that depends on the size and shape of the scattering element, as well as the interacting wavelength. Mie scattering preferentially distributes energy in the forward direction relative to the direction of the incident photon.

As a result of Rayleigh and Mie scattering, and reflection and scattering from large-scale environmental structures, the solar UV radiation waveband is comprised of a direct component and a diffuse component. Since short solar UV wavelengths are scattered preferentially in the dominating Rayleigh process, a large proportion of the diffuse component is comprised of UVB wavelengths. At 300 nm more than half of solar UVB radiation is diffuse (Pickett 1994). The portion of diffuse UV radiation that contributes to the global solar UV waveband is large compared to the direct proportion and increases at large SZA. At SZA of more than 45°, between 70% and 100% of the solar UVB waveband, and more than 55% of the solar UVA waveband is diffuse UV radiation (Feister & Grewe 1995).

The changing geometry of the Earth-Sun system due to the Earth's rotation and orbit results in continual changes in atmospheric path lengths for the direct component of solar radiation. The atmospheric path length increases with increasing SZA. With

increasing path length comes a greater air mass between the Sun and Earth's surface, which increases the probability of absorption and scattering interactions within the atmosphere (Ortiz de Galisteo *et al.* 2008).

3.3.2 Effects of Clouds

Short-term fluctuations of solar UV radiation occur within the troposphere due to absorption and Mie scattering of solar radiation from cloud droplets under various weather conditions. Within any given climate zone, clouds are the dominant source of atmospheric variability of solar UV radiation (Lubin, Jensen & Gies 1998).

During conditions of heavy cloud cover, solar UVB irradiance may be reduced to zero (Mantis *et al.* 2000). The extent of attenuation by clouds depends on cloud type, cloud coverage, cloud altitude and SZA (Blumthaler, Ambach & Salzgeber 1994; Kuchinke & Nunez 1999; Josefsson & Landelius 2000; Piacentini, Cede & Barcena 2003). Conversely, many instances of elevated UV irradiance above clear-sky irradiance during broken cloud and cloud-haze conditions have been reported. Such enhancements result from radiation reflected from cumuliform clouds (Mims II & Frederick 1994; Weihs *et al.* 2000; Sabburg, Parisi & Wong 2001).

3.3.3 The Altitude Effect

At higher atmospheric pressures, the effective optical path length is greater due to the higher concentrations of atmospheric gas molecules, tropospheric ozone, aerosols, and a greater abundance of clouds (Schmucki & Phiipona 2002). Scattering and absorption of UV radiation are therefore greater at sea level than at high altitudes, and there is a direct relationship between altitude and UV irradiance. The altitude effect (AE) is given as a percentage increase in irradiance per kilometre by

$$\mathrm{AE} = \Delta y \left(\frac{I_m - I_v}{I_v} \right) \times 100 \qquad (3.3)$$

where I_m is the high altitude (mountain) irradiance, I_v is the low altitude (valley) irradiance and Δy is the difference in altitude in kilometres (Blumthaler, Ambach & Ellinger 1997).

The decrease in scattering element concentrations with increasing altitude results in a change in the ratio of diffuse to direct irradiance, with a rapid increase in direct irradiance while the diffuse component remains constant or decreases (Blumthaler & Webb 2003, p. 47-8). The decrease in tropospheric ozone with altitude, and the preferential scattering of shorter wavelengths in the Rayleigh process cause a shift in spectral UV irradiance toward shorter wavelengths. The AE is therefore greater at UVB wavelengths. Lorente *et al.* (2004) for example, found clear-sky AE values of 6% km^{-1} for solar UVA irradiance, 9% km^{-1} for UVB, and 11% to 14% for biologically effective UV irradiance. This is the probable cause of the higher incidence of ocular SCC in horses at high-altitude locations as noted in the previous chapter.

3.4 Spatial Distribution

3.4.1 Latitudinal Dependence

The angle of incidence of solar radiation is greater at higher latitudes since SZA is a function of latitude, and hence the reduction in direct irradiance due to the cosine weighting is greater. In addition, the path length through the atmosphere is greater at higher latitudes, increasing the probability of absorption and scattering. Consequently, at any given moment in time there exists a decreasing latitudinal UV irradiance gradient on the daytime side of the Earth that extends from the equator to the polar regions.

3.4.2 Hemispherical Differences

The Southern Hemisphere on average receives greater UV exposure than the Northern Hemisphere (Seckmeyer *et al.* 1995; Madronich *et al.* 1998, p. 2). The greater population of the Northern Hemisphere due to the larger landmass results in greater anthropogenic emissions compared to the Southern Hemisphere. The greater

atmospheric aerosol loading and greater tropospheric ozone concentrations due to human activity result in lower ground level UV irradiance in the Northern Hemisphere (Blumthaler & Webb 2003, pp. 49-50).

In addition to the effects of aerosols and tropospheric ozone, the Earth-Sun geometry also contributes to the imbalance of solar UV irradiance between the hemispheres. The winter solstice coincides with perihelion, which results in a 3.3% closer proximity of southern hemisphere to the Sun during summer compared to the northern hemisphere in summer. Consequently, the mid-summer southern hemisphere UV irradiance is about 6.6% greater than that of the northern hemisphere (McKenzie 1991).

3.4.3 Surface Albedo

The Earth's UV surface albedo quantifies the fraction of global UV irradiance incident upon the Earth's surface that is returned to the atmosphere by reflection. Albedo depends primarily on the nature of the reflecting surface and the wavelength of the incident radiation, and hence varies from one location to another. Typical albedo values range from 0.01 to 0.03 for grass, around 0.1 for sand, and 0.50 to 0.6 for snow (Feister & Grewe 1995; Lester & Parisi 2002; Chadyšienė & Girgždys 2008). In the case of fresh snow, UV albedo values approaching unity have been reported (Grenfell, Warren & Mullen 1994; Wuttke, Seckmeyer & König-Langlo 1996). The measurements presented by these and other authors indicate that UV albedo also tends to increase with wavelength for natural surfaces. The superimposed effects of surface albedo and atmospheric turbidity also influence the altitude effect resulting in complex seasonal variations in global UV irradiance (Blumthaler, Ambach & Ellinger 1997; Schmucki & Phiipona 2002).

3.5 Stratospheric Ozone and Total Column Ozone

Total column ozone (TCO) is measured in Dobson units[1] (DU) from the ground to the atmosphere's perimeter and includes both tropospheric ozone and the

[1] The Dobson unit is defined as an ozone thickness of 0.01 mm at standard temperature and pressure, or a concentration of 2.69×10^{20} m^{-2}.

stratospheric ozone layer. Although tropospheric ozone plays a significant role in the altitude affect, it contributes only about 10% to the TCO. The ozone layer therefore plays the most important role in protecting the Earth's surface from damaging high-energy UVB radiation.

Stratospheric ozone concentrations vary significantly in time and with latitude, resulting in both temporal and spatial variations in UVB irradiance. The inverse relationship between UVB irradiance by TCO has been well established (e.g. Fioletov, Kerr & Wardle 1997; Lam *et al.* 2002; Koshy *et al.* 2006). A decline in stratospheric ozone results in a spectral irradiance increase at the shortest UVB wavelengths of the solar terrestrial UV waveband.

The sensitivity of biologically effective UV radiation to changes in ozone concentration is known as the radiation amplification factor (RAF), and provides the percentage change in biologically effective radiation that results from a 1% change in ozone concentration. The severity of many biological responses is inversely related to UVB wavelength. The RAF is therefore dependent on both the given response and wavelength of induction. Estimates of the RAF range from 1.1% to 2.3% for erythemal (sunburning) irradiance (Blumthaler, Salzgeber & Ambach 1994; Mendeva *et al.* 2005). Changes in biologically effective UV irradiance (UV_{BE}) can be estimated directly from the RAF for small changes in ozone. For changes of more than a few percent in ozone, UV_{BE} changes become nonlinear and are estimated by

$$UV_{BE} \sim (TCO)^{-RAF} \tag{3.4}$$

under the assumption that UV_{BE} for the given response decreases approximately exponentially with wavelength (Madronich *et al.* 1998, p. 5).

Stratospheric ozone concentrations over the polar regions have been steadily declining since the early 1980s due to anthropogenic emissions of ozone depleting chemicals such as chlorofluorocarbons (CFCs) and halocarbons into the atmosphere. Consequently, solar UVB irradiance arriving at Earth's surface at some locations has increased over this period (e.g. McKenzie, Connor & Bodeker 1999).

The severity of ozone depletion is greatest over the Antarctic due to the unique atmospheric conditions of the polar regions. Polar stratospheric clouds (PSC) form

under the cold conditions of the winter circumpolar vortex, and act as a substrate for the formation of chlorine monoxide (ClO) and bromine monoxide (BrO) from CFCs and halogens. The arrival of springtime sunlight initiates photochemical reactions between these chemical species and ozone, resulting in massive ozone losses of 1% to 2% per day over Antarctica during the austral spring (Tolba 1992; Nichol *et al.* 2001). The ozone loss and spatial extent of this ozone hole has increased significantly since 1980. The TCO over Antarctica during the August-October period in the 1960s and early 1970s was 275 DU to 300 DU. In 1984, the TCO declined to 180 DU (Shaw & Stroup 1995, p. 9), and a new minimum of 126 DU was reported in September 2000 (Nichol *et al.* 2001). The area of the springtime ozone hole has increased from less than 3 million km^2 in 1980 to almost 29 million km^2 in 2000. The second largest area of ozone depletion of 28 million km^2 occurred in September 2003 (NOAA n.d.).

The Montreal Protocol established in 1987, along with its subsequent revisions, aims to reduce global emissions of ozone depleting gases (Fraser & Prather 1999). Due to the long half-life of many ozone depleting substances, the exponential nature of the resulting decrease due to the Montreal Protocol, and the possibility that some substances may still be increasing, the restoration of the ozone layer is uncertain. The total atmospheric burden of ozone depleting substances may not peak until 2010 (Montzka *et al.* 1999).

3.6 Summary and Conclusions

Solar ultraviolet radiation continually varies at the Earth's surface in a complex manner due to a large number of superimposed spatial and temporal factors. These factors modulate both the irradiance and spectral distribution of the UV waveband. Atmospheric ozone and aerosol concentrations alter the refractive index of atmospheric layers causing changes in absorption and scattering of UV radiation. Changing SZA results in the expected diurnal and seasonal cosine modulation of irradiance, and also interacts with atmospheric processes via changes in atmospheric path length causing irradiance fluctuations over many different time scales. Furthermore, due to the spectrally selective nature of atmospheric attenuation, these

processes work in conjunction with path length to alter ground level spectral irradiance.

As discussed in chapter 2, biological responses induced by UV radiation have strong spectral dependencies, with shorter wavelengths generally having a greater biological effectiveness. Although the irradiance of the solar UVB waveband is significantly lower than that of the UVA due to spectral atmospheric attenuation, the UVB waveband delivers substantially more energy and is absorbed more efficiently by protein and DNA molecules. The inverse relationships between wavelength and several important biological weighting functions were shown in figure 2.3. Due to the shift of the solar distribution to shorter wavelengths by atmospheric processes, meteorological conditions have an important impact on variations in biologically effective irradiance at the Earth's surface.

Stratospheric ozone depletion has caused a long-term shift of the spectral UV distribution to shorter wavelengths, especially near the polar regions, with a resulting nonlinear increase in biologically effective UV irradiance. Despite international efforts to reduce anthropogenic emissions of ozone depleting gases into the atmosphere, the timeframe for ozone layer recovery remains uncertain.

Measurements of biologically effective UV radiation are therefore necessary to assess the biological effects of ambient UV exposures under various conditions of atmospheric variability and geometrical modulations. Measurements are also required to quantify amplification of UV irradiance due to ozone depletion, altitude, surface albedo and clouds, and the resulting biological consequences. Furthermore, due to the significant variability of UV irradiance, a detector developed for these measurements must be capable of maintaining a reasonable degree of accuracy under a radiation field that is constantly changing in both irradiance and spectral distribution during the course of the measurement. Since UV dosimeters naturally integrate all temporal UV variations into the response, dosimetry is a methodology well suited to solar UV exposure measurements.

Chapter 4

Optical Properties of Absorbance-Based UV Actinometers

4.1 Introduction

Some cause gives rise to an effect in all detectors. For a UV radiation detector, the cause is the absorption of incident UV radiation and the effect is the response of the detector to that absorbed radiation. The response of an ideal detector for biologically effective solar UV measurements has optical properties that exactly match the behaviour of the biological response of interest. However, deviations of the optical properties of a detector are always present, and must be quantified in order to evaluate the performance of the detector.

Radiant energy incident on the surface of a material is either absorbed or reflected depending on the nature of the material and the angle of incidence of the radiation. A material is suitable for dosimetry only if it is capable of absorbing radiation in an appropriate waveband, and the quantum yield resulting from that absorption is large enough to be quantified by some means. In actinometry, molecular bonds of the actinometer material are primarily responsible for the absorption of radiant energy. If the absorbed radiation is sufficiently energetic, molecules of the actinometer material are excited to a chemically active state resulting in photochemical reactions that are responsible for a chemical response of the material. Otherwise the radiant energy is redistributed thermally among the molecules and no response occurs.

A range of methods are used for quantifying the UV induced response depending on the type of dosimeter employed. Biodosimeters frequently employ the quantification of cyclobutane pyrimidine dimer (CPD) type photolesion concentrations or protein production after incubation and staining. Some forms of chemical solution actinometry require high performance liquid chromatography (HPLC) analysis to determine chemical concentrations, while others depend on quantification of quantum yields or reaction rate constants. The simplest form of response quantification employs photometry, in which the response is a direct measure of the change in optical absorbance of the dosimeter material due to UV radiation exposure. This type of response quantification is the most cost effective, and may be conducted in any standard optical laboratory. In adhering to efficient and low cost methodologies, absorbance related optical properties applicable to solar UV actinometry are reviewed in this chapter.

4.2 Optical Absorbance and Response

A photochemical change takes place within an actinometer material when the quantum yield due to the absorption of radiation is greater than zero. This photochemical change when quantified, gives a measure of the response of the material to UV radiation. Since the variation in response defines the optical properties of an actinometer, an efficient method for quantifying response is required. The most cost effective and versatile methods of UV actinometry employ a photosensitive material that experiences a change in optical absorbance due to the photolysis of the material by UV radiation. Quantifying this change is the underlying principle for this type of actinometry.

The optical absorbance A of translucent materials is often expressed as

$$A = \log\left(\frac{I_0}{I}\right) \tag{4.1}$$

where I_0 is the radiation intensity before absorption, and I is that after absorption; or in a solution as,

$$A = \log\left(\frac{I_0}{I}\right) = \varepsilon l c \tag{4.2}$$

where ε is the molar absorptivity of the material, l is the path length through the material, and c is the concentration of the solution (Yadav 2005, p. 7).

The change in optical absorbance ΔA of an actinometer material due to a given UV dose H is calculated from the difference between the absorbance before exposure and after exposure. The response is therefore given by

$$\Delta A(H) = A(H = 0) - A(H) \tag{4.3}$$

where $A(H = 0)$ is the absorbance before exposure and $A(H)$ is the absorbance after a given dose H. The absorbance of the material before and after exposure may be determined by equation 4.1 for a film type actinometer, or by equation 4.2 for a solution type. Alternatively, and perhaps more conveniently, these absorbances may

be measured directly with photometric equipment such as a spectrophotometer. Equation 4.3 assumes that the response is a monotonically changing function of dose (see section 4.4), and hence the sign of the response given by equation 4.3 is unimportant.

The absorbance of an actinometer material is usually spectrally selective, and characterised by an absorbance spectrum $A(\lambda)$. Hence the measurement of the actinometer's response may depend on the wavelength of the radiation used for the response measurement. Equation 4.3 therefore becomes

$$\Delta A\left(H,\lambda_{L}\right)=A\left(H=0,\lambda_{L}\right)-A\left(H,\lambda_{L}\right) \tag{4.4}$$

where λ_L is the constant wavelength used for the measurement of the absorbance. The absorbance spectrum of the actinometer material after exposure is not necessarily the same as that before exposure. This allows the response measurement to be optimised for sensitivity by means of the response spectrum

$$\Delta A\left(H,\lambda\right)=A\left(H=0,\lambda\right)-A\left(H,\lambda\right) \tag{4.5}$$

in which case λ is a variable measurement wavelength ranging from 280 nm to 400 nm. The wavelength at which $\Delta A(H,\lambda)$ is maximised provides the greatest measurement sensitivity of the response when this wavelength is substituted for λ_L in equation 4.4.

4.3 Sensitivity

The UV induced changes in a photosensitive material depend primarily on the overall sensitivity of the material to UV exposure. In most cases, actinometer materials exhibit interrelated sensitivities to spectral irradiance and to exposure.

4.3.1 Exposure Sensitivity

The exposure sensitivity S_H is the change in absorbance ΔA per unit UV dose $H(t)$ received during the exposure period t, or

$$S_H = \frac{\Delta A}{H(t)} \tag{4.6}$$

where the spectral irradiance distribution of the source of $H(t)$ is constant. Due to the spectral sensitivity of a dosimeter material, the exposure sensitivity must be evaluated employing a monochromatic UV radiation source at some reference wavelength.

In the general case for actinometers, the photochemical reactions that drive the response of the actinometer become exhausted resulting in optical saturation. As saturation proceeds, the rate of change of the response induced by a given UV dose declines. Hence as saturation increases, the exposure sensitivity declines while the response variance either remains constant or increases (Diffey, Oliver & Davis 1982; González-López 2007). The dose resolution of an actinometer therefore decreases while measurement uncertainties increase due to saturation related reductions in sensitivity.

4.3.2 Spectral Sensitivity

The change in sensitivity per unit change in wavelength defines the spectral sensitivity of an actinometer material. When the dose sensitivity of a material is linear, the monochromatic spectral sensitivity $S(\lambda)$ is given by

$$S(\lambda) = \frac{d\Delta R(\lambda)}{d\lambda} \tag{4.7}$$

where $d\Delta R(\lambda)$ is the response that results from an infinitesimal change in wavelength $d\lambda$. Equation 4.7 does not hold when the exposure sensitivity is nonlinear since each wavelength has a range of sensitivities that depend additionally on dose (Bauer 1968).

In such cases, the relative spectral sensitivity must be employed. The ratio of the spectral sensitivity at any given wavelength $S(\lambda)$ to the spectral sensitivity at a reference wavelength $S(\lambda_0)$ defines the relative spectral sensitivity $S(\lambda)_{\text{rel}}$ as

$$S(\lambda)_{\text{rel}} = \frac{S(\lambda)}{S(\lambda_0)} \tag{4.8}$$

(Bauer 1968). If $S(\lambda_0)$ is defined as the wavelength that maximises the response of the material, then the reciprocal of equation 4.8 gives a weighting function of the material known as the spectral response $R(\lambda)$, which is given by

$$R(\lambda) = \frac{H(\lambda_0, t)}{H(\lambda, t)} \tag{4.9}$$

where $H(\lambda,t)$ is the monochromatic dose at a wavelength of λ, and $H(\lambda_0,t)$ is the dose at which $H(\lambda,t)$ is minimised due to the maximum effectiveness of the wavelength λ_0. The spectral absorbance often resembles the spectral response, but may differ somewhat since photolysis and absorption cross-section are often independent functions of wavelength.

Note that equations 2.1 and 4.9 are algebraically equivalent. The spectral response of an actinometer material is therefore analogous to a biological action spectrum, and hence the quantity $R(\lambda)H(\lambda,t)$ expresses the dose $H(\lambda,t)$ as an equivalent monochromatic dose at the wavelength of λ_0. An actinometer material with equivalence between its spectral response and a given biological action spectrum is therefore particularly useful for quantifying biologically effective exposure for that response.

4.4 Dose-Response and Calibration Functions

In order for a dosimeter to provide UV dose measurements, its response must be cumulative, and must also be a function of UV radiation dose that changes monotonically. This dose-response function relates each level of the dosimeter's response to a unique UV dose. If a suitable UV monitoring instrument is used to measure the dose, then the dose-response function provides a calibration of the dosimeter against that instrument.

Due to the decline in sensitivity that results after optical saturation of an actinometer material, the dose-response function approaches a constant as dose increases, and

hence the dose-responses of many materials assume logarithmic or exponential forms. Since there should be no change in the response of a material before UV exposure, the first point on the dose-response curve is at the origin. Least squares regression curves of logarithmic or exponential forms therefore cannot be used. A useful property of the dose-response function however, is that since it is monotonic it has an inverse. The inverses of logarithmic and exponential functions can be very closely approximated by polynomials. Whether the dose-response or its inverse is used for calibration depends on the suitability of a least squares fit to the data. The use of least squares regressions with large R^2 (Pearson coefficient of correlation) values largely removes the effects of nonlinearity of the material's dose-response.

The spectral sensitivity of a photosensitive material implies that its dose-response function is affected by the spectral irradiance distribution of the source. In some cases, a monochromatic calibration function determined by exposing a photosensitive material to a specific UV wavelength can be used to determine the calibration function for any other monochromatic wavelength. The monochromatic dose $H(\lambda)$ is given by

$$H(\lambda) = \frac{f(D)}{R(\lambda)} \tag{4.10}$$

(Diffey 1989, pp. 138-9) where $f(D)$ is the monochromatic calibration function and $R(\lambda)$ is the relative spectral response of the dosimeter material normalised to unity at some reference wavelength. For convenience, the wavelength used for normalisation is usually that which maximises the material's response, but other wavelengths may also be used (Diffey 1989, pp. 139-41; Abdel-Rehim, Ebrahim & Abdel-Fattah 1993).

Monochromatic calibrations however, are not well suited to measurements of polychromatic biologically effective exposure due to the nonlinearity of most action spectra. As mentioned in the previous section, a photosensitive material with a spectral response that is in close agreement with a given biological action spectrum makes a suitable candidate for a dosimeter material to quantify biologically effective dose for that response. Currently, the spectral responses of photosensitive materials only coarsely approximate biological action spectra. The discrepancy between

spectral response and action spectrum can be accounted for by the correction factor Q given by Davis, Deane & Diffey (1976) as

$$Q = \frac{\int_{\lambda_1}^{\lambda_2} P(\lambda) A(\lambda) d\lambda}{\int_{\lambda_1}^{\lambda_2} P(\lambda) R(\lambda) d\lambda} \tag{4.11}$$

where $P(\lambda)$ is the relative spectral irradiance of the source, $A(\lambda)$ is the action spectrum, and $R(\lambda)$ is the spectral response of the material. In equation 4.11, $P(\lambda)$, $A(\lambda)$, and $R(\lambda)$ are all normalised to the same reference wavelength. The biologically effective dose, H_{BE}, is then calculated by

$$H_{BE} = HQ \text{ (J m}^{-2}\text{)} \tag{4.12}$$

where H is the monochromatic dose administered at the reference wavelength λ_0 that would produce a response in the photosensitive material equivalent to that of the actual broadband dose. Calibration errors are further minimised by calibrating the material against a detector that is weighted for the same biological response that the material's spectral response resembles.

4.5 Dynamic Range

In general, the dynamic range is the range of exposures over which the cause and effect of a detector are related. The UV dose-capacity of a dosimeter is the largest dose that can be accurately measured, while the dose-threshold is the smallest dose that can be measured by a dosimeter. Typically a trade-off exists between dose-capacity and sensitivity. A high-sensitivity material exhibits a large change in response for a given UV radiation dose, but tends toward saturation more rapidly than a lower sensitivity material. The dynamic range is therefore calculated by subtracting the dose-threshold from the dose-capacity. In terms of the dose-response function (or its inverse), the dynamic range encompasses the segment of the curve between the dose-threshold and the region of optical saturation. The dynamic range

can be expressed relative to the dose-capacity as the relative dose range (RDR), given by

$$RDR = \frac{H_C - H_T}{H_C} \tag{4.13}$$

where H_C is the dose-capacity and H_T is the dose-threshold.

4.6 Angular Response

The angle of incidence of a large portion of solar UV irradiance incident at the surface of a detector is non-normal due to changing SZA and the random directions of photons comprising the diffuse component of global solar UV irradiance. An understanding of the angular response of dosimeter materials intended for measurements of solar UV radiation is therefore required. The response of an ideal detector to a collimated uniform irradiance source decreases in as the cosine of the angle of incidence of the beam. The cosine error is the deviation of the angular response of the detector from the cosine function. The cosine error is commonly expressed as the f_2 error,

$$f_2(\theta,\varphi) = \frac{S(\theta,\varphi)}{S(\theta=0,\varphi)\cos\theta} - 1 \tag{4.14}$$

where $S(\theta,\varphi)$ is the response of the detector, θ is the angle of incidence of the source irradiance and φ is the azimuth angle (Schreder, Blumthaler & Huber 1999).

4.7 Time-Irradiance Reciprocity

Radiation dose is directly proportional to irradiance. The conversion factor between these two quantities is time. An instrument that measures dose must therefore measure irradiance as well as time, such that the product of the two is linearly proportional to the measured dose. If a dosimeter material is to be used to measure dose in physical units, then the dose measured by means of the response of the material must also be proportional to the product of irradiance and time. This proportionality is known as the Bunsen-Roscoe law of reciprocity. In

photochemistry, this law requires that a radiation induced response due to a given dose is the same regardless of the exposure time and irradiance for primary reactions. The photochemical form of the Bunsen-Roscoe law is $It = \mathrm{C}$ where It is the exposure (product of irradiance and time) and C is a constant.

The review of reciprocity experiments by Martin, Chin & Nguyen (2003) indicates that the majority of biological responses obey reciprocity. Currently however, the dose-range over which reciprocity holds is unclear, and it has been suspected that biological responses may conform to reciprocity only within narrow dose-ranges. According to WHO (1997), biological responses are most likely the endpoints of secondary photobiological reactions to which reciprocity does not apply. Nonlinear biological responses resulting from very short exposures, and the action of repair mechanisms over long duration exposures contribute to deviations from reciprocity outside of a given dose-range (Sliney 2005).

4.8 Temperature Dependence

For the measurement of solar UV radiation by passive dosimetry techniques, the environmental conditions completely govern the temperature at which the detectors are deployed, and the temperature variations that occur during the exposure measurement. Although the temperature stability has been reported for only a small number of actinometer materials, the responses of the majority of these materials are independent of temperature (Kuhn, Braslavsky & Schmidt 2004). The kinetic mechanisms involved in photochemical responses are primarily photolytic. The photochemical quantum yield is usually temperature independent and thermal input does not usually contribute significantly (if at all) to the response of photosensitive materials (Moore & Zhou 1994).

This independence of response and temperature however, is not always the case. Jankowski *et al.* (2000) for example, developed UV actinometers based on the photolysis of nitrate and nitrite, and found a 3% error corresponding to a 2°C temperature change. The dependence of the response of an actinometer on temperature therefore requires quantification during its development such that the range of temperatures under which the actinometer can be deployed using a single

calibration can be established, and temperature correction coefficients determined for temperatures outside of this range.

4.9 Dark Reaction

Materials sensitive to UV radiation frequently have a slight post-exposure instability that results in changes in the materials response after UV radiation exposure has been terminated (Davis, Deane & Diffey 1976). Such post-exposure changes in response over time in the absence of radiation are collectively known as the dark reaction, although darkness is not required for these reactions to proceed. Since the dark reaction is based on chemical reactions within the actinometer material and not on photolysis, it is likely that the dark reaction will have at least some dependence on the temperature at which the actinometer is stored after exposure. If the actinometers are stored at a constant temperature after exposure, then the dark reaction can be quantified as functions of post-exposure time and temperature by

$$\Delta A_{Dk}\left(\lambda_{\mathrm{L}}, t_p, T_p\right) = A\left(\lambda_{\mathrm{L}}, t_p, T_p\right) - A\left(\lambda_{\mathrm{L}}, t_p = 0, T_p\right) \tag{4.15}$$

where $\Delta A_{Dk}(\lambda_{\mathrm{L}},t_p,T_p)$ is the change in absorbance induced by the dark reaction measured at the wavelength of λ_{L} after the material has been stored at a temperature of T_p for a time of t_p after the exposure. According to equation 4.15, an increase in absorbance due to the dark reaction results in a positive dark response. If the dark reaction is not in the same direction as the UV induced response, then it is necessary to consider both the sign of the dark reaction and the sign of the response.

4.10 Summary and Conclusions

The response of an actinometer may be quantified either directly or indirectly by means of optical absorbance. The absorption of UV radiation by solution type actinometers allows the quantum yield and the photolysis rate constant to be determined, which provides a measure of response to UV irradiance or exposure. The change in optical absorbance of film type actinometers provides a direct measure of UV exposure. The exposure sensitivity and spectral sensitivity of an UV detector are

superimposed to give a dose-response or calibration curve that depends on both the spectral response of the material and the spectral distribution of the source.

Calibration uncertainties arise from the discrepancies in spectral distribution between the calibration source and the UV source under measurement. This arises as a result of the dependence of both dose-response (equation 4.10) and the correction factor *Q* (equation 4.11) on the source spectrum. Solar radiation continually changes in dose-rate and spectral distribution due to the geometrical and atmospheric parameters discussed in the previous chapter. Further uncertainties therefore arise from deviations of the actinometer material's response from time-irradiance reciprocity and from the cosine response. Reciprocity errors may also be magnified by differences in reciprocity between an actinometer material and the UV induced biological response for which an actinometer material may be weighted. Due to the uncertainty of the dose ranges within which reciprocity holds for the various biological responses, such reciprocity related errors cannot currently be quantified. Given the effects of solar variation on the response of a detector, the most accurate calibrations for solar UV actinometry are achieved by minimising any differences between the calibration source and the UV source under measurement. For solar dose calibrations, this is most easily achieved by exposing both calibration and measurement actinometers to solar radiation simultaneously, and nearby a solar radiation monitoring instrument against which the actinometers are to be calibrated.

Chapter 5

Evaluation of Currently Available UV Dosimetry Methods

5.1 Introduction

5.2 Biodosimetry

5.3 Actinometry

5.4 Summary and Conclusions

5.1 Introduction

The first step in developing an actinometer suitable for large-dose UV measurements is to investigate and compare the dynamic ranges of currently available actinometer materials. Although the dynamic range is an important parameter for large-dose measurements, other optical properties relevant to the measurement of solar UV radiation must also be considered.

The various optical properties of dosimeter and actinometer materials are reviewed and compared in this chapter. As previously mentioned, biodosimetry is currently the leading technique for the measurement of large UV radiation doses. The objective of this research however, is to develop a cost-effective actinometer that can be analysed by optical equipment available in a standard physics laboratory. The optical properties of the dominating biodosimetric methods will therefore be considered, but only as a reference for developing an actinometer that may be competitive with biodosimeters for large-dose UV measurements.

The dynamic range is essentially meaningless unless it is considered in relation to the spectral response of the material. For example, if a material that is sensitive to only UVB wavelengths is exposed to a source of UVA irradiance, then the dynamic range is infinite since the material will never respond. Hence the dynamic range can be made arbitrarily large by exposing the material to wavelengths to which it does not respond. This presents a problem in comparing the dynamic ranges of materials that have been determined using different wavebands. In an attempt to overcome this difficulty, erythemally weighted exposures that are reported in the literature are converted to an approximate equivalent unweighted UVB dose according to McKenzie, Smale and Kotkamp (2004) by

$$\mathrm{UVB}_{280-315\mathrm{nm}} = 7.55\mathrm{UV}_{\mathrm{Ery}} \tag{5.1}$$

when the spectral response of the material is known to be weighted toward the UVB. An error of at least 10% applies to this conversion. In some cases, the spectral response of the material is unknown, or the spectral distribution of the irradiance source is not reported. In such cases, the dynamic range of the material cannot be directly compared with others.

5.2 Biodosimetry

Biodosimetry utilizes UV radiation induced biological damage to rudimentary biological materials. A large number of such materials have been employed for the quantification of solar UV exposure, either by suspending the material in a solution or immobilizing by fixing the material to a film or glass plate.

5.2.1 Vitamin D, Iodouracil, and DNA

Methods of biodosimetry have been developed employing provitamin-D (Terenetskaya 2003), iodouracil (Rahn & Lee 1998), and calf thymas DNA (Ishigaki *et al.* 1999). The maximum conceivable dose-capacity of the provitamin-D solution based method was 4.1 kJ m^{-2} for UVB exposure. Greater dose-capacities have been realised by the iodouracil solution and calf thymas DNA film type dosimeters, with estimated UVB dose-capacities of 30 kJ m^{-2} for iodouracil, and 40 kJ m^{-2} to 100 kJ m^{-2} for thymas DNA depending on the filter type employed. The dose-thresholds for these dosimeters have not been reported, and the optical properties have not been clearly characterised.

5.2.2 Bacillus Subtilis

One of the most common methods of biodosimetry utilises the common bacteria found in soil, *Bacillus subtilis*, in the form of film or plate type biodosimeters. These include DLR-biofilm (Institute of Aerospace Medicine, Cologne, Germany), and Viospor (BioSense, Bornheim, Germany). The sensitivity of *B. subtilis* films to UV radiation depends on the strain employed. DNA repair deficient strains have a higher sensitivity and are well suited to applications requiring a high resolution of dose (Rettburg & Cockell 2004). DLR-biofilm was used to quantify solar UV doses of up to about 28 MED or a UVB equivalent dose of about 42 kJ m^{-2} over a 24 hour period (Rettburg & Cockell 2004). The authors state that DLR-biofilms are suitable for both short-term exposure measurements of at least ten minutes and long-term measurements of two months at most. This implies an estimated dose-threshold and dose-capacity of about 5 J m^{-2} and 2.5 MJ m^{-2} respectively, or a RDR of almost

100%. The authors also state that DLR-biofilms conform to reciprocity and have an angular response that approximates the cosine response. The peak spectral sensitivity of DLR-biofilm was shown to be 270 nm with a close correspondence to the DNA damage action spectrum in the UVB waveband but deviates toward overestimation at longer wavelengths.

VioSpor biodosimeters are detailed by Quintern *et al.* (1992) and are also capable of large UV dose measurements (Moehrle & Garbe 2000). The dose-capacities of VioSpor extend from around 22.7 kJ m^{-2} to 680 kJ m^{-2} of UVB depending on the dosimeter type (BioSense n.d.). The BlueLine Viospor type-V dosimeter has the largest dose-capacity and has a dose-threshold of about 11 kJ m^{-2} providing an RDR of 98.3%. The UV radiation response of *B. subtilis* follows the law of reciprocity (Quintern *et al.* 1992) and corresponds closely to the erythemal action spectrum (Moehrle & Garbe 2000). According to the technical specifications, VioSpor has a reproducibility of 5% to 20% depending on dose, and has an absolute calibration uncertainty of ± 2.5 kJ m^{-2} (BioSense n.d.).

5.2.3 Uracil Thin Layer

RNA based uracil thin layer biodosimeters utilising polycrystalline layers of uracil have been developed (Gróf, Gáspár & Bérces 1994; Gáspár *et al.* 1995), and possess a large dynamic range. This dosimeter is capable of measuring UV radiation doses from about 50 to 400 MED using spectrophotometric post-exposure analysis (Gróf, Gáspár & Rontó 1996) or 75.5 kJ m^{-2} to about 604 kJ m^{-2} of equivalent UVB dose, giving this material a UVB dynamic range of 530 kJ m^{-2} or a RDR of 87.5%. The standard spectrophotometric and optical waveguide lightmode spectroscopy methods employed by Horváth *et al.* (2001) showed much lower dose-thresholds giving a RDR of better than 95%, but optical saturation reduced the dose-capacity to about 700 J m^{-2}.

5.3 Actinometry

UV actinometry involves a photosensitive non-biological material either suspended in solution or fixed to a translucent film or glass plate. The actinometer response is

usually obtained as a direct measurement of an optical or chemical property of the actinometer material that changes due to the photolytic action of UV radiation exposure.

5.3.1 Chemical Solution Actinometers

A number of chemical solution actinometers have been developed for UV radiation measurements. These include solutions of 2-nitrobenzaldehyde (Allen, Allen & Baertschi 2000) and 3,4-dimethoxynitrobenzene (Zhang, Esrom & Boyd 1999), benzophenone-benzhydrol (Rosenthal & Bercovici 1976), potassium iodide and iodate types (Rahn 1997; Rahn *et al.* 2003), sulfamethoxazol (Moore & Zhou 1994), and many others. The literature indicates that the expertise of a chemical technician is generally required for the preparations of these types of actinometers, and substantial labour and time is involved. Post-exposure analysis frequently requires determination of the quantum yield by HPLC analysis, although in some cases the response can be quantified by means of spectrophotometry. Furthermore, reaction vessels (usually quartz glass) are required which complicate the optical properties of the detector and adds to the cost of solution type actinometry.

Although a substantial amount of research has been published relating to the development of solution type actinometers, the chemical film types dominate solar exposure research. This is most likely due to the lower costs, labour, and equipment demands required for these methods compared to both biodosimetry and solution type actinometry.

5.3.2 Polysulphone Film

Polysulphone film is perhaps the most extensively employed UV-sensitive material employed for UV actinometry, and has been well characterised. The research by Diffey (1989 pp. 143-4) shows that the onset of optical saturation occurs after polysulphone receives a dose approximately equivalent to 7.5 kJ m^{-2} of UVB. In addition to declining dose resolution, the coefficient of variation (CV) increases rapidly with increasing exposure within the region of saturation. The CV is 10% for an UVB equivalent dose of about 11.3 kJ m^{-2}, and increases to around 30% at a dose

of 17 kJ m^{-2}. The effective UVB dose-capacity of polysulphone film is therefore about 11.3 kJ m^{-2} if measurement uncertainties are to remain within 10%. CIE (1992) states the dose-threshold and dose-capacity of polysulphone as 1 kJ m^{-2} and 11 kJ m^{-2} respectively, and hence a RDR of 91%.

Although the dynamic range of the polysulphone actinometer is relatively small, a number of optical properties of polysulphone film make it well suited for solar UV actinometry, particularly for erythemal exposure measurements. The erythemal action spectrum (figures 2.2 and 2.3) is approximated by the spectral sensitivity of polysulphone film (Diffey 1989, pp. 139-43) (figure 5.1). This type of actinometer is therefore highly utilised for the erythemal dose measurements required in dermotological research. Polysulphone also exhibits an angular response with small deviation from the cosine response (Krins *et al.* 2000), and reciprocity is obeyed over most of the dynamic range from 2.5 kJ m^{-2} to 10 kJ m^{-2} (Davis, Deane & Diffey 1976).

The main disadvantage of polysulphone film as an actinometer material is its inability to directly quantify doses larger than about 12 kJ m^{-2} due to its limited dynamic range. The dynamic range of polysulphone has been extended by means of a wire mesh foil used as a grey filter. A single foil filter increases the dose-threshold and dose-capacity to 5 kJ m^{-2} and 60 kJ m^{-2} respectively, while a double foil increases these to 25 kJ m^{-2} and 300 kJ m^{-2} (CIE 1992). Another composite system formulated by Parisi & Kimlin (2004) employs a black and white developed photographic film as a filter. The combined response of the polysulphone film and the filter then provide the UV dose via a suitable calibration. This method extended the dynamic range of polysulphone to a UVB equivalent dose of about 151 kJ m^{-2}. The addition of filters however, increases the costs and labour involved in the fabrication of these types of actinometers.

5.3.3 Dyed Polyvinyl Alcohol and Polyvinyl Butanol Films

A polyvinyl alcohol (PVA) film dyed with both hexahydroxyethyl pararosaniline cyanide dye (HPR-CN) and sandolan yellow N-3GL dye (SYN-3GL) was investigated for use in UVB actinometry by Abdel-Rehim, Ebrahim & Abdel-Fattah

(1993). The authors exposed the film to doses of up to 4 kJ m^{-2} of monochromatic UVB radiation to discern a cubic polynomial calibration function. No signs of saturation were evident within this dose range. Monochromatic exposures indicated a greater sensitivity of the film to UVB wavelengths, but also showed considerable response in the UVA compared to the erythemal action spectrum (figure 5.1). This actinometer material showed high sensitivity with a dose-threshold of around 260 J m^{-2}, and offers precision with a reproducibility of 3% including calibration. However, a deviation from reciprocity was seen to increase steadily from 5% for doses greater than 2 kJ m^{-2}. The PVA film provides superior exposure sensitivity and low dose-thresholds, but no evidence of dose measurements greater than 4 kJ m^{-2} was found in the literature. Given the general relationship between dose-threshold and dose-capacity, it may be expected that this film cannot support a large dose-capacity. The possibility exists however, of reducing the concentrations of HPR-CN and SYN-3GA in an attempt to reduce the sensitivity, and hence increase the dose-capacity of the PVA film.

Dyed chemical films have also been investigated by Ebraheem *et al.* (2000). These films were fabricated from PVA and polyvinyl butanol (PVB) and dyed with triphenyl tetrazolium chloroide (TTC). Monochromatic dose-response curves were obtained for both the PVA/TTC and PVB/TTC films at 492 nm and 366 nm, which indicated that both film types have nonlinear responses tending toward saturation with doses in excess of 16 kJ m^{-2} to 20 kJ m^{-2} of UVA exposure. The spectral sensitivity of the PVA/TTC film to wavelengths longer than 300 nm increases rapidly, while that of PVB/TTC steadily declines in this region (figure 5.1). Although greater in dynamic range compared to polysulphone, these films may present difficulties for solar dose measurements due to the large differences between their spectral responses and the common biological action spectra.

5.3.4 Photosensitised Polyvinyl Chloride Films

Photosensitive chemicals blended with polyvinyl chloride (PVC) have often been used in UV actinometry. Although PVC does respond to UV radiation, it is much more stable than the photosensitive chemical additive. The primary response is therefore presumed to be that of the chemical additive.

A dose-response function was established for a PVC film photosensitised with benoxaprofen (Diffey, Oliver & Davis 1982). This actinometer material provides a dose-capacity of about 80 kJ m^{-2} and an estimated dose-threshold of 2.9 kJ m^{-2} for 320 nm monochromatic irradiance (RDR = 96.3%). The authors also determined the spectral response over the solar UV waveband that shows a peak at 320 nm (figure 5.1). A close correspondence between the angular response of the film and the cosine function was shown, and reciprocity was demonstrated for a dose of 5 kJ m^{-2}. No post-exposure dark reaction was observed.

Other photosensitising agents used in PVC films include nalidixic acid (NA) (Tate, Diffey & Davis 1980; Gobbs & Young 1982), phenothiazine (Diffey *et al.* 1977), and 8-methoxypsoralen (8-MOP) (Diffey & Davis 1978). The broadband UV dose-capacities of these materials were investigated and compared by Parisi & Wong (1999). The given dose-capacities were 150 kJ m^{-2}, 100 kJ m^{-2}, and 400 kJ m^{-2} for NA, phenothiazine and 8-MOP respectively. The authors also determined the broadband UV dose-capacity of 150 kJ m^{-2} for polysulphone. The spectral responses of each actinometer material given by the aforementioned authors are confirmed and compared by Parisi, Wong & Moore (1997). Of these actinometers, NA provides the closest spectral response match to the erythemal action spectrum.

Dyed and photosensitised films have the advantage that the chemical additive concentration may be altered to achieve the optimum sensitivity for a given application. Some of the sensitised PVC films have broadband dose-capacities that are equal to, or up to 2.7 times greater than that of polysulphone. However, these dose-capacities are relatively small compared to the dose-capacity of poly(phenylene oxide) film discussed below.

5.3.5 Poly(Dimethyl Phenylene Oxide) Film

Davis, Deane & Diffey (1976) initially proposed poly(2,6-dimethyl-1,4-phenylene oxide) (PPO) as a material for use in UV actinometry. PPO film actinometers were tested for applications in building material weathering research by Berre and Lala (1989). The films were calibrated for very large broadband UV doses in excess of 15 MJ m^{-2} in the 295 nm to 385 nm waveband with no signs of saturation. The

broadband dose-threshold estimated from the lowest dose data point of the calibration by Berre & Lala (1989) was 410 kJ m^{-2} suggesting a RDR of 97.3%. The spectral response of PPO film has not been reported, and hence the dose-capacity cannot be estimated in terms of an equivalent UVB dose.

It may be reasonable to presume that the spectral response of PPO film is weighted toward the UVB due to the chemical structural similarities between PPO and polysulphone, and the fact that most polymers of this nature absorb more efficiently in the UVB waveband. In this case, the 15 MJ m^{-2} broadband UV dose-capacity of PPO film would be largely overestimated due to the contribution of radiation in the UVA waveband. The broadband UV dose-capacity of polysulphone as reported by Parisi and Wong (1999) is about twelve times greater than the UVB dose-capacity given by CIE (1992). Hence assuming a similar spectral response of PPO film to that of polysulphone, the UVB dose-capacity of PPO film may be roughly estimated as 1.4 MJ m^{-2}. Or from another perspective, if the broadband dose-capacity of PPO film were reduced by more than 95% due to the elimination of wavelengths that do not contribute to its response (regardless of its response), then the dynamic range of PPO film would remain competitive with that of Viospor.

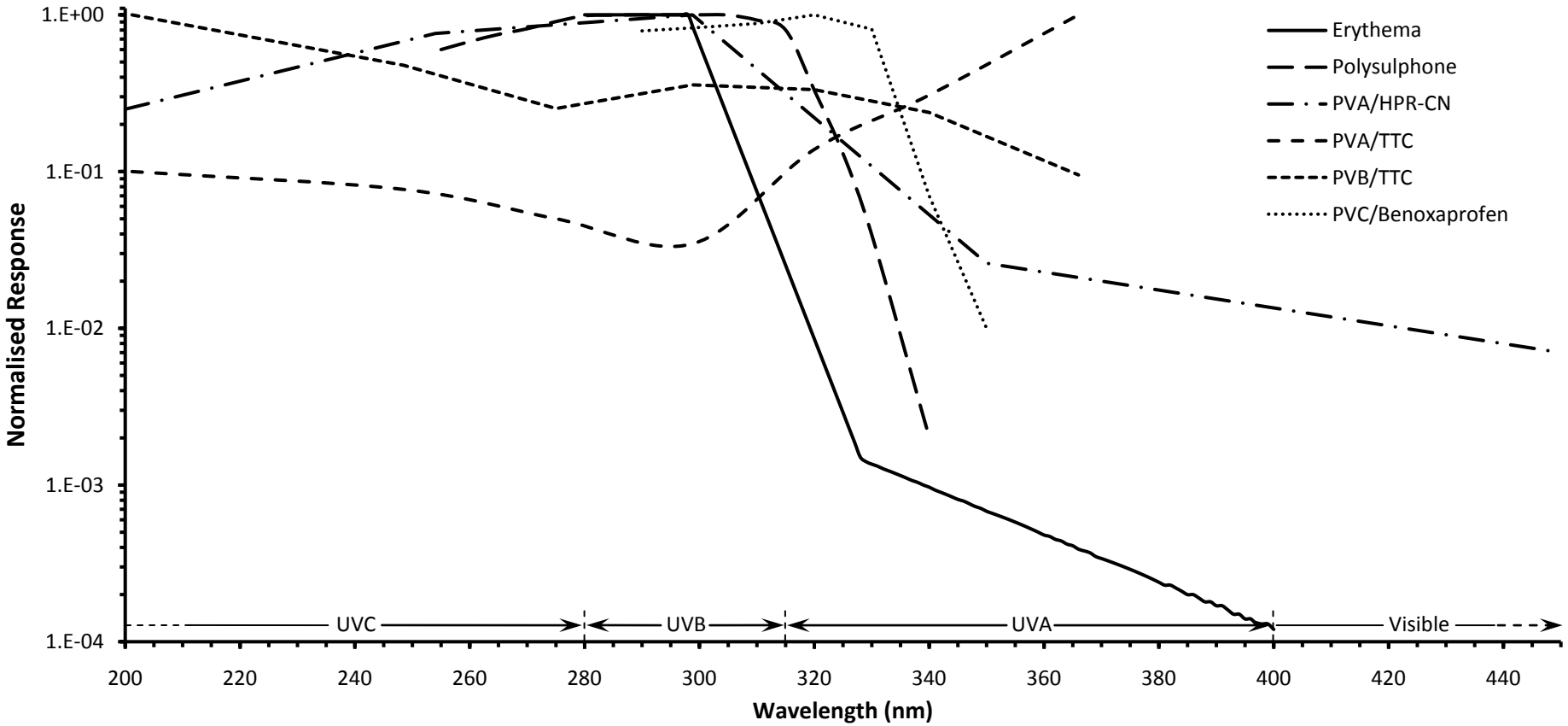

Figure 5.1: A comparison of the spectral responses of several of the actinometer materials reviewed in this chapter. These include polysulphone (Diffey 1989), PVA/HPR-CN (Abdel-Rehim, Ebrahim & Abded-Fattah 1993), PVA/TTC and PVB/TTC (Ebraheem *et al.* 2000), and PVC/benoxaprofen (Diffey, Oliver & Davis 1982). The erythemal action spectrum (CIE 1987) is included for reference.

5.4 Summary and Conclusions

Biodosimeters have the largest dynamic ranges available. The most impressive are those based on *B. Subtilis* with dose-capacities in excess of 680 kJ m^{-2} and RDRs of better than 98%. However, inspection of the materials and methods of biodosimetry presented in the literature indicates these techniques are labour intensive, time consuming, expensive, and often require specialised equipment.

A number of UV sensitive actinometric materials are available as an alternative to biodosimetry. Due to optical saturation, actinometer materials tend to be disadvantaged by their relatively small dynamic ranges compared to *B. Subtilis* based biodosimeters. The literature indicates however, that the most cost effective and most versatile method currently available for solar UV exposure quantification is chemical film actinometry.

In the literature, little attention has been given to the dynamic ranges of actinometer materials. The properties reported for the materials discussed above however, indicate some possibility of providing a larger dynamic range than polysulphone. This is achieved either through the intrinsic optical properties of the material, or through developing composite systems that incorporate either photosensitising agents external filters.

The chemical films that showed the greatest potential for large-dose measurements were photosensitised PVC films with 8-MOP having the largest reported broadband UV dose-capacity of 400 kJ m^{-2}. The chemical preparation of these films however, is more expensive and time consuming than the preparation of a pure film such as unfiltered polysulphone. The estimated broadband dose-capacity of PPO film was over 37 times greater than that of 8-MOP without additives or filters. Although a number of possibilities exist for developing an actinometer with a larger dynamic range, the literature suggests that the utilisation of PPO film as an actinometer material may be the most cost effective since no dyes, sensitising chemicals, or filters, are required. The initial research by Berre and Lala (1989) also suggests that PPO film may provide a dynamic range that is competitive with biodosimetry.

Although there may be more risk in pursuing PPO film as a large-dose actinometer due to the lack of published optical characteristics compared to some of the materials discussed in this chapter, the large dose-capacity of PPO film warrants further investigation. The pilot study in appendix A is used to assess the feasibility of further development of PPO film for large-dose solar exposure measurements. A return to this point and a re-evaluation of the materials may be required, depending on the outcome of the pilot study.

Chapter 6

Physical Development and Optical Characterisation of Poly(Dimethyl Phenylene Oxide) Film Actinometers

6.1 Introduction

In order to fulfil the objective of large UV dose quantification, a highly durable actinometer material is required that has the ability to absorb substantial amounts of solar UV radiation before saturating. The review of UV sensitive materials in chapter 5 indicates that PPO film may best meet this latter requirement. The pilot study (appendix A) also provides preliminary experimental evidence of the larger dynamic range of PPO film, as well as evidence of suitable optical properties for solar UV actinometry. The durability of PPO film however, has not been reported in the literature. Assessment of the long-term durability of PPO film was required before acknowledging PPO as a suitable chemical film.

For chemical film actinometers, the fundamental property of interest is the UV induced change in optical absorbance, which can be calibrated against a suitable instrument to provide a measure of UV radiation exposure. The optical properties of a given chemical film encompass the spectral dependence of the magnitude of the film's change in absorbance, and the behaviour of the absorbance change in relation to the UV radiation climate in which the film is deployed. The physical development and durability assessment of PPO film actinometers, and the characterisation of the optical properties relevant to solar UV radiation exposure quantification are presented in the following sections.

6.2 Equipment and Instrumentation

6.2.1 Casting Table

Sheets of PPO film were fabricated using a polymer film casting table (figure 6.1). The main components of the casting table are a highly polished glass plate (216 mm × 280 mm) and a stainless steel casting blade. The casting blade is driven across the length of the glass plate by an electric motor. The height of the casting blade is adjustable allowing the distance between the glass plate and the casting blade to be changed, accommodating for the casting of films of any desired thickness.

Figure 6.1: The polymer film casting table employed by physicists at the University of Southern Queensland for the fabrication of various chemical films for use in UV actinometry.

6.2.2 UV Radiation Sources

The primary sources of UV radiation employed in the optical characterisation experiments were artificial radiation generated by either xenon arc lamps or mercury lamps. Natural solar UV radiation at Toowoomba, Australia (27º33' S) was also used for solar radiation calibrations. An example solar UV spectrum is shown in figure 6.2(*d*).

A fluorescent UV lamp (model FS40/12, Philips, Lawrence and Hanson, Toowoomba, Australia) was used as a laboratory source for exposing large numbers of actinometers simultaneously. This lamp employs a 1.5 m, 38 mm diameter fluorescent tube. Although the spectral irradiance of this lamp has two peaks at 313 nm and 365 nm, the spectral irradiance between these maxima is broadly distributed with about 43% and 57% of the irradiance in the UVB and UVA wavebands respectively (figure 6.2(*a*)).

For experiments requiring collimated broadband irradiance, a solar UV simulator (model 15S, Solar Light Co., Philadelphia, USA) was employed. The irradiance source of the simulator was a 150 W xenon arc lamp. An output filtering system provides a spectrum that resembles that of the Sun. The simulator lamp was powered by the Solar Light XPS-200 stabilised power supply. The spectral irradiance of the solar UV simulator is shown in figure 6.2(*c*).

Monochromatic irradiance was provided by an irradiation monochromator (figure 6.3). This instrument is comprised of an air cooled LX/450-2 xenon arc lamp powered by a LPS255 HR universal arc lamp power supply, and a GM 252 single monochromator supplied by Spectral Energy, New Jersey, USA. Width adjustments of the monochromator input and output slits allow the bandwidth to be varied. The output irradiance is inversely related to the bandwidth. Several examples of the relative spectral distribution of different wavebands produced by the irradiation monochromator are shown in figure 6.2(*b*).

The time required for the artificial sources to stabilise after activation was estimated by determining the raw uncalibrated output of each source with a spectroradiometer (described in section 6.2.3) immediately after lamp start-up and then at three to five

minute intervals thereon. The time interval between the start-up measurement and the time at which an uncalibrated measurement of the given source was within 2% (corresponding to the estimated precision of the spectroradiometer) of the previous measurement was used for this estimate. The stabilisation time for the fluorescent UV lamp, solar UV simulator, and irradiation monochromator were estimated to be 12 minutes, 8 minutes, and 15 minutes respectively. These lamp stabilisation times were used for all experiments employing artificial radiation sources.

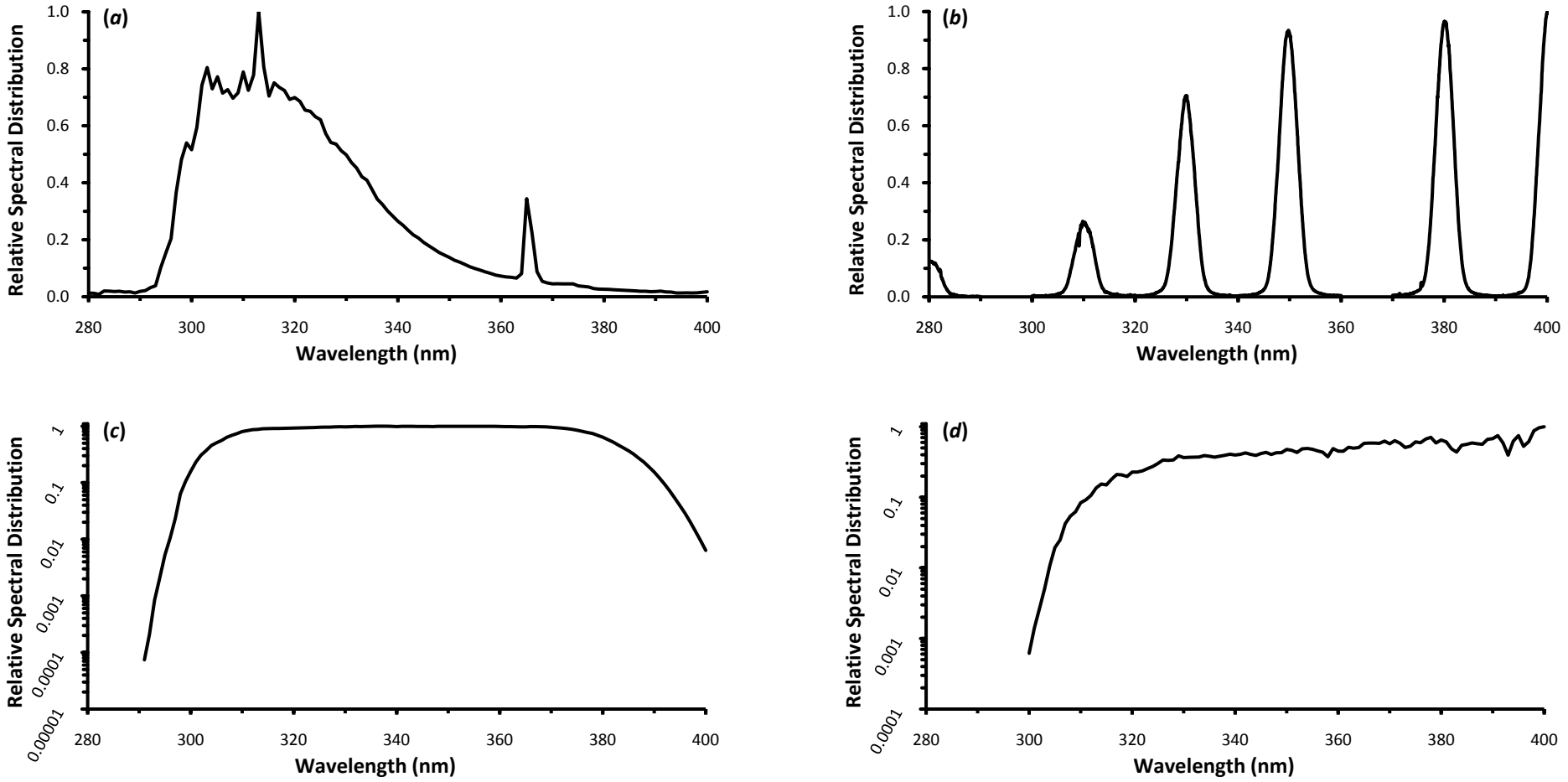

Figure 6.2: Relative spectral distributions of the fluorescent UV lamp (*a*), the irradiation monochromator at various UV wavebands of 4.4 nm FWHM bandwidth (*b*), the solar UV simulator (*c*), and natural solar UV radiation (*d*).

Figure 6.3: The irradiation monochromator at the University of Southern Queensland's physics laboratory. The lamp housing is seen toward the rear of the instrument and the monochromator is toward the front. A PPO film actinometer is held in front of the output aperture by a retort stand for irradiation with monochromatic UV.

6.2.3 Irradiance Measurements and Calculations

Several instruments were employed to determine the irradiance of the UV sources that were described in section 6.2.2. The primary instrument used for measurement of both natural and artificial sources of UV radiation was a scanning spectroradiometer. This instrument is comprised of a 15 cm diameter integrating-sphere (model OL IS640, Optronics Laboratories, Orlando, USA), a 1200 lines mm^{-1} double holographic grating monochromator (model DH10, Jobin Yvon Co., France) and a UV photomultiplier tube (model R212, Hamamatsu Co., Japan) temperature stabilised to 15.0 ± 0.5ºC. The spectroradiometer was calibrated for wavelength against the 365.0 nm mercury emission line of a mercury electric discharge lamp to within ± 0.1 nm, and against an air-cooled secondary standard quartz-tungsten halogen lamp for spectral irradiance. The secondary standard was powered by a Kenwood regulated power supply (model PD36 20AD) at a current of 9.500 ± 0.005 A, monitored by a calibrated MX 56 Metrix multimeter. The secondary standard irradiance is traceable to the National Standards Laboratory at the CSIRO, Lindfield, Australia. The precision of the spectroradiometer was estimated by analysing the raw data from six scans of the secondary standard. The integrated data varied by less than 2% between these scans. However, the accuracy of calibrated absolute spectral irradiance measurements is uncertain by an estimated 10%.

The spectral responsivity of the spectroradiometer was determined by performing a dark scan, and a secondary standard scan over the desired waveband using the wavelength increment $d\lambda$. The integrating-sphere and monochromator were maintained in complete darkness during the dark scans. The spectral responsivity $R(\lambda)$ was calculated over the waveband of interest by

$$R(\lambda) = \frac{S_C(\lambda)}{S_S(\lambda) - dk} \tag{6.1}$$

where $S_C(\lambda)$ is the spectral irradiance of the secondary standard as determined by the National Standards Laboratory, and $S_S(\lambda)$ is the spectroradiometer reading of the secondary standard over the waveband of interest. The dark response determined by the dark scans was independent of wavelength. The mean dark response *dk* over all wavelengths was therefore used in calculating the spectral responsivity.

The spectral irradiance above the dark response was calculated by

$$I(\lambda) = R(\lambda)\left[S_{SC}(\lambda) - dk\right] \text{ (W m}^{-2}\text{ nm}^{-1}\text{)} \tag{6.2}$$

where $S_{SC}(\lambda)$ is the spectroradiometer reading of the irradiance source under measurement. The irradiance I was then calculated by

$$I = \int_{\lambda_1}^{\lambda_2} I(\lambda) d\lambda \text{ (W m}^{-2}\text{)} \tag{6.3}$$

where λ_1 and λ_2 are the short and long wavelength limits respectively of the waveband of interest, and $I(\lambda)$ is the measured spectral irradiance. The values of λ_1 and λ_2 were set to 280 nm and 400 nm respectively, and a $d\lambda$ of 1.0 nm was used in the measurement of all radiation sources except for the irradiation monochromator. In this case, the irradiation monochromator output wavelength of interest was selected, and λ_1 and λ_2 were set to 10 nm below and 10 nm above this wavelength respectively. Due to the small full width half maximum (FWHM) of the irradiation monochromator, accurate irradiance calculations required a $d\lambda$ of 0.1 nm.

Irradiances from the fluorescent UV lamp were filtered by cellulose acetate (CA) to remove the small but significant UVC content of the spectrum, since this waveband is irrelevant to ground level solar irradiance. Due to the decrease in transmission of CA with increasing UV dose, the CA filter was replaced every 8 h for all exposures. The average transmission $T(\lambda)$ of the CA filter for an 8 h exposure (figure 6.4) was determined, and all spectral irradiance measurements of the fluorescent UV lamp were weighted by $T(\lambda)$ by

$$I_{Fl} = \int_{\lambda_1}^{\lambda_2} I_{Fl}(\lambda) T(\lambda) d\lambda \tag{6.4}$$

where I_{Fl} is the irradiance of the fluorescent UV lamp after correction for CA filtering, and $I_{Fl}(\lambda)$ is the spectral irradiance of the lamp.

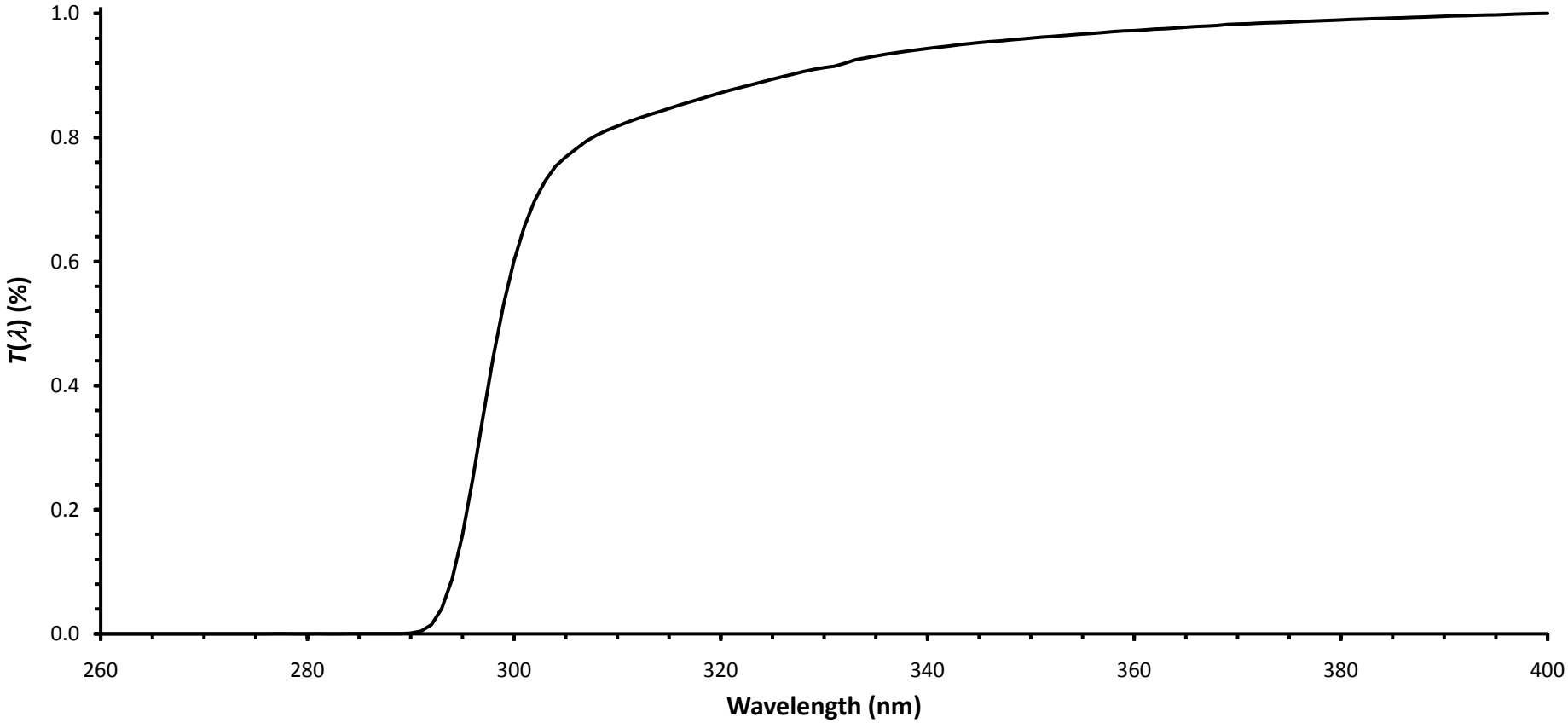

Figure 6.4: Average relative transmission spectrum $T(\lambda)$ of cellulose acetate film for an 8 h broadband exposure (272 kJ m^{-2}) to the fluorescent UV lamp.

UV dose is a function of the irradiance incident on the exposed surface and the duration of the exposure. Since the artificial UV radiation sources used in this research are constant, the doses from these sources were calculated by

$$H = It \text{ (J m}^{-2}\text{)} \tag{6.5}$$

where I is the irradiance of the source calculated by equation 6.3 or 6.4 and t is the exposure time. Due to the continual variation of natural solar radiation, solar UV irradiance was measured at regular time intervals. The solar UV dose was then calculated by

$$H = \int_0^T \int_{\lambda_1}^{\lambda_2} I(\lambda) d\lambda dt \text{ (J m}^{-2}\text{)} \tag{6.6}$$

where T is the duration of the total exposure and dt is the length of each exposure time interval. The biologically effective dose was calculated by weighting $I(\lambda)$ (equation 6.2) against the action spectrum for the biological response of interest according to equation 2.2.

A portable radiometer/photometer (model IL1400A, International Light Technologies, Massachusetts) employing a SEL400 20.5 mm diameter vacuum photodiode detector with a bandpass UV filter was operated in signal mode was also used to monitor the output irradiance of the artificial radiation sources. The manufacturer specified uncertainty of this instrument is 6% at best for radiometric measurements. The small dimensions of the SEL400 detector allowed the lamp irradiances to be checked during experiments involving the fluorescent UV lamp, and between the sequential exposures of actinometers involving the collimated sources.

An outdoor erythemal meter (model 501, UV-biometer, Solar Light Co., Philadelphia, USA) was also used to monitor solar UV exposure. The 501 UV-biometer is comprised of a quartz-glass dome covering a green glass and phosphor filter. Situated below the filter is a gallium-arsenide diode photodetector. The system is temperature stabilised (± 0.2ºC), and has a response that approximates the CIE

erythemal action spectrum (CIE 1992). This instrument is regularly calibrated against the scanning spectroradiometer, and thus has an estimated uncertainty of 10% at best. The UV-biometer data is integrated over 300 second intervals and recorded in units of MED as defined for type I skin. The spectral sensitivity of the UV-biometer is shown in figure 6.5.

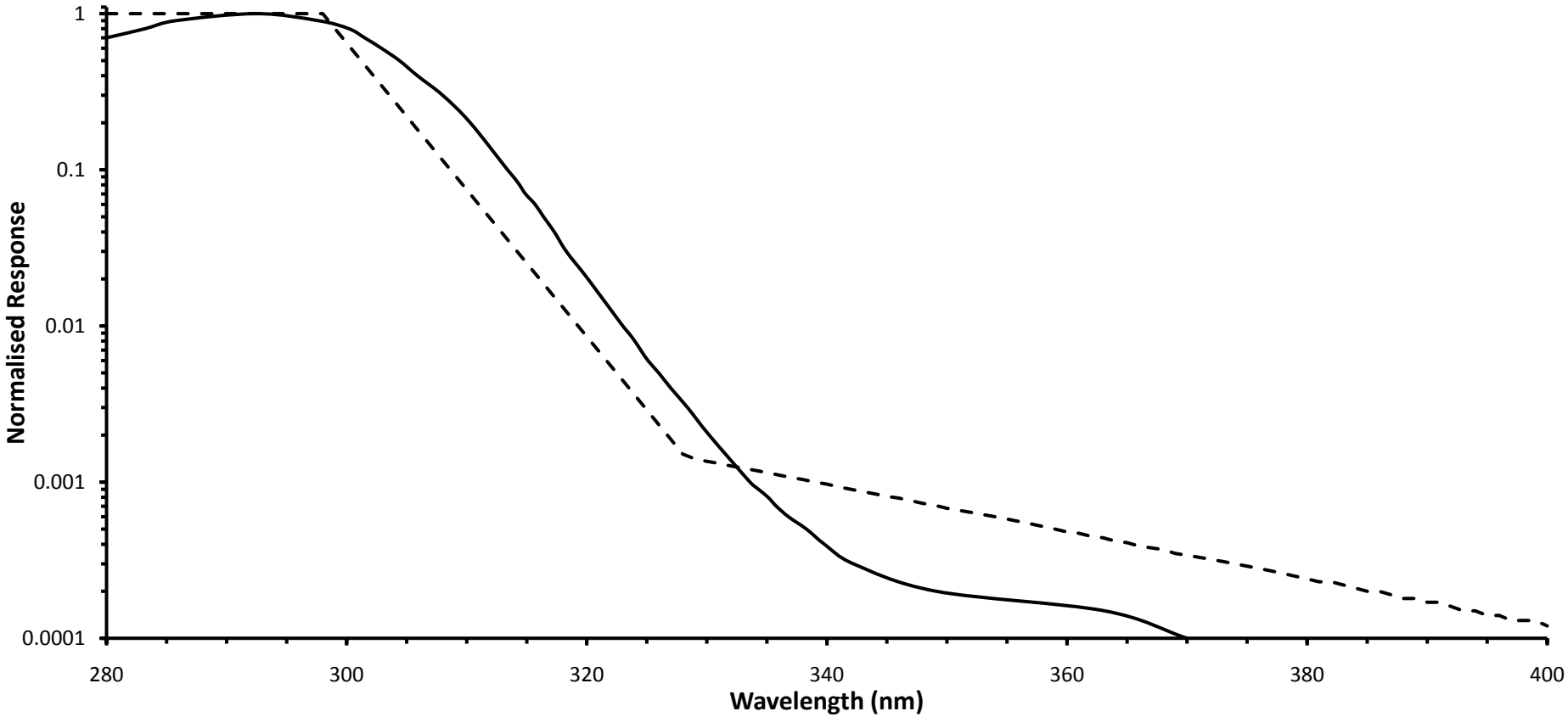

Figure 6.5: Spectral sensitivity of the Solar Light 501 UV-biometer (solid curve) normalised to the maximum sensitivity at 293 nm compared to the CIE erythemal action spectrum (dashed line) (CIE 1987).

6.2.4 Optical Absorbance Measurements and Calculations

Initially the effects of temperature and dark reaction on the response of PPO film were unknown. In order to minimise any such effects, the exposures were undertaken at a constant temperature, and the absorbance measurements were made within a short time after the exposure. The UV-1601 Shimadzu spectrophotometer was employed for optical absorbance measurements of PPO film. The manufacturer specified uncertainty of this instrument for absorbance measurements is ± 0.002. The preliminary adoption of the wavelength of 340 nm for λ_L according to Berre & Lala (1989) allowed equation 4.4 to be employed to determine the UV induced change in absorbance. Absorbance spectra were obtained by measurements of absorbance at 1 nm increments from 290 nm to 400 nm employing the scanning capability of the spectrophotometer. Change-in-absorbance spectra, or response spectra, were investigated by means of equation 4.5.

Possible effects of dust or small film defects were minimised by measuring the absorbance at four different orthogonal orientations of the spectrophotometer beam with respect to the film surface and averaging these measurements. The spectrophotometer beam orientations were identical for measurements of both $A(H = 0,\lambda_L)$ and $A(H,\lambda_L)$, eliminating the effects of unquantified variations in irradiance across the beam of the collimated sources used in the investigations of the film's optical properties.

6.3 Physical Development and Actinometer Fabrication

6.3.1 General Development Procedure

PPO actinometer films were fabricated by dissolving PPO powder in chloroform ($CHCl_3$) and applying the solution to the polymer casting table. The casting blade spreads the solution into a thin uniform layer over the glass plate, from which the chloroform evaporates leaving a thin film of PPO. Films of various thicknesses were cast by adjusting the distance between the glass plate and the casting blade. A feeler

gauge was used to ensure the distance between the glass plate and blade was uniform across the width of the glass plate. The films were separated from the glass plate by the surface tension of distilled water that was sprayed over the edges of the film. The newly manufactured PPO film was found to contract over a period of 12 hours to 18 hours after casting. The films were therefore stored in a darkroom for a period of at least 24 hours after casting to allow for physical stabilisation before use. Sheets of PPO film of sufficient quality and durability were then cut to size to cover the 12 mm × 16 mm apertures of 30 mm × 30 mm square PVC frames to form the PPO film actinometers (figure 6.5).

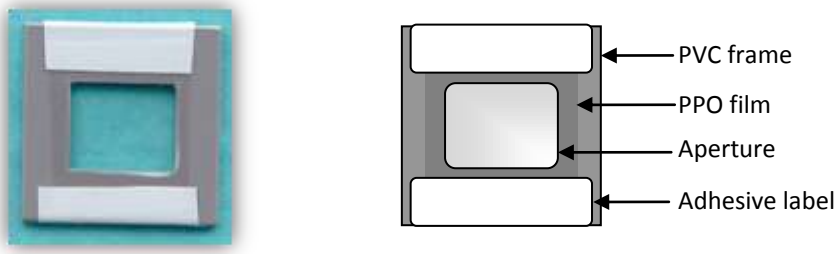

Figure 6.6: An actual size PPO film actinometer displayed on a blue background (left) and the PPO film actinometer schematic (right).

6.3.2 PPO Film Quality and Durability

The quality of PPO film was investigated before exposure to UV radiation, and its durability was investigated both before and after exposure. The quality of the films was assessed subjectively in terms of visual transparency and surface blemishes, which were determined through visual inspection. Observing the ease at which tearing and fractures occurred during removal of the film from the casting table was used to assess pre-exposure durability. The ability of dosimeters to withstand outdoor environmental forces, and the normal handling required for post-exposure analysis after a near-saturation exposure without sustaining damage was used as an indicator of sufficient post-exposure durability. The PPO dry mass to chloroform volume ratio

(mixing ratio), film thickness, and chloroform evaporation rate were found to affect the quality and durability of the film.

Film Thickness

PPO films of acceptable quality and pre-exposure durability could be cast at thicknesses of up to 60 μm using a mixing ratio of 0.12. Film thicknesses greater than 60 μm were brittle and could not be removed from the casting table. Although the 60 μm films did endure UV radiation exposures up to the saturation exposure (section 6.4.1), their post-exposure durability was dubious. These films became brittle and fragile well before the saturation exposure was reached, and were very easily damaged during the post-exposure analysis.

Mixing Ratio and Chloroform Evaporation Rate

High quality films with acceptable pre-exposure durability could be cast in the range of $0.06 \leq$ mixing ratio ≤ 0.32, where the mixing ratio is defined as the mass of dry PPO powder to the volume of chloroform used in the PPO solution for casting. Due to the very low viscosity and the large solidification time required for films cast using mixing ratios of less than 0.06, adjusting the distance between the casting blade and the glass plate did not control the film thickness. Such ratios resulted in poor quality films of non-uniform thickness. Mixing ratios greater than 0.36 resulted in saturation of the chloroform and failure of the PPO powder to completely dissolve. The high viscosity and rapid solidification of films cast at mixing ratios greater than 0.32 also resulted in very poor quality films. The best casting results were achieved for mixing ratios of around 0.13, near the midpoint of the range. In order to decrease the time required for the PPO powder to dissolve, the mixing ratio was systematically decreased from 0.32 until visible decreases in film quality and/or pre-exposure durability were observed. No difference was observed in these properties until a mixing ratio of less than 0.12 was used. The effect of mixing ratio on the UV dose-response function of PPO film was found to be negligible (section 6.4.1). All subsequent PPO films were therefore cast using a mixing ratio of 0.12, providing the shortest dissolution time and a suitable solidification time.

The evaporation rate of the solvent from solution during casting is known to have an effect on the surface properties of polymer films. The fume hood in which the casting was done was not temperature stabilised, resulting in different evaporation rates depending on the ambient temperature of the laboratory. Casting at temperatures above about 25°C resulted in a rippled or frosted appearance of the film causing low visible transparency. The casting table enclosure was partially covered to prevent condensation from the walls of the fume hood dripping onto the casting table. During the summer months, this also served to reduce the chloroform evaporation rate allowing high quality PPO films to be cast at temperatures greater than 25°C.

6.3.3 Film Thickness Measurements

The distance between the casting-blade and the glass plate were altered to provide different film thicknesses of 15 μm, 20 μm, 40 μm, 50 μm and 60 μm. The mixing ratio was 0.12 for all film thicknesses other than the 15 μm film, which required a mixing ratio of 0.06.

The thicknesses of the PPO films were measured by means of optical wedge interferometry (appendix B). An optical wedge was formed by two optically flat glass plates (50 mm × 60 mm × 10 mm) stacked horizontally with one edge in contact and a sliver of PPO film between the edges at the opposite end to form an air wedge between the glass plates (figure B-1). The glass plates were then mounted on a travelling microscope in order to view the interference pattern created by the wedge. A sodium lamp was mounted above the eyepiece of the travelling microscope to illuminate the wedge with monochromatic radiation of 589 nm.

The lamp was mounted such that the radiation was normally incident on the upper surface of the glass plate. Due to constructive and destructive interference between radiation reflected from the lower surface of the upper glass plate and the upper surface of the lower glass plate, bright and dark fringes parallel to the contacting edges were observed through the travelling microscope. The number of fringes per unit length of the wedge was used in conjunction with the wedge geometry to calculate the film thickness. The theory behind this technique is given in appendix B.

The accuracy and precision of the optical wedge were assessed by employing the wedge to measure the thickness of 20 μm, 30 μm, 40 μm and 50 μm feeler gauges. The gauges were measured five times in random order. The data are provided in table 6.1. Errors of up to 16.6% were encountered for individual measurements. However, the mean of five measurements was within 5.3% of the specified feeler gauge leaf thickness. This indicates that multiple measurements of a given PPO film sample using the optical wedge will be required to provide film thickness measurements with a reproducibility of better than 6%.

Table 6.1: Results of the feeler gauge leaf thickness measurements made using the optical wedge interference technique to test the accuracy of PPO film thickness measurements using this method.

Sample	Leaf Thickness (μm)			
	20	**30**	**40**	**50**
1	17.79	33.44	42.67	49.49
2	19.36	31.31	40.46	47.78
3	23.31	32.93	37.56	48.98
4	21.47	27.52	41.99	53.49
5	22.89	32.71	38.34	49.18
Mean (μm)	**20.96**	**31.58**	**40.20**	**49.78**
Std Dev (μm)	**2.35**	**2.40**	**2.22**	**2.17**
Error (%)	**4.28**	**5.27**	**0.510**	**0.432**

6.4 Optical Characterisation of PPO Film Actinometers

6.4.1 Effects of Mixing Ratio and Film Thickness on Dose-Response

Mixing Ratio

The effects of mixing ratio and film thickness on dose-response functions are investigated in this section. Any changes in the dose-response function due to mixing ratio or to film thickness will be used to optimise the dynamic range and dose-threshold of the actinometer.

The effect of different mixing ratios was investigated by casting two films of 20 μm thickness with different mixing ratios of 0.06 and 0.12. Two batches of five actinometers were fabricated from these films and the pre-exposure optical density was measured. As mentioned earlier, λ_L has yet to be optimised, and hence $\lambda_L = 340$ nm is used for the spectrophotometer lamp wavelength for this experiment.

The actinometer batches were centred both lengthwise and breadthwise below the fluorescent UV lamp in an array of five by two rows (15 cm × 6 cm) parallel to the fluorescent tube. The actinometers were suspended below the lamp at a distance of 6 cm from the tube. In this configuration, irradiance variations related to the lengthwise geometry of the lamp were avoided since any given actinometer was at least 67.5 cm from either end of the lamp. The spectrum of the fluorescent UV lamp has a small component of UVC radiation. In order to keep the irradiance waveband consistent with solar UV radiation, the actinometers were placed under a layer of CA to remove the UVC wavelengths from the spectrum. After the stabilisation period of the fluorescent UV lamp and prior to exposure of the actinometers, the lamp output was measured with the scanning spectroradiometer. Equations 6.1 to 6.5 were used to calculate the UV radiation dose from the lamp. The actinometers were removed from exposure for measurement of $\Delta A(340\text{ nm})$ with the spectrophotometer at various exposure time intervals. The lamp output was also remeasured with the IL1400A

radiometer at these intervals. After scanning, the actinometers were immediately returned to exposure under the fluorescent UV lamp. In order to minimise possible effects of spatial irradiance variations due to lamp geometry or centering of the actinometers under the lamp, the position of each actinometer in the array was randomised after each interval. The exposure time intervals ranged from 30 minutes to 8 hours. As indicated by the pilot study (appendix A), the rate of change in optical density decreases with increasing UV dose. The time intervals were therefore slowly increased during the course of the experiment. The optical absorbance of cellulose acetate increases slowly with UV radiation exposure, and was therefore replaced after each 8 hours of exposure. The exposure was continued until the films began to disintegrate. The maximum variation in lamp irradiance measured at the various time intervals by the IL1400A during the exposure was less than 4% and was within the uncertainty of the radiometer.

Figure 6.6 shows the dose-response curves for the two films produced using the different mixing ratios of 0.06 and 0.12. The response difference falls within the estimated experimental error of 6% for all doses greater than 100 kJ m^{-2}, but is always positive indicating a slightly higher sensitivity for the lower mixing ratio film. The difference however, may also be due to a slight difference in thickness between the two films. The shape of the dose-response curves for both mixing ratios is essentially the same.

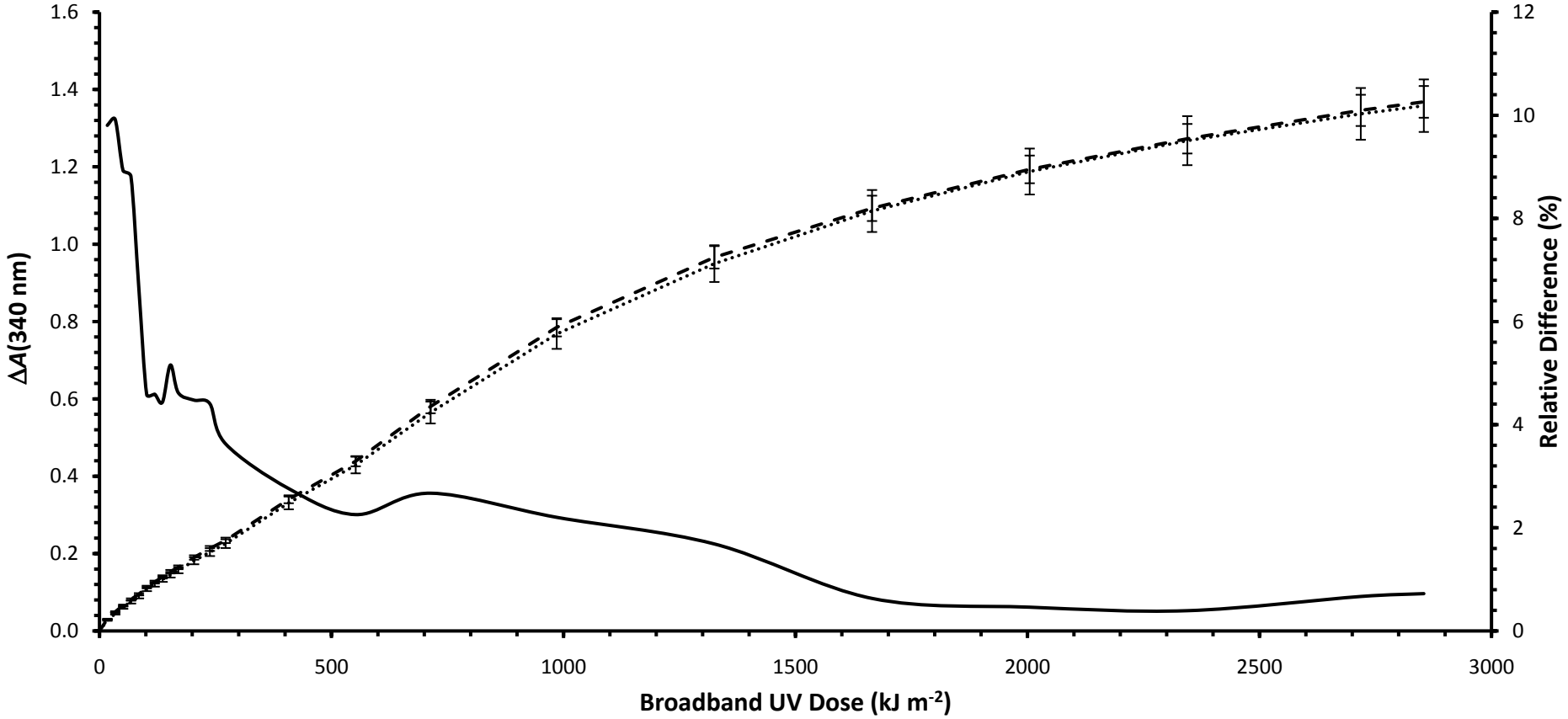

Figure 6.7: Dose-response comparison for 20 μm PPO film cast using mixing ratios of 0.06 (dashed curve) and 0.12 (dotted curve). The relative difference between the responses at the two mixing ratios is given by the solid curve (right axis). The error bars represent an estimated 6% error in the response due to film thickness variations, timing errors, and lamp alignment errors.

Film Thickness

As indicated by the pilot study in appendix A, the $\Delta A(\lambda)$ spectrum differs significantly for different film thicknesses. It may therefore be possible to optimise the dynamic range of PPO film actinometers by altering the film thickness. Investigations of the effects of film thickness on dose-response were conducted by the exposure of batches of five actinometers fabricated from PPO films cast at thicknesses of 15 μm, 20 μm, 40 μm, 50 μm, and 60 μm. The exposure source and time interval regime were the same as for the mixing ratio experiment described in the previous section. The IL1400A radiometer measurements after the stabilisation period and after the maximum exposure period of each film thickness showed a variation of about 6%. The UV induced ΔA(340 nm) responses for each film thickness are plotted in figure 6.7.

The dose-responses of the 15 μm and 20 μm films are approximately linear up to a dose of about 1 MJ m^{-2}, whereas the thicker films increase as a power of dose in this range. The slopes of the dose-response curves are very similar for doses larger than about 2 MJ m^{-2}, indicating that all films approach optical saturation at approximately the same rate. These observations indicate that the actinometer's sensitivity, and hence dose-threshold, can be improved substantially without significantly affecting the dose-capacity by employing thicker PPO films. The relative difference between the response of 15 μm and 60 μm films after an exposure of 17 kJ m^{-2}, for example, is 93.8%.

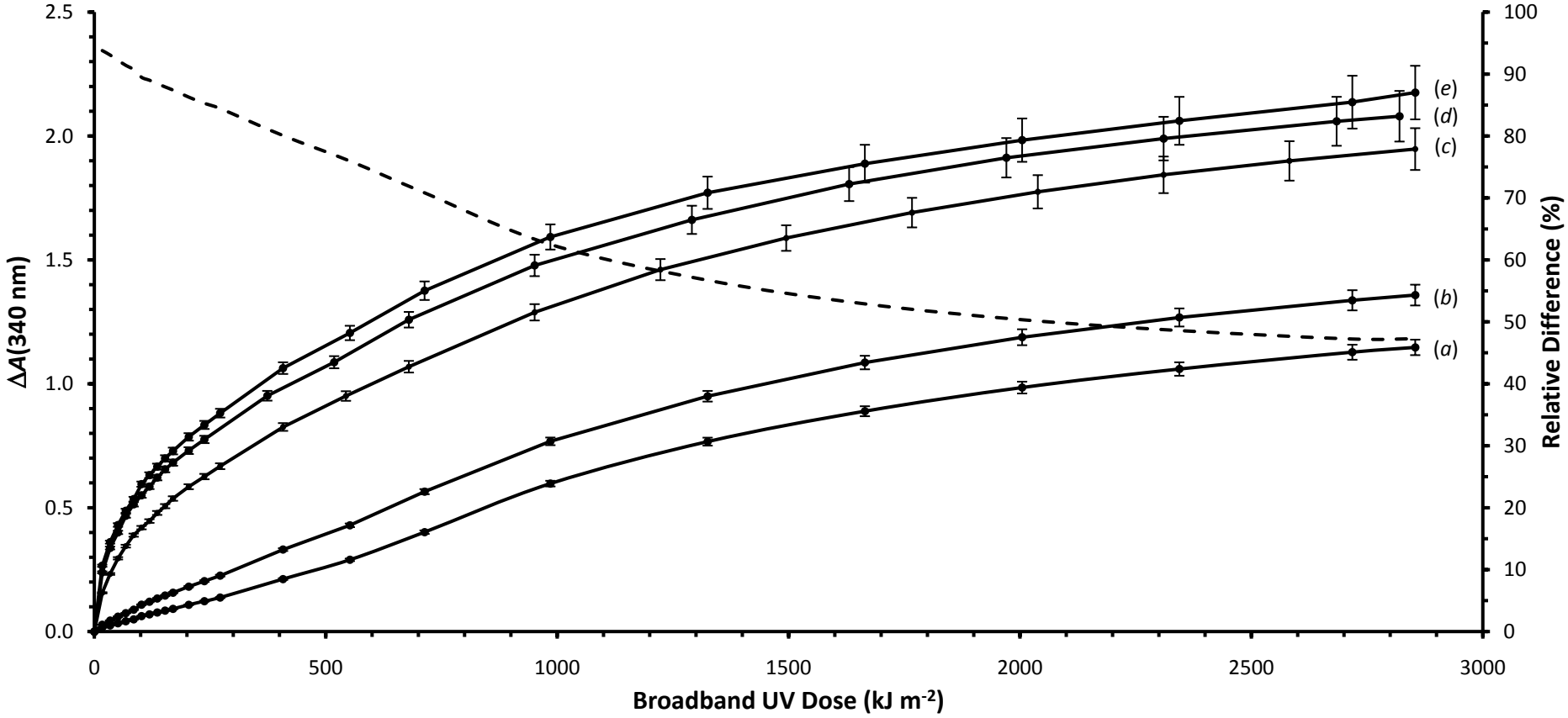

Figure 6.8: Dose-response curves (left axis) resulting from the broadband UV exposure of PPO films of thicknesses 15 μm (*a*), 20 μm (*b*), 40 μm (*c*), 50 μm (*d*) and 60 μm (*e*). The dashed curve represents the relative difference between the ΔA(340 nm) of 15 μm and 60 μm films (right axis). The error bars represent an estimated 6% error in the response due to film thickness variations, timing errors, and lamp alignment errors.

Returning to the subject of durability (section 6.3.2), this film thickness experiment indicated that 60 μm films became brittle after large exposures and are not sufficiently durable for use as large-dose actinometer films. Films cast at 50 μm could be used for indoor measurements of artificial UV sources, but are unlikely to withstand inclement outdoor conditions and are therefore not considered suitable for large exposure measurements of solar UV radiation. However, 40 μm films were demonstrably robust and are unlikely to be damaged even in severe outdoor conditions. The casting of PPO films of 40 μm using a mixing ratio of 0.12 is therefore adopted as the casting method for actinometer films.

6.4.2 Spectrophotometer Measurement Wavelength

The optical absorbance spectra of PPO film were obtained for films exposed to a wide range of UV doses in order to determine the spectrophotometer lamp wavelength λ_L at which the UV induced response measurement is maximised. λ_L was investigated by exposing a batch of five film samples to broadband UV radiation from the fluorescent UV lamp. Broadband exposure was used since the spectral response of PPO film has yet to be determined. The response spectrum given by equation 4.5 was determined at five different time intervals ranging from 0.5 h to 68 h during the exposure, corresponding to UV doses of 17 kJ m^{-2}, 272 kJ m^{-2}, 544 kJ m^{-2}, 1223 kJ m^{-2} and 2310 kJ m^{-2}. The mean $\Delta A(\lambda)$ of the batch was determined after each of the exposure periods. Figure 6.8 shows an increase in the absorbance spectrum with increasing dose. A wavelength dependent monotonic increase in $\Delta A(\lambda)$ is observed in the $320 \leq \lambda \leq 400$ nm range. At shorter wavelengths a local maximum occurs between 302 nm and 307 nm depending on the dose. These features shifted to slightly longer wavelengths with increasing UV exposure.

The $\Delta A(\lambda)$ drops rapidly to zero on the short wavelength side of this maximum almost independently of dose and λ, as seen in figure 6.8. The greatest $\Delta A(\lambda)$ at wavelengths longer than the short wavelength maximum was observed at approximately 320 nm. Compared to the region of the short wavelength maximum, the 320 nm point on the spectrum does not shift significantly with dose. The maximum exposure sensitivity providing stable $\Delta A(\lambda)$ measurements for doses of up

to 2.31 MJ m^{-2} is therefore achieved by adopting a spectrophotometer lamp wavelength of λ_L = 320 nm. The results shown in figure 6.8 were obtained for a film thickness of 40 μm.

Reanalysis of the film thickness data from section 6.4.1 using λ_L = 320 nm for absorbance measurements showed a dose dependent improvement in response measurement sensitivity in 40 μm, 50 μm and 60 μm films. These improvements ranged from 2.1% to 6.8% for a dose of 17 kJ m^{-2}, and increased with dose to 11.2% to 12.6% at 2.9 MJ m^{-2}, with the thicker films contributing more to this improvement. Due to the improvement in the sensitivity of response measurements, all subsequent measurements of optical absorbance used in this work are made at the spectrophotometer lamp wavelength of λ_L = 320 nm.

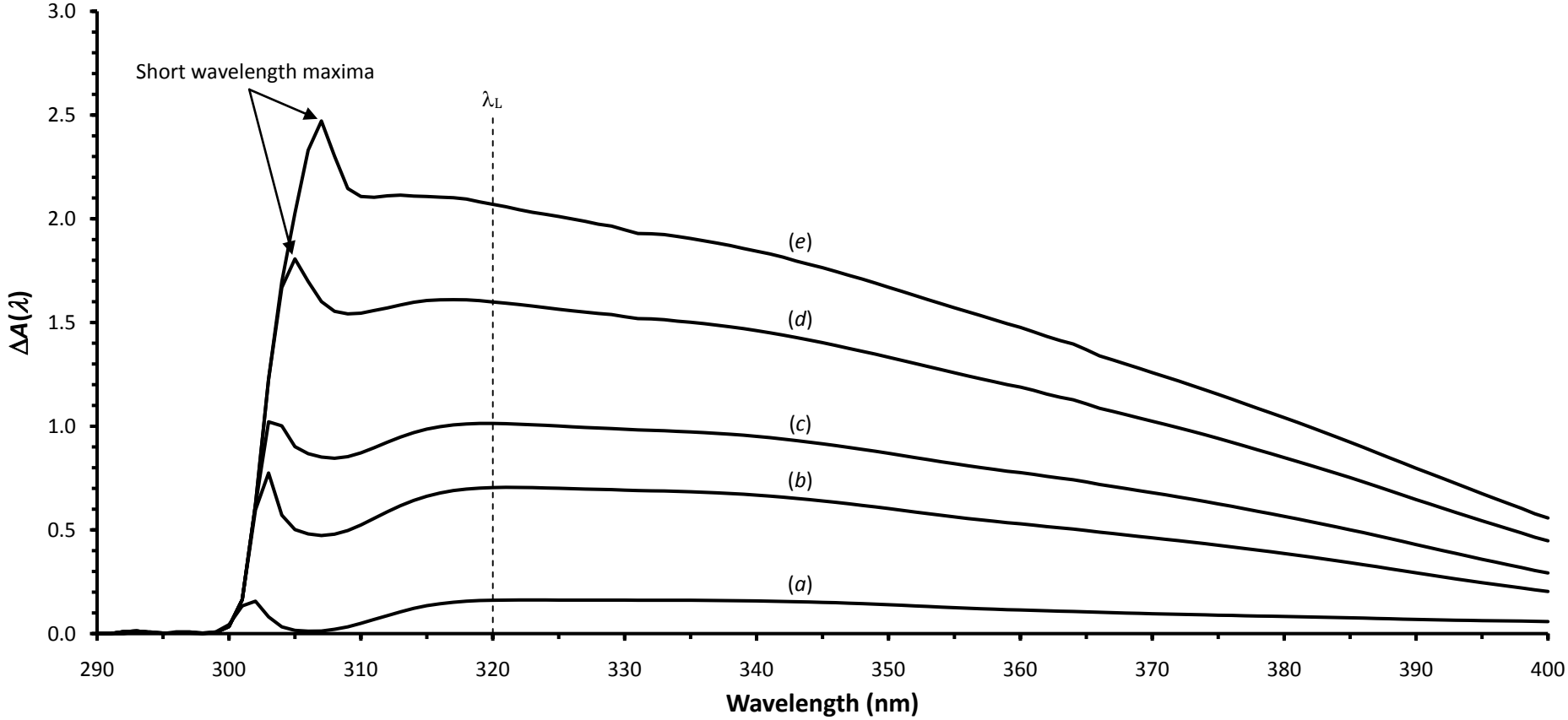

Figure 6.9: Optical absorbance spectra of 40 μm PPO film samples after exposure to broadband UV doses of 17 kJ m^{-2} (*a*), 272 kJ m^{-2} (*b*), 544 kJ m^{-2} (*c*), 1223 kJ m^{-2} (*d*), and 2310 kJ m^{-2} (*e*).

6.4.3 Effect of Spectrophotometer Beam

The spectrophotometer lamp wavelength that maximises the sensitivity of the response measurements lies within the waveband to which the PPO film is sensitive. It is therefore necessary to quantify any effects of the spectrophotometer beam on optical absorbance of PPO film.

The absorbance of an unexposed PPO film actinometer was measured ten times repeatedly at the same film location at the spectrophotometer beam wavelength of λ_L = 320 nm. This was repeated for a total of fifteen actinometers. The ten measurements served to provide the film with a dose from the spectrophotometer beam of five times that required for analysis. The mean optical absorbance of the fifteen actinometers was determined before a further set of ten measurements (μ_1) and again after the last set of ten (μ_{10}). This experiment was repeated for unexposed 40 μm PPO film samples, and films that had received a UV dose of 1.22 MJ m^{-2}. For all films, the alternate hypothesis $\mu_{10} > \mu_1$ was easily rejected by a one-tailed paired *t*-test at the 95% confidence level (appendix C) indicating that the 320 nm spectrophotometer beam causes no detectable change in the film's absorbance during analysis.

6.4.4 Response Reproducibility

The simultaneous exposure of five PPO film actinometers in the film thickness experiment (section 6.4.1) suggests that the response of this film can be reproduced for any given UV dose with reasonable precision. The ability of the actinometer to resolve UV doses depends on this reproducibility. In this section, the reproducibility of PPO film response is examined with a larger sample size in order to provide the coefficient of variation (CV) over the entire dynamic range.

Fourteen actinometers were simultaneously exposed to broadband irradiance from the fluorescent UV lamp for a total time of 84 h. During the first five hours of exposure, the ΔA(320 nm) response of each actinometer was measured at intervals of 0.5 h. The measurement interval was increased to 12 h during the remaining exposure time. The spectroradiometer was used in conjunction with equations 6.1 to

6.5 to measure the lamp irradiance and calculate the UV dose received by the actinometers at each time interval. The mean and standard deviation of the fourteen response measurements were then used to calculate the CV for each dose.

The CV is shown in figure 6.9 as a function of the UV dose, along with the corresponding response for each dose. The CV was less than 4% for doses up to about 700 kJ m^{-2} (ΔA(320 nm) < 1.4). A steady increase in the CV occurred with increasing exposure to a maximum of 6.5% at a dose of 2851 kJ m^{-2} (ΔA(320 nm) ≈ 2.3. The response variations result from both intrinsic and extrinsic factors. Intrinsic factors include the film's optical quality, contamination of PPO during fabrication, and deviations in film thickness. Lamp alignment errors, fluctuations in lamp output, spectrophotometer measurement uncertainties, exposure timing errors, and changes in the optical absorbance of the cellulose acetate filter all contribute to the extrinsic factors of the obtained reproducibility. The quadratic regression fitted to the CV data shown in figure 6.8 allows an estimate of the CV to be calculated for any given response in the range of $17 \leq \Delta A$(320 nm) ≤ 2851 kJ m^{-2} with an R^2 value of 0.947. The estimated CV is given by

$$\mathrm{CV} = 1.1647x^2 - 0.4618x + 3.1 \qquad (6.7)$$

where the ΔA(320 nm) response is denoted by x.

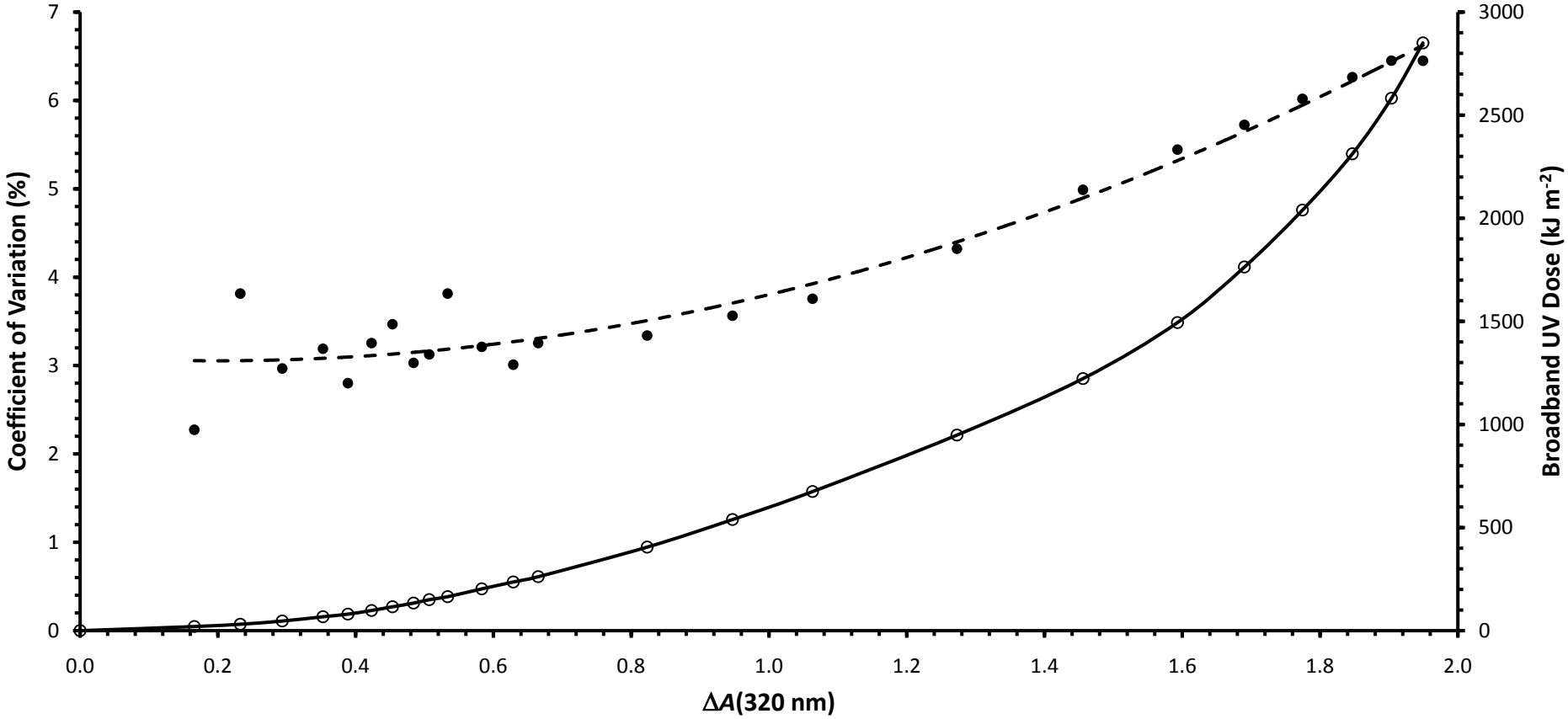

Figure 6.10: Reproducibility of broadband UV doses in terms of the coefficient of variation (CV) as a function of dose (●). The dashed curve represents the least squares regression $y = 1.1647x^2 - 0.4618x + 3.1$ fitted to the CV data (R^2 = 0.947). The calibration curve (○) employing the mean ΔA(320 nm) at each dose is included for reference.

6.4.5 Temperature Dependence

In order to determine the effect of temperature on the ΔA(320 nm) response, six batches of ten 40 μm PPO film actinometers were submerged in a 40 litre heated water bath suspended from a floating platform at a depth of 1.5 cm. Evaporation was minimised by insulating the water surface with polystyrene beads, and by increasing the water volume by interconnecting five 40 litre water tanks with the water bath by syphons. A small rectangular slot (4 cm × 10 cm) above the floating platform was kept free of beads by a wire frame so that the actinometers could be irradiated from above. An equal broadband UV dose was administered to each batch by the fluorescent UV lamp at a different water temperature (table 6.2). The low temperatures were obtained by initially cooling the water with icepacks, and then maintaining these temperatures with an immersion cooler during the course of the exposure. The mean ΔA(320 nm) of each batch was measured after exposure and are compared in figure 6.10.

Table 6.2: Response measurements of 40 μm PPO film actinometers after exposure at six different temperature levels.

Water Temperature (°C)	Mean ΔA(320 nm)	Uncertainty (°C)
1.5	1.9498	± 0.5
10	1.9233	± 0.5
20	1.8977	-1, +2
30	1.9459	± 0.5
40	1.8920	± 0.5
50	1.9475	± 1.5

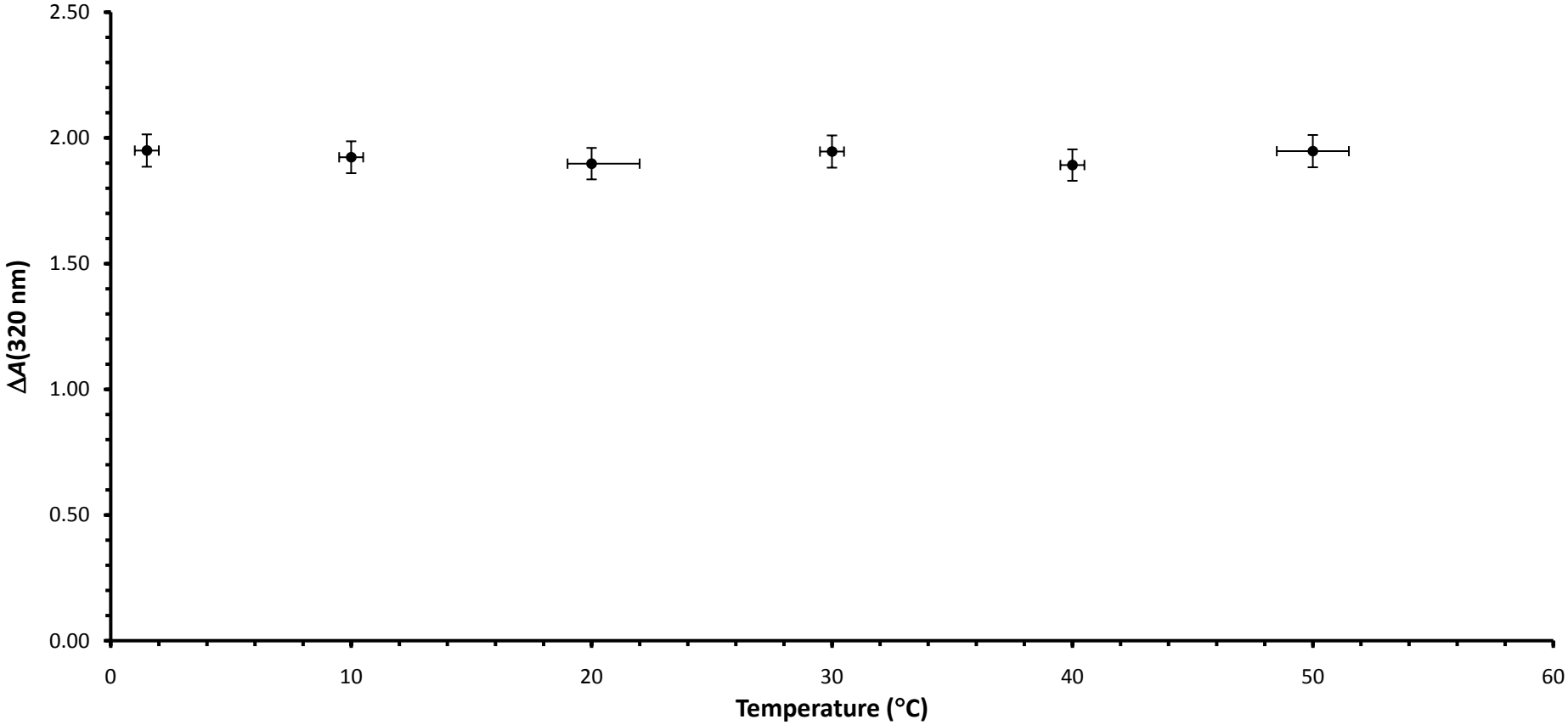

Figure 6.11: Effect of temperature during exposure on the UV induced response of 40 μm PPO film actinometers from 1.5°C to 50°C. The *x*-error bars indicate the uncertainty in temperature during the exposure, and the *y*-error bars are based on a 6.6% CV predicted by equation 6.7.

Analysis of variance showed no significant difference between actinometer responses at the six temperature levels (p = 0.593) (appendix D). The variation in response between actinometers was about 5% at each temperature level, and the temperature variation at each level was less than 2%. As expected, the response of PPO film actinometers is independent of temperature in the temperature range from 1.5°C to 50°C.

6.4.6 Artificial Source Calibration Functions

As indicated by figure 6.7 the calibration equations depend strongly on film thickness. The entire set of calibration equations are given in appendix E. The work in the previous sections indicates that a PPO film thickness of 40 μm with responses measured at λ_L = 320 nm optimises the exposure sensitivity. A broadband fluorescent UV lamp calibration equation was obtained employing these parameters (figure 6.11(□)) by reanalysing the 40 μm data from section 6.4.1. It should be noted that the UVB irradiance of the fluorescent UV lamp relative to the total irradiance is significantly greater than that of natural solar radiation. Furthermore, unlike the solar radiation field, the spectral distribution, dose rate, and angular distribution of the fluorescent UV lamp radiation field are constant. The calibrations presented in this section are therefore used to examine the potential of PPO film actinometry for quantifying biologically effective dose, but cannot be employed directly as a calibration for accurate solar dose measurements.

Third order cubic regressions are frequently used in actinometry for calibration as it is well suited to data associated with optical saturation related phenomena. The R^2 values were substantially closer to unity for the third order cubic than for lower order polynomials. The calibration equation given by the regression for broadband UV exposure is

$$H = 213.47x^3 - 21.53x^2 + 266.14x \text{ (kJ m}^{-2}\text{)} \qquad (6.8)$$

with an R^2 value of 0.997, where H denotes the broadband UV dose calculated from the measured spectral irradiance using equations 6.4 and 6.5, and x is the ΔA(320 nm).

The UVB and UVA doses were determined by applying equations 6.4 and 6.5 to the irradiance measurements described in section 6.4.1, and the biologically effective doses for the common biological responses were also calculated by equations 2.3 and 6.5. The calibrations for these wavebands are shown in figure 6.11. The scaling factors for the common biologically effective dose calibrations were also determined from the ratio of biologically effective UV irradiance to broadband irradiance (table 6.3).

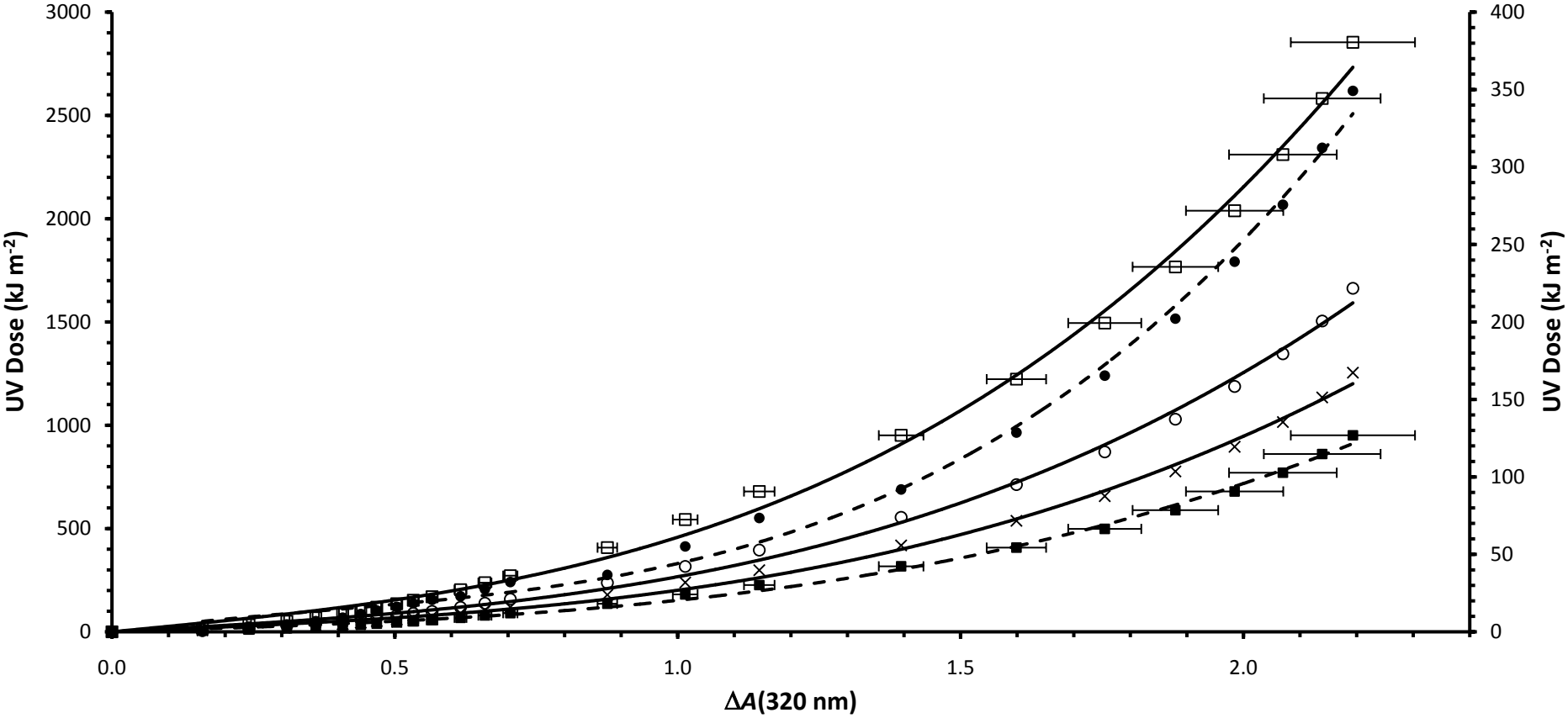

Figure 6.12: Fluorescent UV lamp calibration curves for broadband UV dose (□), UVB dose (×), UVA dose (○), erythemal dose (●), and photokeratitis weighted dose (■). Solid lines are scaled against the left axis while dashed lines are scaled against the right axis. The error bars represent the CV as estimated for each ΔA(320 nm) by equation 6.7. The error bars are identical for all calibration curves.

Table 6.3: Fluorescent UV lamp irradiances for various UV wavebands and biological weightings, and the ratio *A* of the irradiance of a given waveband or weighting to the broadband UV irradiance.

Waveband or Weighting	Irradiance ($W\ m^{-2}$)	Ratio (*A*)
UV	9.438	1
UVB	4.148	4.395×10^{-1}
UVA	5.499	5.826×10^{-1}
Erythemal	1.276	1.352×10^{-1}
Vitamin D	2.129	2.256×10^{-1}
Actinic	5.661×10^{-1}	5.998×10^{-2}
DNA Damage	8.882×10^{-2}	9.411×10^{-3}
Photoconjunctivitis	2.798×10^{-2}	2.965×10^{-3}
Photokeratitis	4.195×10^{-1}	4.445×10^{-2}

The calibration equations for the wavebands or biological weightings given in table 6.3 are given by

$$H' = AH \ (\text{kJ m}^{-2}) \tag{6.9}$$

where H' is either the dose within a given waveband or the biologically effective dose as appropriate, A is the ratio given in table 6.3, and H is the broadband dose calibration given by equation 6.8. In addition to the UV wavebands, figure 6.11 shows the calibration curves for erythemally weighted and photokeratitis weighted dose.

6.4.7 Time-Irradiance Reciprocity

A time-irradiance reciprocity experiment was designed to assess the reciprocity of 40 μm PPO film actinometers for a large UV dose. A broadband dose of 1.9 MJ m^{-2} was administered to batches of ten actinometers from the fluorescent UV lamp. The dose rate was altered for each batch by irradiating the batches at different distances from the lamp. The spectroradiometer was employed to measure the irradiance output of

the fluorescent tube at six different distances from the tube. Equations 6.4 and 6.5 were used to calculate the time required for the lamp to produce the broadband dose of 1.9 MJ m^{-2} from the six different lamp distances. The lamp distances and the corresponding measured irradiances and calculated exposure times are listed in table 6.4, and the reciprocity results are plotted in figure 6.12.

Table 6.4: Distances, measured irradiances and calculated exposure times used in the time-irradiance reciprocity experiment.

Lamp Distance (m)	Irradiance (W m^{-2})	Exposure Time (h)
0.52	1.01	522.8
0.42	1.13	466.0
0.32	1.43	367.1
0.17	2.07	255.2
0.12	3.67	143.7
0.06	11.74	44.9

The Bunsen-Roscoe law of reciprocity is valid for the actinometer if the ΔA(320 nm) responses are equal for the different dose rates. The average response to the 1.9 MJ m^{-2} dose was a ΔA(320 nm) of 1.5. The responses were equal within the CV of 4% expected for this magnitude of response for irradiances from 2.1 W m^{-2} to 11.7 W m^{-2}. However, the response begins to accelerate for the given dose when the irradiance falls below 2.1 W m^{-2}. This low irradiance deviation from reciprocity reaches 13% at 1.0 W m^{-2}.

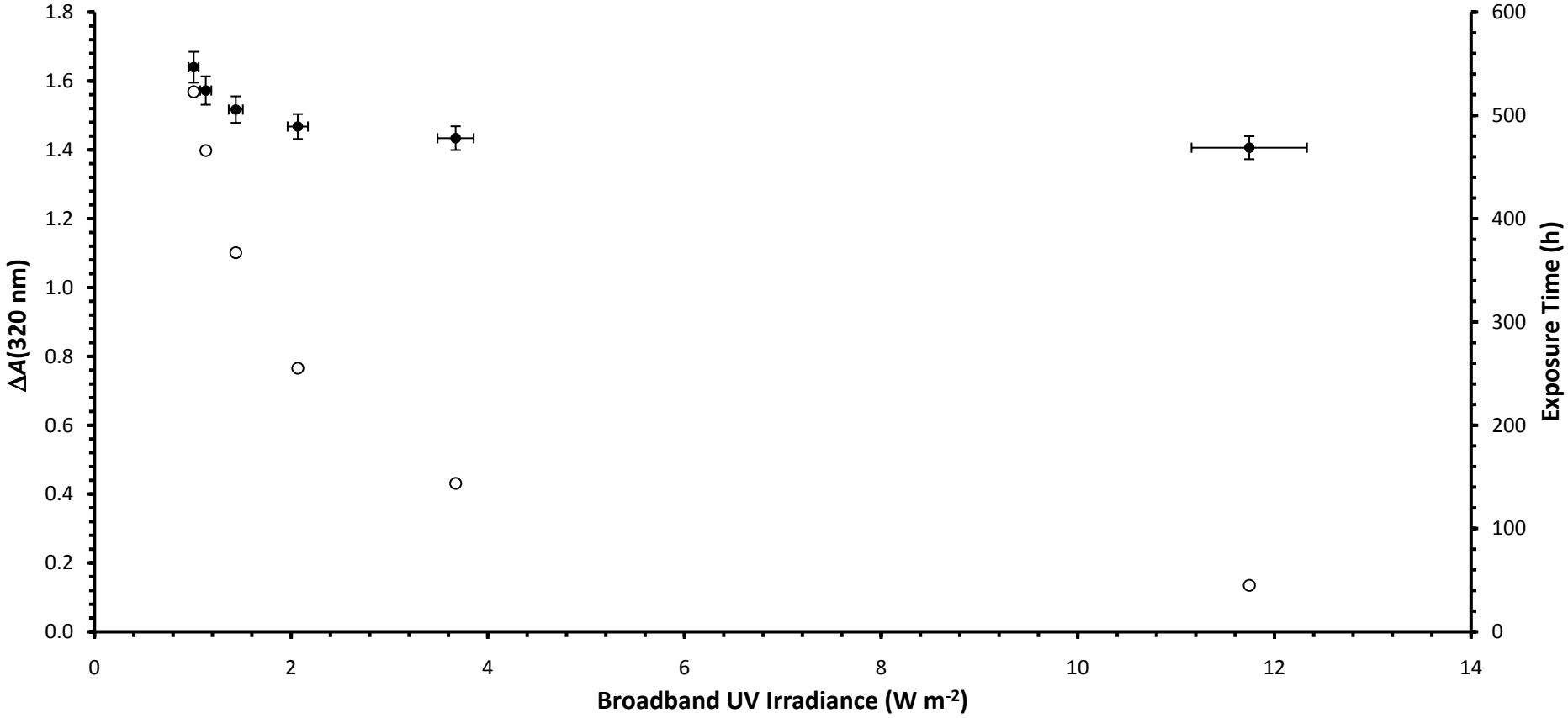

Figure 6.13: Reciprocity result for 40 μm PPO film actinometers exposed to a broadband dose of 1.9 MJ m^{-2}. The ΔA(320 nm) (●) is plotted against the irradiance required to administer a dose of 1.9 MJ m^{-2} over the given exposure time period (○) (right axis). The *x*-error bars indicate the estimated 10% error associated with measurements of irradiance, and the *y*-error bars indicate a CV ranging from 3.3% to 4.5% predicted by equation 6.7 for each ΔA(320 nm) response.

6.4.8 Spectral Response

The importance of quantifying the spectral response of an actinometer material was discussed in section 4.3.2. The irradiation monochromator was employed for this objective. Since the output irradiance of this instrument varies substantially with wavelength (figure 6.2(*b*)), and the response of PPO film deviates from reciprocity at irradiances of less than 2.1 W m^{-2}, a minimum irradiance of 2.1 W m^{-2} was required from the irradiation monochromator. The monochromator output was measured with the spectroradiometer. Due to physical constraints, the closest approach of the input aperture of the integrating sphere to the monochromator's output aperture was 4.5 cm. At this distance, an irradiance of 2.2 W m^{-2} was measured at 280 nm using input and output slit widths of both 1 mm. The irradiances of a further 20 wavebands of nearly the same FWHM (4.4 ± 0.3 nm) were measured from 285 nm to 380 nm, each separated by 5 nm between the wavelength of peak irradiance of each band. An overall increase in irradiance to 3.45 W m^{-2} was observed with increasing peak wavelength.

Actinometers containing 40 μm PPO films were sequentially exposed to the different wavebands of the irradiation monochromator at a distance of 4.5 cm from the output aperture. At 280 nm, an exposure time of 76 h providing a narrowband UV dose of 601.92 kJ m^{-2} was required to produce a ΔA(320 nm) of 1.0. The exposure times were adjusted according to equation 6.5 such that each actinometer received the same dose regardless of the waveband.

The ΔA(320 nm) response data showed a maximum spectral sensitivity to the waveband centred on 305 nm. A calibration equation for the irradiation monochromator was determined at that waveband by exposing a single actinometer to the beam and measuring the ΔA(320 nm) at regular time intervals throughout the exposure. The spectral response, $R(\lambda)$, was then calculated by

$$R(\lambda) = \frac{142.38x^3 + 104.58x^2 + 10.744x}{601.92} \qquad (6.10)$$

according to equation 4.10 where the numerator is the irradiation monochromator calibration curve in kJ m^{-2} and x denotes the ΔA(320 nm) response. The spectral

response exposures were repeated two to three times at most wavelengths. The reproducibility of actinometer responses at any given wavelength was within 8.8%. Fluctuations in the output of the irradiation monochromator contributed to the measurement uncertainties in this experiment. The spectral response of PPO film is presented in figure 6.13 and shows maximum wavelength sensitivity at 305 nm. Responses were not detectable with the given UV dose at wavelengths longer than 340 nm.

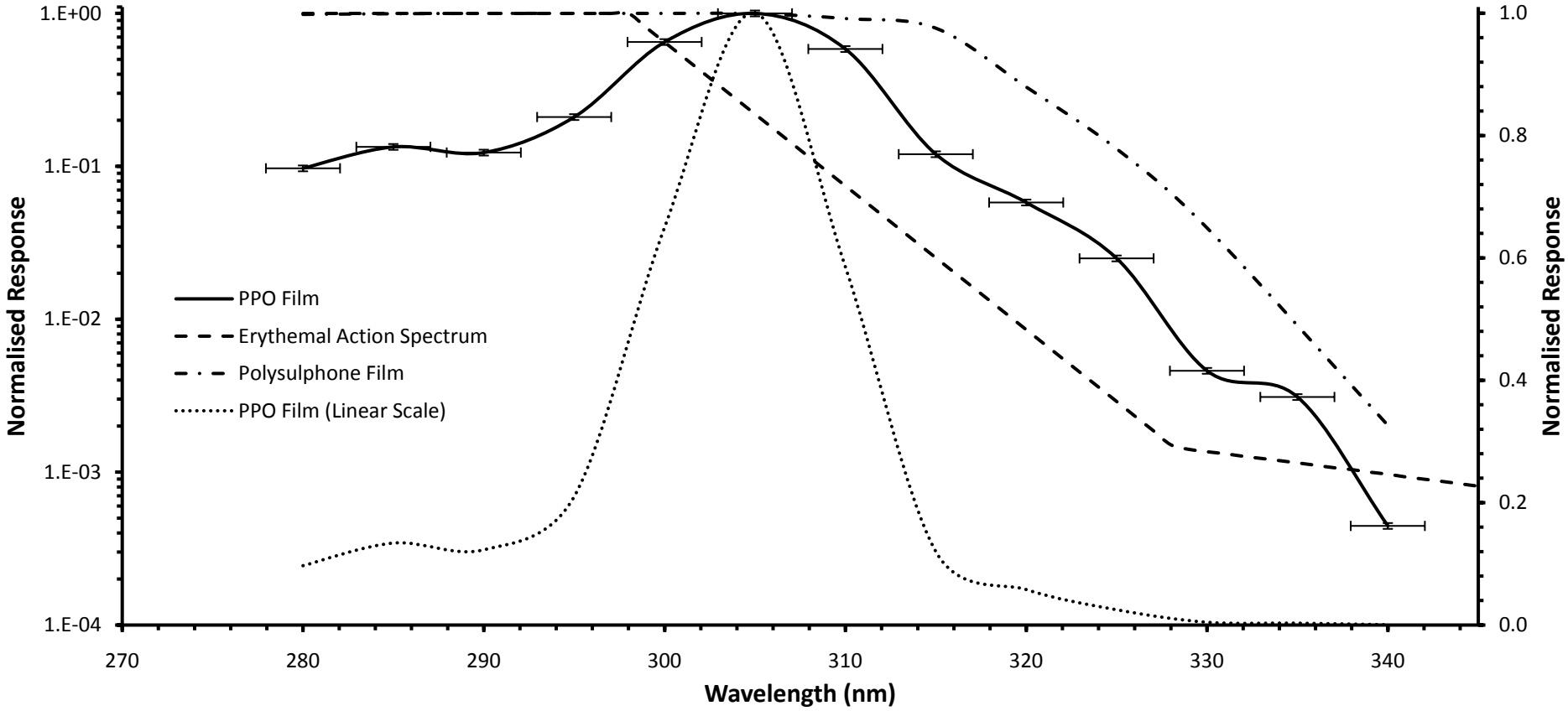

Figure 6.14: Experimentally determined spectral response of 40 μm PPO film shown on logarithmic (solid curve, left axis) and linear (dotted curve, right axis) scales. The response is normalised to the maximum response that occurs at 305 nm. The *y*-error bars represent the reproducibility of 8.8% for this experiment. The *x*-error bars indicate the 4.4 nm FWHM of each exposure waveband. The spectral response of polysulphone film (left axis) and the erythemal action spectrum (left axis) are included for comparison.

6.4.9 Angular Response

Due to the constantly changing angle of incidence of direct solar irradiance and the omnidirectional nature of diffuse solar irradiance, quantification of the angular response of 40 μm PPO film actinometers to UV radiation was undertaken. The angular response was determined by sequentially irradiating actinometers with the collimated beam of the solar UV simulator each at a different angle, in increments of 10° ranging from 0° to 80° in the azimuth plane, and from 0° to 70° in the altitude plane. A rotatable holder was designed to position an actinometer at any desired angle to the beam. Normal incidence (0°) was defined by placing a small plane mirror in the rotatable holder and aligning the reflected beam with the centre of the output aperture of the solar simulator.

Each actinometer was exposed for a period of 2 h at a distance of 16 cm from the output aperture of the solar simulator. The irradiance measured with the spectroradiometer at this distance was 71.7 W m^{-2}. Exposure at normal incidence resulted in a ΔA(320 nm) of 0.55. Assuming an ideal cosine angular response, the irradiance incident on an actinometer at an angle of 80° is about 12.5 W m^{-2}. Hence for all angles, the irradiance is outside the range for which reciprocity was determined. Due to the expense and limited lifespan of the xenon arc lamp of the simulator, longer exposures at lower irradiance were not feasible. The reciprocity experiment (section 6.4.7) however, shows smaller deviations from reciprocity at larger irradiances (up to 12 W m^{-2}). It is therefore assumed that reciprocity deviations are negligible at the larger irradiances employed in this experiment.

In order to minimise the effects of nonlinearity of the dose-response of PPO film, a calibration function was determined for the solar UV simulator using the same technique as described for the irradiation monochromator in section 6.4.8. The normalised R_N response was then calculated from

$$R_N = \frac{-8.150x^3 + 17.99x^2 + 1.696x}{-8.150x_0^{\,3} + 17.99x_0^{\,2} + 1.696x_0} \tag{6.11}$$

where the polynomials in the numerator and denominator are the solar simulator calibration equation. In this case, x is the ΔA(320 nm) induced at any angle, and x_0 is

that induced at normal incidence. The angular response for PPO film actinometers is presented in figure 6.14. The maximum deviation of the response from the cosine function in the azimuth plane was 7.9% and the average deviation was 4.5%. In the altitude plane, the average deviation was 13.2%. The two largest deviations in the altitude plane were 12.8% and 13.2% at angles of 60° and 80° respectively. It is interesting to note that the error at 70° was only 3%, indicating the possibility that the responses at 60° and 80° in the altitude plane are outliers. The average cosine error for both planes was 4.9%. The cosine errors appear to be randomly scattered with respect to angle. However, the majority of the deviations are positive, which in this case indicates that the cosine function is on average slightly underestimated.

Three exposures were made at an angle of 45° in the azimuth plane to estimate the reproducibility of this experiment. The angle was reset before each exposure so as to include angle alignment errors in the reproducibility. The ΔA(320 nm) responses due to each exposure fell within a range of 4%.

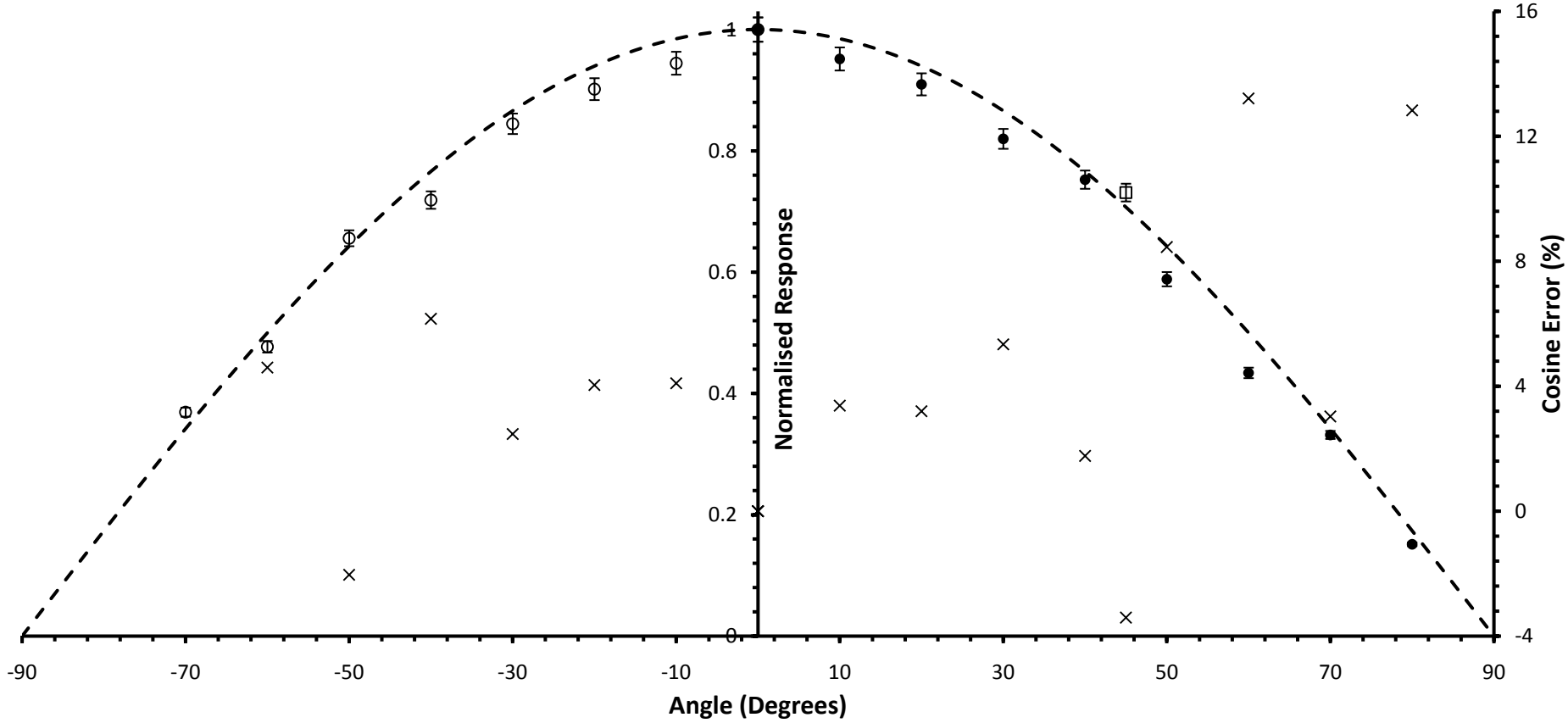

Figure 6.15: The angular response of 40 μm PPO film actinometers in the azimuth plane (○) and the altitude plane (●) (central axis), and the cosine error (×) for each angle (right axis). Three repeated measurements were made at 45° of altitude (□) to provide an estimate of the reproducibility of about 4% for this experiment, as indicated by the error bars.

6.4.10 Solar Erythemal Exposure Calibration

The spectral response of PPO film determined in section 6.4.8 indicates that these actinometers are best suited for the monitoring of UVB exposure, and have a response that approximates the erythemal action spectrum (figure 6.13). Calibration of the actinometers against the solar UV-biometer served to determine the solar erythemal dynamic range and to estimate the solar UVB dynamic range[1] by means of equation 5.1.

The exposure of 26 PPO film actinometers to solar radiation was performed over a period of 18 days during August 2002 in Toowoomba (27.6° S). Two actinometers were removed from solar exposure each day at 12:00 pm and 5:00 pm local time for the first nine days. For the remaining eight days, one actinometer was removed from exposure at 5:00 pm each day. The cumulative erythemal exposure retrieved from the UV-biometer for each exposure period was plotted against the ΔA(320 nm) response, providing the calibration curve depicted in figure 6.15. The cubic regression for this calibration gives

$$H_{Er} = -0.8774x^3 + 4.9124x^2 + 35.446x \text{ (MED)} \qquad (6.12)$$

with an R^2 value of 0.995, where H_{Er} is the solar erythemal dose and x is the ΔA(320 nm) response of the actinometer. As is seen in figure 6.15, ΔA(320 nm) is very nearly a linear function of erythemal dose, and may be closely approximated by the linear regression

$$H_{Er} = 41.536x \text{ (MED)} \qquad (6.13)$$

with an R^2 value of 0.993. The data in the region of saturation are not included in the either of the regressions. The linear regression deviates from the cubic function by 15.7% at the smallest dose. However, for doses greater than 20 MED, the difference between the functions is well within the experimental uncertainty and decreases to less than 1.9% with increasing dose.

[1] This estimation was required since at the time that these experiments were conducted, there were no detectors available for the long-term monitoring of unweighted solar UVB irradiance.

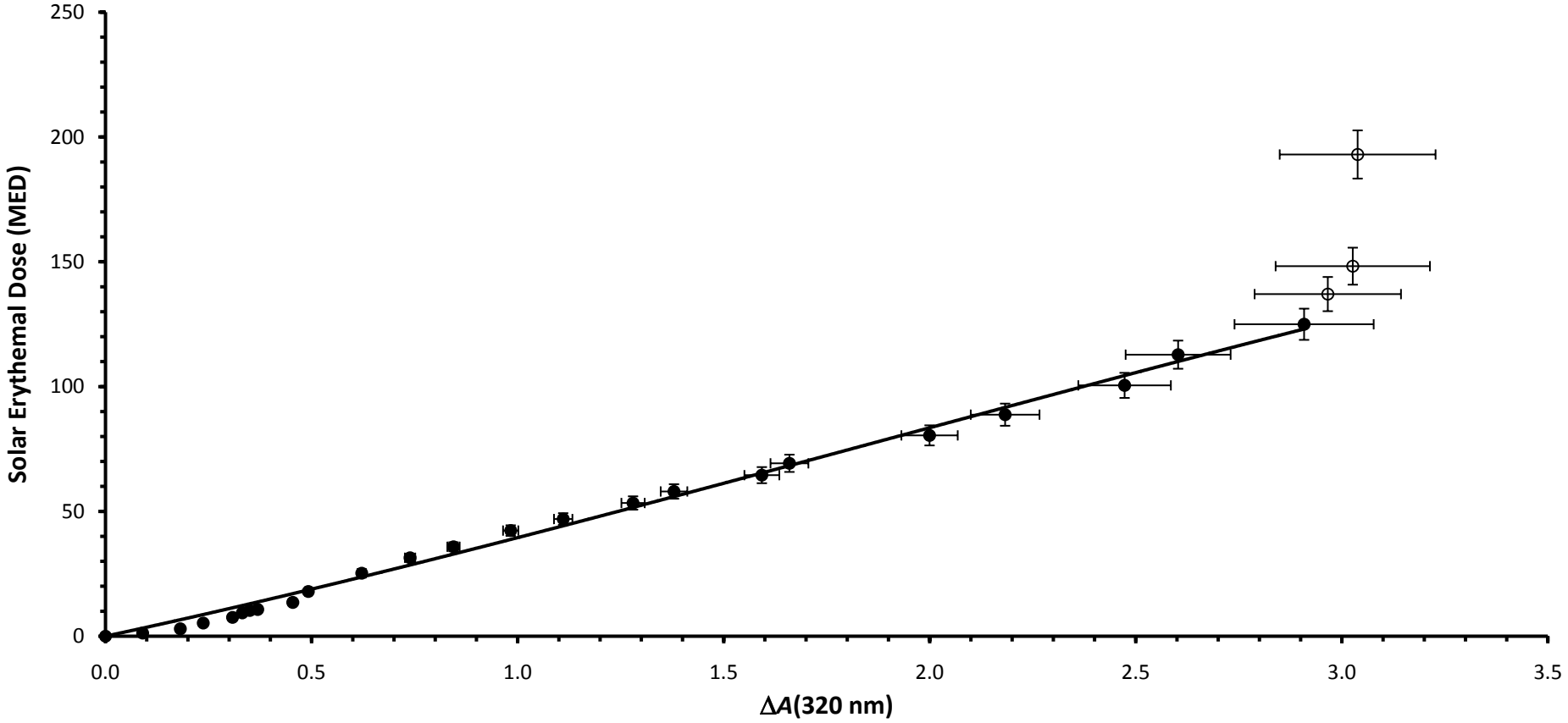

Figure 6.16: Solar erythemal exposure calibration curve of 40 μm PPO film actinometers. The curve represents the third order cubic regression (equation 6.12). The three open circles represent the data points that occur within the region of optical saturation as they deviate substantially from the regression line. The *y*-error bars show the uncertainty of about 10% in the UV-biometer measurements, and the *x*-error bars represent the CV of the response ranging from 3% to 12.4% as estimated by equation 6.7.

In addition to variations in the response quantified by the CV, all dosimetric methods incur calibration errors introduced through the transfer of data from the calibration instrument to the dosimetry calibration function. The accuracy of a dosimetry method for absolute dose measurements is therefore at best as good as that of the calibration instrument. Total errors in solar erythemal dose measurements determined from this calibration of up to 16.5% should be expected due to the combined uncertainty of the UV-biometer and the CV of PPO film.

6.4.11 Dynamic Range

The rate of change of the response of PPO film decreases with increasing UV exposure, and consequently the sensitivity, and hence the dose resolution diminishes with increasing dose. This effect is clearly seen in the results of the film thickness experiment (section 6.4.1). The calibration curve is useful only to the point that individual doses are resolvable within experimental uncertainty. For the purpose of removing subjectiveness from the definition of optical saturation of PPO film, it is defined here as the largest ΔA(320 nm) that cannot be distinguished from the maximum ΔA(320 nm) due to reproducibility, where the maximum ΔA(320 nm) is the last recorded response before mechanical failure of the film. The saturation dose is then defined as the UV dose that induces the saturation response. By this definition, the dynamic range depends on both the intrinsic nature of the film and the precision of the measurements involved.

In section 6.4.6 the artificial source calibration functions shown in figure 6.11 begin saturation at the third-last data point on each curve, since the CV error bar of this point is the first to overlap with that of the last data point (the point that precedes failure of the film). The saturation dose for broadband UV is 2310 kJ m^{-2} and the minimum recorded dose was 17 kJ m^{-2}. The corresponding dose-capacities and thresholds for the UVB and UVA wavebands, and for the various biologically weighted doses may be found by weighting the broadband UV dose-capacity and dose-threshold by the appropriate ratio (A) given in table 6.3. The estimated RDR for all wavebands and weightings is 99.3%.

The onset of saturation was sudden in the solar exposure calibration described in section 6.4.10. The saturation dose was 125 MED[1] (figure 6.15). At larger doses the ΔA(320 nm) remained essentially constant with increasing exposure. The solar erythemal dose-capacity of PPO film is therefore about 27 kJ m^{-2}, or about 204 kJ m^{-2} for unweighted UVB according to equation 5.1. The minimum distinguishable erythemal dose recorded in this calibration was 267.7 J m^{-2} or an estimated UVB dose of 2.02 kJ m^{-2}. Hence the UVB RDR for PPO film is about 99.0%.

6.4.12 Dark Reaction

The dark reaction of 40 μm PPO film actinometers, denoted by ΔA_{DK}(320 nm) as given by equation 4.15, and its temperature dependence was investigated by simultaneously exposing four pairs of actinometers to a broadband dose of 729.5 kJ m^{-2} from the fluorescent UV lamp. The mean ΔA(320 nm) response was determined immediately after exposure. Each pair was stored after exposure in darkness at temperatures of -16°C, 2°C, 24°C, and 40°C. The mean A_{DK}(320 nm) of the pairs were remeasured at various times of up to 40 days after the initial exposure and were plotted as a function of post-exposure time (figure 6.16).

The dark reaction was less than 0.7% at -16°C and was indistinguishable from that at 2°C until about 70 h after the exposure, and remained below 2.7% at 2°C. Hence the dark reaction is within the range of experimental reproducibility at these temperatures and is thus negligible up to 40 days after the exposure. At higher temperatures however, the dark reaction reached 12% at 24°C and nearly 21% at 40°C after a post-exposure time of 941 h. Power curve regressions fit the 24°C and 40°C data allowing correction factors to be applied in the case that the post-exposure response measurements of calibration actinometers and field actinometers are made at different times after their respective exposures.

[1] The MED as measured by the UV-biometer was defined as 214 J m^{-2} at the time of the measurements.

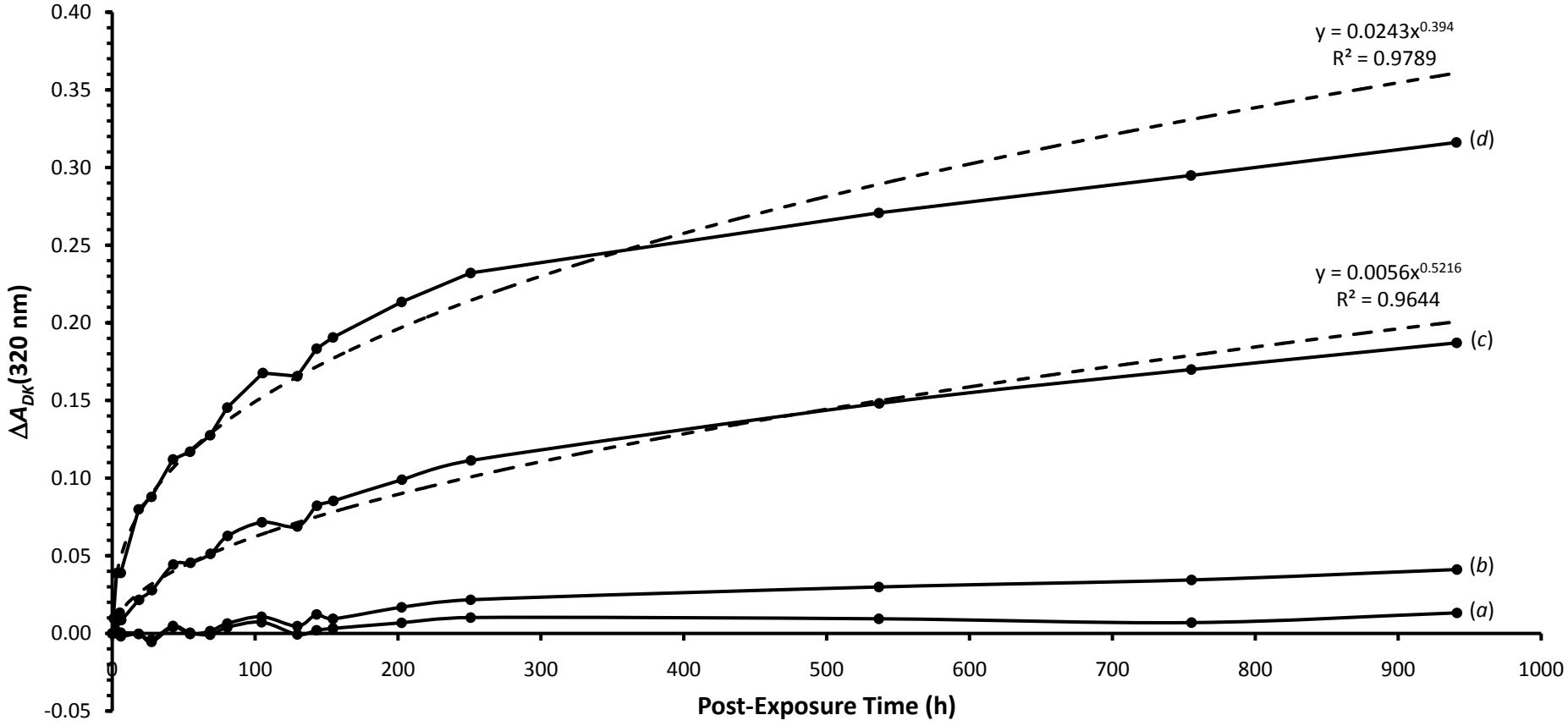

Figure 6.17: Dark reaction of 40 μm PPO film actinometers stored at temperatures of -16°C (*a*), 2°C (*b*), 24°C (*c*), and 40°C (*d*) after exposure to a broadband dose of 729.5 kJ m^{-2}. The dashed curves represent power curve regression lines for temperatures of 24°C and 40°C.

The regression curve for 24°C is given by

$$\Delta A_{DK}\left(320\text{ nm}\right) \approx 0.0056 t_p^{\,0.5216} \tag{6.14}$$

($R^2 = 0.964$) where t_p is the post-exposure time in hours before measurement of the response. The power curve regressions are valid for $1 \leq t_p \leq 941$ h. Equation 6.14 assumes that the dark reaction is independent of the UV dose received during exposure.

The dependence of the dark reaction of PPO film on UV dose was therefore also investigated. Four pairs of actinometers were exposed to four different broadband doses from the fluorescent UV lamp, and the mean ΔA_{DK}(320 nm) of each pair was determined at six different post-exposure times (table 6.5). The percentage increase in response due to the dark reaction is plotted against the ΔA(320 nm) response induced by the UV doses in figure 6.17, revealing an inverse linear dependence of ΔA_{DK}(320 nm) on ΔA(320 nm). The series in figure 6.17 from bottom to top shows an increase in dark reaction with increasing post-exposure time. The negative slope of each series indicates an inverse dependence of the dark reaction on dose. The largest ΔA_{DK}(320 nm) over the dose range investigated was 3.4%. Extrapolating from zero to the saturation response (ΔA(320 nm) ≈ 2.9) using the average slope of the curves in figure 6.17 ($m \approx -2.2$) gives a maximum possible dose related ΔA_{DK}(320 nm) of 6.4%. The slopes of the linear regressions are similar indicating that post-exposure time has little or no effect on the dose dependence of the dark reaction.

Table 6.5: Post-exposure times and response measurements of 40 μm PPO film actinometers after four different broadband UV doses.

	Broadband UV Dose (kJ m^{-2})			
	162	544	950	1495
Post-Exposure Time (h)	ΔA_{DK}(320 nm)			
22.5 ± 5.5	0.0714	0.5724	0.8832	1.2789
49.5 ± 5.5	0.0727	0.5931	0.8941	1.3219
72.0 ± 5.0	0.0811	0.6201	0.9119	1.3111
104 ± 12	0.0921	0.6222	0.9200	1.3321
176.5 ± 11.5	0.1322	0.6361	0.9298	1.3391
493.5 ± 42.5	0.1103	0.6519	0.9699	1.4127

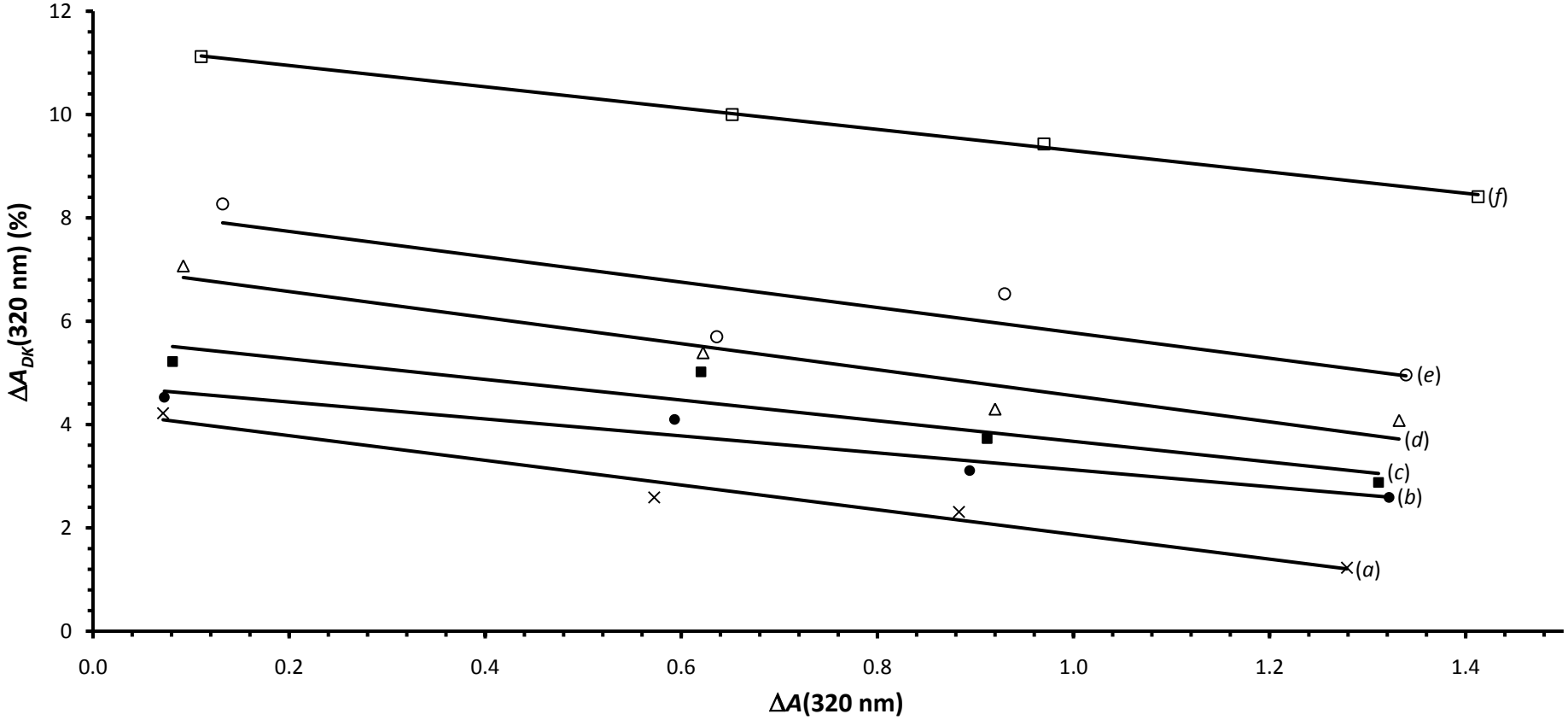

Figure 6.18: Dependence of the dark reaction of 40 μm PPO film actinometers on dose. The percent change in ΔA_{DK}(320 nm) is plotted against the ΔA(320 nm) response induced by the broadband doses given in table 6.5. The ΔA_{DK}(320 nm) was determined at post-exposure times of 22.5 h (*a*, ×), 49.5 h (*b*, ●), 72 h (*c*, ■), 104 h (*d*, △), 176.5 h (*e*, ○), and 493.5 h (*f*, □). The curves represent least squares linear regressions.

6.5 Summary and Conclusions

This chapter has provided an account of the development and characterisation of the optical properties of PPO film actinometers. Casting experiments and broadband dose-response curves were used to establish the optimum PPO dry mass to chloroform mixing ratio and the film thickness that provides the optimum dynamic range and exposure sensitivity. The mixing ratio of 0.12 enabled the casting of high quality PPO films with sufficient durability, and the sensitivity was maximised while maintaining film quality by casting films at a thickness of 40 μm and measuring the pre-exposure and post-exposure A(320 nm) at the spectrophotometer wavelength of 320 nm. The reproducibility of the ΔA(320 nm) response in terms of the CV was found to increase from about 3% to 6.5% according to equation 6.7 in the response range of $0 \leq \Delta A(320\text{ nm}) \leq 1.88$, or the broadband UV dose range of $0 \leq H \leq 2851$ kJ m^{-2}. The angular response averaged over both the azimuth and altitude planes was better than 5%, and no temperature dependence of the response was detected from 1.5°C to 50°C. The spectral response experiment found the spectral sensitivity peak of PPO film at 305 nm and a fairly close correspondence with the CIE erythemal action spectrum between 300 nm and 335 nm. The PPO film actinometer is therefore most suited to measurements of erythemally weighted UV dose. Time-irradiance reciprocity remained within experimental uncertainty for the irradiance range of $2.1 \leq I \leq 11.7$ W m^{-2}, but deviated inversely for irradiances lower than 2.1 W m^{-2} by up to 13%.

Broadband exposures were calibrated against the spectroradiometer in section 6.4.6 for unweighted and weighted UV doses, and for solar erythemal dose in section 6.4.10. Equation 6.8 provided the calibration function for broadband dose, and the weighting factors for important biological responses were given in table 6.3. Given that no response was observed at wavelengths longer than 340 nm in the spectral response experiment, the UVA calibration is valid only for a constant spectral irradiance. The solar erythemal calibration function was given by equation 6.12 and was near linear as indicated by equation 6.13. Significant differences exist between both the scaling factor and the kernel of the erythemal calibration performed under the fluorescent UV lamp and that under natural solar radiation. The large difference in linearity can be seen by comparing figures 6.11 and 6.15. The erythemal dose-

capacity as given by the lamp calibration was about 276 kJ m^{-2}, while that given by the solar radiation was 125 MED or an erythemally weighted dose of about 26.3 kJ m^{-2}. This latter dose-capacity is a surprising and somewhat disappointing result, being more than a factor of ten smaller. However, the result demonstrates a dynamic range for solar erythemal dose of PPO film of more than twice that of polysulphone.

A dark reaction dependent on post-exposure time was quantified, that is closely approximated by equation 6.14 for post-exposure temperatures of around room temperature. An inverse dependence of the dark reaction on UV dose was observed indicating a maximum dose related variation of the dark reaction of 6.4%. A dark reaction correction factor may be employed by means of equation 6.14 in the case that calibration and experimental actinometers are stored at room temperature and are measured at different times. Due to the dose dependence however, this correction factor could be in error by as much as 6.4% depending on the difference in the range of doses to which the actinometers are exposed.

Refrigeration of the actinometers after exposure significantly reduced the dark reaction. At temperatures of 2°C or lower, the dark reaction remained within experimental uncertainty. This allows the dark reaction to be essentially eliminated provided that all actinometers from a given experiment are maintained at the same low temperature after exposure. Alternatively, the dark reaction can be minimised by measuring the response of each actinometer from a given experiment within a short period of time after the exposure.

Chapter 7

Conclusions

7.1 Introduction

7.2 Consolidation of the Research Objectives

7.3 Further Research

7.4 Final Conclusion

7.1 Introduction

A myriad of spectrally dependent and exposure dependent biological effects are induced by UV radiation. Biologically effective solar radiation is modulated at the Earth's surface by continual fluctuations in UV irradiance and spectral distribution caused by variations in geometrical and atmospheric parameters. An important aspect of environmental risk assessment is therefore the quantification of biologically effective radiation under a highly variable UV radiation field.

Dosimetry methods have been employed extensively for solar UV dose measurements due to their low cost, versatility and ability to integrate all variability into a single dose measurement. Chapter 5 revealed that a number of dosimetric and actinometric materials techniques are available. The polysulphone film actinometer minimises the labour and costs associated with solar UV exposure quantification and is one of the most versatile UV detectors. It also provides a response that approximates the CIE erythemal action spectrum, and hence is the most extensively employed actinometer type in UV exposure research. The main disadvantage of polysulphone film however, is its limited dynamic range. Although the dynamic range of polysulphone can be overcome by employing filters, or by summing the doses of sequentially exposed actinometers, this adds to the fabrication cost in terms of both materials and labour, and may in the latter case incur increased integration errors.

The overall objective of this research was to reduce the labour and costs associated with large-dose measurements of solar UV exposure. Biological dosimeters have larger dynamic ranges than chemical actinometers, but are disadvantaged by their cost, and their demands on expensive equipment for post-exposure analysis that are not generally available in a physics laboratory equipped with standard optical instruments. The primary objective was therefore fulfilled by the development and characterisation of a chemical film actinometer employing poly(2,6-dimethyl-1,4-phenylene oxide) polymer in the form of a thin film (PPO film), which was found to provide a larger dynamic range than polysulphone, and thus allows larger doses to be quantified with a single measurement.

7.2 Consolidation of Research Objectives

PPO film was identified through a literature search as a convincing candidate for development as a large-dose actinometer. Evidence from the literature suggested the possibility of extending the dynamic range of actinometry into the MJ m^{-2} range by use of PPO film. The literature review also revealed polysulphone actinometry as the cheapest form of actinometry in terms of both labour and cost, and one of the most versatile methods available for quantifying UV dose. The material costs, equipment demands, and labour involved in this method are also substantially lower than those required by the common forms of biological dosimetry that were reviewed.

Through the experimental work of this project, the spectral response of PPO film was found to peak in the UVB waveband at 305 nm. The response approximates the CIE erythemal action spectrum, and does so more closely than polysulphone from 300 nm to 340 nm. Although a deviation from the CIE erythemal action spectrum exists at wavelengths shorter than 300 nm, a significant response was observed at these wavelengths allowing calibration against an erythemal radiometer. PPO film actinometers are therefore suitable for either UVB or erythemally weighted dose measurements. Fluorescent UV lamp exposures conducted in section 6.4.6 demonstrate the ability of PPO film actinometers to quantify biologically effective dose for UVB related responses when calibrated against a spectroradiometer. If a spectral irradiance monitoring instrument is available during the calibration stage, then PPO film actinometers have the capability of quantifying biologically effective dose weighted for various biological responses including erythema, actinic response, DNA damage, photoconjunctivitis, photokeratosis, and vitamin D synthesis.

The demonstrated close correspondence between the cosine function and the angular response of PPO film actinometers allows these detectors to integrate both direct and diffuse irradiance with an accuracy of about 5% regardless of the SZA. The cosine response and temperature independence of PPO film combined allow deployment of the actinometers at any latitude and during any season. The Bunsen-Roscoe law of reciprocity was obeyed by PPO film at irradiances greater than 2.1 W m^{-2}. An upward trend in the response was observed at lower irradiances. This is potentially a serious source of error if calibration actinometers are exposed to a source that is

significantly different in dose-rate to the source measured by experimental actinometers. For example, an experimental design in which actinometers are calibrated in full sunlight with irradiances generally greater than 2.1 W m^{-2} while experimental dosimeters are used to measure doses in a shaded area and receive irradiances less than 2.1 W m^{-2} will incur a reciprocity related calibration error. Such an experimental design would be improved by exposing the calibration dosimeters in a similar shaded environment as the experimental dosimeters, and applying a shadowband to the instrument against which the actinometers are calibrated. As mentioned in section 4.10, the most accurate calibrations are obtained by minimising any differences between the calibration source and the source under measurement. Therefore, with regard to PPO film actinometers, these differences include both spectral distribution and irradiance.

Broadband exposures employing the fluorescent UV lamp showed the dynamic range of PPO film to have a dose-capacity of up to 2.31 MJ m^{-2}. The erythemal and UVB dose-capacities were 276 kJ m^{-2} and 1015 kJ m^{-2} respectively. The dose-capacity for natural solar erythemal exposure calibrated against the UV-biometer was 26.3 kJ m^{-2}. Although the latter dose-capacity does not compare favourably with those of biodosimeters, it does represent an increase in the dynamic range of a factor of 2.4 compared to polysulphone film actinometers for solar erythemal exposure. The difference between the R^2 values of cubic and linear regressions fit to the solar erythemal calibration data is only 0.18%. This linearity offers the advantage that fewer calibration points are required compared to nonlinear calibrations, and thus further reduces labour and costs. Furthermore, the reproducibility of PPO film actinometer responses compares favourably to other dosimetry methods over the entire dynamic range (cf. 10% to 30% for polysulphone actinometry), with a maximum CV of 6.5%.

The dark reaction of PPO film was found to be significant and dependent on temperature, and to a lesser extent on dose. As for polysulphone actinometry, the presence of the dark reaction does not detract from the accuracy or contribute to the labour or costs of the method if managed correctly. Techniques for managing the dark reaction of PPO film actinometers are discussed in section 6.4.12 and section 6.5.

The deviations of the optical properties of PPO film actinometers from an ideal solar UV radiation detector were found to be sufficiently small that these actinometers are well suited to the measurements of UVB and biologically weighted dose. The effects of deviations from the ideal can be minimised by calibrating the actinometers under the same or a similar irradiance source. The performance may also be enhanced by calibrating the actinometers for erythemal dose, since the spectral response of PPO film approximates the CIE erythemal action spectrum.

PPO powder is inexpensive and employs the same solvent as polysulphone. The labour and costs involved in fabricating PPO film actinometers is therefore equivalent to those for polysulphone film actinometers. The demonstrated ability of PPO film actinometers to provide a dynamic range of more than twice that of polysulphone without the need for chemical additives or physical filters proves that fewer actinometers and hence less materials and fabrication time are required for large-dose measurements. Although some further research would be advantageous as discussed below, the method of PPO film actinometry as developed in this research can be employed for measurements of up to 26.3 kJ m^{-2} of erythemally weighted dose with a precision that is at least equal to that of current forms of actinometry.

7.3 Further Research

The calibration functions determined in this project under fluorescent UV lamp irradiance and natural solar radiation showed large differences in both dynamic range and linearity. Under the assumption that this difference results from the significant difference between the source spectra, the form of the calibration function may vary according to season and latitude. Determining and comparing calibration functions for different seasons, latitudes, and weather conditions will therefore provide a greater understanding of the nature and accuracy of various calibrations and the effect of solar variability on these calibrations. For example, it would be interesting to compare the calibration functions for diffuse and direct solar exposure. A diffuse calibration could be achieved (at mid to equatorial latitudes) by exposing actinometers only during early morning and late afternoon periods in which the SZA is small and diffuse solar irradiance dominates. Alternatively, the actinometers could be exposed in a shaded area and calibrated against a shadowband radiometer. A

direct exposure calibration would be accomplished by exposing actinometers only during the midday hours to reduce the effects of the diffuse component. Since solar spectral irradiance depends on SZA, such comparisons may elucidate the combined effect of spectral distribution, dose-rate, and effect of diffuse and direct irradiance on the calibration function. This information is necessary in a situation where experimental dosimeters are exposed at a large distance from, or at a different latitude to the calibration.

The time-irradiance reciprocity was tested only for a single large UV dose. It was assumed that if the Bunsen-Roscoe law was obeyed for a large dose, then it would also be obeyed for all smaller doses. Experimental verification of this assumption could be achieved by repeating the reciprocity experiment described in section 6.4.7 for various doses within the dynamic range of the actinometer. In addition, the effect of the constantly changing nature of solar UV radiation and the fractionation of exposure by the night-time periods on reciprocity has not been quantified. A reciprocity experiment incorporating simulated diurnal UV exposure variations and nocturnal fractionation could be implemented by cyclically increasing and decreasing the distance between the fluorescent UV lamp and actinometers, and switching the lamp off at regular intervals during an experiment. Experimental runs employing different variation cycles and different on-off periods that give the same cumulative UV dose should provide an evaluation of UV variability and exposure fractionation on the reciprocity of PPO film actinometers. The value of examining reciprocity in more detail is to investigate the possibility of determining a correction factor for experimental dosimeters that are subjected to an irradiance of less than 2.1 W m^{-2} at which point a deviation from the Bunsen-Roscoe law occurs. Such a correction factor would allow a single calibration to be applied to a larger number of environmental situations. For example, a full-sun calibration could be applied after correction to low irradiance measurements in shade.

The dark reaction proceeds through the night-time periods, but the contribution of the nocturnal dark reactions to the total response are unquantified. The dark reaction experiments of section 6.4.12 indicate that the overnight change in response is negligible; about 0.02 over a period of 12 hours. If the dark reaction to fractionated exposure is cumulative, then after a 17 day exposure such as in the calibration of section 6.4.10, the dark reaction may have contributed 0.32 to the response, or an

erythemal dose equivalent of about 12 kJ m^{-2}. A hypothetical material that is optically equivalent to PPO film but has no dark reaction therefore has the potential to provide a larger dynamic range. This information may be employed in future searches for actinometer materials that may provide large dynamic ranges. The nocturnal dark reaction could easily be quantified by the long-term exposure of an actinometer and the measurement of its response before nightfall and again before sunrise each day. Such an experiment should also confirm (or otherwise) the dependence of the dark reaction on UV dose.

Davis, Diffey and Tate (1981) showed that the spectral sensitivity of polysulphone film depends on the thickness of the film, and according to CIE (1992), thinner polysulphone films may correspond more closely to the erythemal action spectrum. The pilot study in appendix A showed the spectral absorbance of 15 μm PPO film to be shifted toward shorter wavelengths compared to a 40 μm film. A possible further avenue of research is therefore the refinement of the spectral response of PPO film by altering the film thickness. A thinner film will result in a loss of sensitivity, but the dose-capacity should not be significantly affected due to the weak dependence between PPO film thickness and dose-capacity.

7.4 Final Conclusion

Polysulphone actinometry has been extensively employed in human exposure research. PPO film actinometry now provides an additional tool for this area of research providing equivalent versatility, as well as labour and cost advantages for large-dose measurements due to its larger dynamic range. The PPO method is at least as precise as polysulphone actinometry and also has the advantage of a near linear solar erythemal calibration function. Applications for PPO film actinometry can be found essentially anywhere that other types of solar UVB actinometry (polysulphone in particular) are employed. Such applications include determination of erythemal dose distributions over models of the human form, the wearing of actinometers by people and animals in various situations, and the quantification of biologically effective dose in plant canopies. PPO film actinometry therefore has the potential to make significant contributions to experimental research in a wide variety of solar UV related fields.

References

Abdel-Rehim, F, Ebrahim, S & Abdel-Fattah 1993, 'The suitibility of a dyed plastic film for biologically effective UVB radiation measurement', *Journal of Photochemistry and Photobiology A: Chemistry*, vol. 73, pp. 247-51.

Ackerman, AB & Mones, JM 2006, 'Solar (actinic) keratosis is squamous cell carcinoma', *British Journal of Dermatology*, vol. 155, pp. 9-22.

Alam, M & Ratner, D 2001, 'Cutaneous squamous cell carcinoma', *New England Journal of Medicine*, vol. 344, no. 13, pp. 975-83.

Allen, JM, Allen, SK & Baertschi, SW 2000, '2-nitrobenzaldehyde: a convenient UV-A and UV-B chemical actinometer for drug photostability testing', *Journal of Pharmaceutical and Biomedical Analysis*, vol. 24, pp. 167-78.

AOCD (American Osteopathic College of Dermatology) n.d., 'Squamous Cell Carcinoma' (published online). Hosted by the AOCD, Kirksville, Missouri. Viewed Feb 2009 at http://www.aocd.org/skin/dermatologic_diseases/index.html.

Appenzeller, T 1993, 'Filling a hole in the ozone argument', *Science*, vol. 262, pp. 990-1.

Ballotti, R & Ortonne, J-P 2002, 'Sunlight and Cutaneous Melanocytes: An Overview', chapter 1 in J-P Ortonne & R Ballotti (eds.), *Mechanisms of Suntanning*, Martin Dunitz Publishers, London.

Battaglia, PR & Brennan, TM 2000, 'Differential effects of short-term exposure to ultraviolet-B radiation upon photosynthesis in cotyledons of a resistant and a susceptible species', *International Journal of Plant Science*, vol. 161, no. 5, pp. 771-8.

Bauer, G 1968, 'The Sensitivity of Nonlinear Detectors', *Applied Optics*, vol. 7, no. 6, pp. 1017-21.

Bérces, A, Gáspár, S & Rontó, G 1999, 'Biological UV dosimetry of environmental radiation based on DNA damage', in C Baumstark-Khan, S Kozubek & G Horneck

(eds.), *Fundamentals for the Assessment of Risks from Environmental Radiation*, Kluwer Academic Publishers, Dordrecht.

Berre, B & Lala, D 1989, 'Investigation on photochemical dosimeters for ultraviolet radiation', *Solar Energy*, vol. 42, no. 5, pp. 405-16.

BioSense n.d., *BioSense.de* (published online). Hosted online by the Laboratory for Biosensory Systems, Bornheim, Germany. Viewed Mar 2009 at http://www.biosense.de/home-e.htm.

Blumthaler, M, Ambach, W & Ellinger, R 1997, 'Increase in solar UV radiation with altitude', *Journal of Photochemistry and Photobiology B: Biology*, vol. 39, pp. 130-4.

Blumthaler, M, Ambach, W & Salzgeber, M 1994, 'Effect of cloudiness on global and diffuse UV irradiance in a high-mountain area', *Theoretical and Applied Climatology*, vol. 50, pp. 23-30.

Blumthaler, M, Salzgeber, M & Ambach, W 1994, 'Ozone and ultraviolet-B irradiances: experimental determination of the radiation amplification factor', *Photochemistry and Photobiology*, vol. 61, no. 2, pp. 159-62.

Blumthaler, M & Webb, AR 2003, 'UVR Climatology', chapter 2 in EW Helbling & HE Zagarese (eds.), *UV Effects in Aquatic Organisms and Ecosystems*, Royal Society of Chemistry, Cambridge.

Bogle, MA 2006, 'Keratosis', chapter 22 in KA Arndt & JTS Hsu (eds.), *Manual of Dermatological Therapeutics: With Essentials of Diagnosis*, 7th edn, Lippincott Williams & Wilkins, Philadelphia.

Breitbart, EW, Greinert, R & Volkmer, M 2006, 'Effectiveness of information campaigns', *Progress in Biophysics and Molecular Biology*, vol. 92, no. 1, pp. 167-72.

Brenner, M & Hearing, VJ 2008, 'The Protective Role of Melanin Against UV Damage in Human Skin', *Photochemistry and Photobiology*, vol. 84, no. 3, pp. 539-49.

Cen, Y-P & Bornman, JF 1990, 'The response of bean plants to UV-B radiation under different irradiances of background visible light', *Journal of Experimental Botany*, vol. 41, no. 11, pp. 1489-95.

Chadyšienė, R & Girgždys, A 2008, 'Ultraviolet radiation albedo of natural surfaces', *Journal of Environmental Engineering and Landscape Management*, vol. 16, no. 2, pp. 83-8.

CIE (Commission Internationale de L'Eclairage) 1986a, 'Photoconjunctivitis', *CIE-Journal*, vol. 5, no. 1, pp. 24-8.

CIE (Commission Internationale de L'Eclairage) 1986b, 'Photokeratitis', *CIE-Journal*, vol. 5, no. 1, pp. 19-23.

CIE (Commission Internationale de L'Eclairage) 1987, *International Lighting Vocabulary*, 4th edn, CIE Publication No. 17.4, International Electrochemical Commission (IEC) / CIE, Vienna.

CIE (Commission Internationale de L'Eclairage) 1992, *Personal dosimetry of UV radiation*, 1st edn, Publication No. CIE 98, CIE, Vienna.

Cockell, CS, Scherer, K, Horneck, G, Rettburg, P, Facius, R, Gugg-Helminger, A, Driscoll, C & Lee, P 2001, 'Exposure of Arctic Field Scientists to Ultraviolet Radiation Evaluated Using Personal Dosimeters', *Photochemistry and Photobiology*, vol. 74, no. 4, pp. 570-8.

Coohill, TP 2001, 'Uses and Effects of Ultraviolet Radiation on Cells and Tissues', chapter 4 in RW Waynant (ed.), *Lasers in Medicine*, CRC Press, New York.

Crespo-Hernádez, CE, Cohen, B & Kohler, B 2005, 'Base stacking controls excited-state dynamics in A-T DNA', *Nature*, vol. 436, pp. 1141-4.

D'Errico, M, Calcagnile, AS, Corona, R, Fucci, M, Annessi, G, Baliva, G & Tosti, G 1997, '*p53* mutations and chromosome instability in basal cell carcinomas developed at an early or late age', *Cancer Research*, vol. 57, pp. 747-52.

Damian, DL, Patterson, DRS, Stapelberg, M, Park, J, Barnetson, RSC & Halliday, GM 2008, 'UV radiation-induced immunosuppression is greater in men and

prevented by topical nicotinamide', *Journal of Investigative Dermatology*, vol. 128, pp. 447-54.

Davis, A, Deane, GHW & Diffey, BL 1976, 'Possible dosimeter for ultraviolet radiation', *Nature*, vol. 261, pp. 169-70.

Davis, A, Diffey, BL & Tate, TK 1981, 'A personal dosimeter for biologically effective solar UV-B radiation', *Photochemistry and Photobiology*, vol. 34, no. 2, pp. 283-6.

de Gruijl, FR 2000, 'Biological action spectra', *Radiation Protection Dosimetry*, vol. 91, no. 1-3, pp. 57-63.

de Gruijl, FR & van der Leun, JC 2000, 'Environment and health: Ozone depletion and ultraviolet radiation', *Canadian Medical Association Journal*, vol. 163, no. 7, pp. 851-5.

Diffey, BL 1989, 'Ultraviolet radiation dosimetry with polysulphone film', chapter 7 in BL Diffey (ed.), *Radiation Measurement in Photobiology*, Academic Press, New York.

Diffey, BL & Davis, A 1978, 'A new dosemeter for the measurement of natural ultraviolet radiation in the study of photodermatoses and drug photosensitivity', *Physics in Medicine and biology*, vol. 23, no. 2, pp. 318-23.

Diffey, BL, Davis, A, Johnson, M & Harrington, TR 1977, 'A dosimeter for long wave ultraviolet radiation', *British Journal of Dermatology*, vol. 97, pp. 127-30.

Diffey, BL, Oliver, I & Davis, A 1982, 'A personal dosimeter for quantifying the biologically effective sunlight exposure of patients receiving benoxaprofin', *Physics in Medicine and biology*, vol. 27, no. 12, pp. 1507-13.

Dunne, RP 1999, 'Polysulphone film as an underwater dosimeter for solar ultraviolet-B radiation in tropical latitudes', *Marine Ecology-Progress Series*, vol. 189, pp. 53-63.

Ebraheem, S, Abdel-Fattah, AA, Said, FI & Ali, ZI 2000, 'Polymer-based triphenyl tetrazolium chloride films for ultraviolet radiation monitoring', *Radiation Physics and Chemistry*, vol. 57, pp. 195-202.

Einspahr, J, Alberts, DS, Aickin, M, Welch, K, Bozzo, P, Grogan, T & Nelson, M 1997, 'Expression of p53 protein in actinic keratosis, adjacent, normal-appearing, and non-sun-exposed human skin', *Cancer Epidemiology Biomarkers & Prevention*, vol. 6, no. 8, pp. 583-7.

Elwood, JM 2004, 'Who gets skin cancer: individual risk factors', chapter 2 in JD Hill, JM Elwood & JR English (eds.), *Prevention of Skin Cancer*, Kluywer Academic Publishers, Dordrecht.

Feister, U & Grewe, G 1995, 'Spectral albedo measurements in the UV and visible region over different types of surfaces', *Photochemistry and Photobiology*, vol. 62, no. 4, pp. 736-44.

Fioletov, VE, Kerr, JB & Wardle, DI 1997, 'The relationship between total ozone and spectral UV irradiance from brewer observations and its use for derivation of total ozone from UV measurements', *Geophysical Research Letters*, vol. 24, no. 23, pp. 2997-3000.

Fiscus, EL & Booker, FL 1995, 'Is increased UV-B a threat to crop photosynthesis and productivity?', *Photosynthesis Research*, vol. 43, no. 2, pp. 81-92.

Fraser, PJ & Prather, MJ 1999, 'Uncertain Road to Ozone Recovery', *Nature*, vol. 398, pp. 663-4.

Garland, C.F., Garland, F.C., Gorham, E.D., Lipkin, M., Newmark, H., Mohr, S.B. & Holick, M.F. 2006, 'The role of vitamin D in cancer prevention', *American Journla of Public Health*, vol. 96, pp. 252-61.

Gáspár, S, Bérces, A, Gróf, P & Rontó, G 1995, 'Ultraviolet radiation dosimetry with uracil thin-layer sensors', in C Nolan & H Bauer (eds.), *Proceedings of the First European Symposium*, pp. 191-4, Office for Official Publications, Brussels.

Gobbs, NK & Young, AR 1982, 'An evaluation of nalidixic acid film as a AV-A radiation dosimeter', *Photochemistry and Photobiology*, vol. 37, no. 3, pp. 345-8.

González-López, A 2007, 'Useful optical density range in film dosimetry: limitations due to noise and saturation', *Physics in Medicine and biology*, vol. 52, no. 15, pp. N321-7.

Grant, W.B. & Holick, M.F. 2005, 'Benefits and requirements of vitamin D for optimal health: a review', *Alternative Medicine Reveiw*, vol. 10(2), pp. 94-111.

Grenfell, TC, Warren, SG & Mullen, PC 1994, 'Reflection of solar radiation by the Antarctic snow surface at ultraviolet, visible, and near-infrared wavelengths', *Journal of Geophysical Research-Atmospheres*, vol. 99, no. D9, pp. 18669-84.

Gróf, P, Gáspár, S & Bérces, A 1994, 'Uracil thin layers in dosimetry of UV-radiation', in K Atsumi, C Borst, WR Cross, HJ Geschwind, D Jocham, J Kvasnicka, HH Scherer, MA Trelles & E Unsoeld (eds.), *Proceedings of SPIE, Medical Applications of Lasers*, vol. 2086, pp. 420-4, The International Society of Optical Engineering, San Diego.

Gróf, P, Gáspár, S & Rontó, G 1996, 'Use of Uracil Thin Layer for Measuring Biologically Effective UV Dose', *Photochemistry and Photobiology*, vol. 64, no. 5, pp. 800-6.

Gross, TL, Ihrke, PJ, Walder, EJ & Affolter, VK 2005, *Skin Diseases of the Dog and Cat: Clinical and Histopathologic Diagnosis*, 2nd edn, Blackwell Science Ltd, New Jersey.

Guruprasad, K, Bhattacharjee, S, Kataria, S, Yadav, S, Tiwari, A, Baroniya, S, A., R & Mohanty, P 2007, 'Growth enhancement of soybean (*Glycine max*) upon exclusion of UV-B and UV-B/A components of solar radiation: characterization of photosynthetic parameters in leaves', *Photosynthesis Research*, vol. 94, no. 2-3, pp. 299-306.

Habegger, S 1999, 'Common Skin Tumors of the Horse', *Horse Previews Magazine* - Veterinary Corner (published online). Viewed Jan 2009 at http://www.horse-previews.com/1299articles/1299vetcorner.html.

Häder, D-P, Kumar, HD, Smith, RC & Worrest, RC 1998, 'Effects on aquatic ecosystems', *Photochemistry & Photobiology B: Biology*, vol. 189, pp. 53-8.

Halliday, D, Resnick, R & Walker, J 1997, *Fundamentals of Physics Extended*, 5th edn, John Wiley & Sons, Brisbane.

Herman, JR, Bhartia, PK, Ziemke, J, Ahmad, Z & Larko, D 1996, 'UV-B increases (1972-1992) from decreases in total ozone', *Geophysical Research Letters*, vol. 23, no. 16, pp. 2117-20.

Ho, CK & Li, G 2005, 'Mutant p53 melanoma cell lines respond differently to CP-31398-induced apoptosis', *British Journal of Dermatology*, vol. 153, no. 5, pp. 900-10.

Holick, MF 2004, 'Vitamin D: Importance in the prevention of cancers, typ 1 diabetes, heart disease and osteoporosis', *American Journal of Clinical Nutrition*, vol. 79, pp. 362-71.

Horváth, R, Kerékgyártó, T, Csúcs, G, Gáspár, S, Illyés, P & Rontó, G 2001, 'The effect of UV irradiation on uracil thin layer measured by optical waveguide lightmode spectroscopy', *Biosensors and Bioelectronics*, vol. 16, pp. 17-21.

HyperPhysics.com n.d., 'Rayleigh Scattering' (published online). Hosted online by the Department of Physics, Georgia State University, Gorgia. Viewed Mar 2009 at http://hyperphysics.phy-astr.gsu.edu/Hbase/atmos/blusky.html#c2.

IRPA (International Radiation Protection Association) 1989, 'Proposed change to the IRPA 1985 guidelines on limits of exposure to ultraviolet radiation', *Health Physics*, vol. 56, pp. 971-2.

Ishigaki, Y, Takayama, A, Yamashita, S & Nikaido 1999, 'Development and characterization of a DNA solar dosimeter', *Journal of Photochemistry and Photobiology B: Biology*, vol. 50, pp. 184-8.

Jankowski, JJ, Kieber, DJ, Mopper, K & Neale, PJ 2000, 'Development and Intercalibration of Ultraviolet Solar Actinometers', *Photochemistry and Photobiology*, vol. 71, no. 4, pp. 431-40.

Jeske, H 1988, 'Skylight intensity distribution', in, *Landolt-Börnstein, Numerical Data and Functional Relationships in Science and Technology*, vol. Group V, vol. 4b, Meteorology: *Physical and Chemical Properties of the Air*, p. 265, Springer-Verlag, New York.

Jones, SK, Moseley, H & Mackie, RM 1987, 'UVA-induced melanocytic lesions', *British Journal of Dermatology*, vol. 117, no. 1, pp. 111-5.

Josefsson, W & Landelius, T 2000, 'Effect of cloud on UV irradiance: as estimated from cloud amount, cloud type, precipitation, global radiation and sunshine duration', *Journal of Geophysical Research-Atmospheres*, vol. 105, no. 4, pp. 4927-35.

Kim, Y-H, Lim, S, Han, S-H, Lee, JC, Song, W-K, Bang, J-W, Kwoon, S-Y, Lee, H-S & Kwok, S-S 2007, 'Differential expression of 10 sweetpotato peroxidases in response to sulfur dioxide, ozone, and ultraviolet radiation', *Plant Physiology and Biochemistry*, vol. 45, no. 125, pp. 908-14.

Kimlin, MG & Parisi, AV 1999, 'Ultraviolet protective capabilities of hats under two different atmospheric conditions', *Second Internet Conference on Photochemistry and Photobiology* (published online). Hosted by Internet Photochemistry and Photobiology. Viewed Jan 2009 at http://www.photobiology.com/photobiology99/index2.htm.

Kimura, S, Tahira, Y, Ishibashi, T, Mori, Y, Mori, T, Hashimoto, J & Sakaguchi, K 2004, 'DNA repair in higher plants; photoreactivation is the major DNA repair pathway in non-proliferating cells while excision repair (nucleotide excision repair and base excision repair) is active in proliferating cells', *Nucleic Acids Research*, vol. 32, no. 9, pp. 2760-7.

Kirkpatrick, JG & Lalman, D n.d., *Pinkeye in Cattle Infectious Bovine Keratoconjunctivitis (IBK)*, Oklahoma Cooprative Extension Fact Sheet VTM-9128 (published online). Hosted by the Oklahoma State University. Viewed Mar 2009 at http://pods.dasnr.okstate.edu/docushare/dsweb/Get/Document-2689.

Knuschke, P & Barth, J 1996, 'Biologically weighted personal UV dosimetry', *Journal of Photochemistry and Photobiology B: Biology*, vol. 36, no. 1, pp. 77-83.

Koshy, K, Maata, M, Samad, AHQ, Sami, G & Tabudravu, J 2006, 'The effect of varying ozone concentration on surface UV-B radiation: a Fiji perspective', *The South Pacific Journal of Natural Science,* vol. 24, pp. 28-31.

Koussoulaki, K, Denielidis, D, Häder, D-P & Santas, R 1997, 'Assessment of *Euglena gracilis* as a bilogical dosimeter for solar UVA and UVB under field conditions', *First Internet Conference: Photochemistry and Photobiology* (published online). Hosted by Internet Photochemistry and Photobiology. Viewed Mar 2009 at http://photobiology.com/v1/contrib.htm.

Krins, A, Bolsée, D, Dörschel, B, Gillatay, D & Knuschke, P 2000, 'Angular dependence of the efficiency of the UV sensor polysulphone film', *Radiation Protection Dosimetry,* vol. 87, pp. 261-6.

Kuchinke, C & Nunez, M 1999, 'Cloud transmission estimates of UV-B erythemal irradiance', *Theoretical and Applied Climatology*, vol. 63, no. 3-4, pp. 149-61.

Kuhn, HJ, Braslavsky, SE & Schmidt, R 2004, 'Chemical Actinometry (IUPAC Technical Report)', *Pure and Applied Chemistry,* vol. 76, no. 12, pp. 2105-46.

Lam, KS, Ding, A, Chan, LY & Wang, T 2002, 'Relationship Between Total Ozone and Surface UV in Hong Kong', *Better Air Quality in Asian and Pacific Rim Cities,* Poster Session, Department of Civil and Structural Engineering, The Hong Kong Polytechnic University, Hong Kong.

Lens, MB & Dawes, M 2004, 'Global perspectives of contemporary trends of cutaneous malignant melanoma', *British Journal of Dermatology,* vol. 150, no. 2, pp. 179-85.

Lester, RA & Parisi, AV 2002, 'Spectral ultraviolet albedo of roofing surfaces and human facial exposure', *International Journal of Environmental Health Research,* vol. 12, pp. 75-81.

Lluria-Prevatt, M & Alberts, DS 2005, 'Skin Cancer Prevention', chapter 11 in DS Alberts & LM Hess (eds.), *Fundamentals of Cancer Prevention*, 2nd edn, Springer-Verlag, Berlin.

Lo, H-L, Nakajima, S, Ma, L, Walter, B, Yasui, A, Ethell, DW & Owen, LB 2005, 'Differential biologic effects of CPD and 6-4PP UV-induced DNA damage on the induction of apoptosis, and cell cycle arrest', *BMC Cancer*, vol. 5, pp. 135-43.

Longstreth, J, de Gruijl, FR, Kripke, ML, Abseck, S, Arnold, F, Slaper, HI, Velders, G, Takizawa, Y & van der Leun, JC 1998, 'Health risks', *Journal of Photochemistry and Photobiology B: Biology*, vol. 46, pp. 20-39.

Lorente, J, De Cabo, X, Campmany, E, Sola, Y, González, JA, Calbó, J, Badosa, J, Alados-Arboledas, L, Martínez-Lozano, A, Cachorro, V, Labajo, A, De La Morena, B, Díaz, AM, Pujadas, M, Horváth, H, Silva, AM & Pavese, G 2004, 'Altitude effect on UV index deduced from the Veleta-2002 experintal campaign (Spain)', in H Fisher & BJ Sohn (eds.), *Current Problems in Atmospheric Radiation: Proceedings of the International Radiation Symposium*, A. Deepak Publishing, Busan.

Lucas, R., McMichael, T., Smith, W. & Armstrong, B. 2006, *Solar Ultraviolet Radiation: Global burdent of disease from solar ultraviolet radiation*, Environmental Burden of Disease Series, No. 13, World Health Organisation, Geneva.

Lubin, D, Jensen, EH & Gies, HP 1998, 'Global surface ultraviolet radiation climatology from TOMS and ERBE data', *Journal of Geophysical Research-Atmospheres*, vol. 103, no. 20, pp. 26061-91.

MacLaughlin, JA, Anderson, RR & Holick, MF 1982, 'Spectral character of sunlight modulates photosynthesis of previtamin D3 and its photoisomers in human skin' *Science*, vol. 216, no. 4549, pp. 1001-3.

Madan, P & Sengupta, UK 2000, 'Flavonoids accumulation and UV-B protection in crop plants', *Indian Journal of Plant Physiology*, vol. 5, no. 1, pp. 96-8.

Madronich, S, McKenzie, R, Björn, RL & Caldwell, M 1998, 'Changes in biologically active ultraviolet radiation reaching the Earth's surface', in DL Albritton, PJ Aucamp, G Megie & RT Watson (eds.), *Environmental effects of ozone depletion: 1998 Assessment*, Secretariat for The Vienna Convention for the Protection of the Ozone Layer and The Montreal Protocol on Substances that Deplete the Ozone layer, United Nations Environmental Programme, Nairobi.

Mantis, HT, Repapis, CC, Philandras, CM, Paliatsos, AG, Zerefos, CS, Bais, AF, Meleti, C & Balis, DS 2000, 'A 5-year climatology of the solar erythemal ultraviolet in Athens, Greece', *International Journal of Climatology*, vol. 20, pp. 1237-47.

Marley, NA, Gaffney, JS, Baird, JC, Blazer, CA, Drayton, PJ & Frederick, JE 2001, 'An empirical method for the determination of the complex refractive index of size-fractionated atmospheric aerosols for radiative transfer calculations', *Aerosol Science and Technology*, vol. 34, no. 6, pp. 535-49.

Martin, JW, Chin, JW & Nguyen, T 2003, 'Reciprocity law experiments in polymeric photodegradation: a critical review', *Progress in Organic Coatings*, vol. 47, pp. 292-311.

Mazza, CA, Battista, D, Zima, AM, Szwarcberg-Bracchitta, M, Giordano, CV, Acevedo, A, Scopal, AL & Ballaré, CL 1999, 'The effects of solar ultraviolet-B radiation on the growth and yield of barley are accompanied by increased DNA damage and antioxidant responses', *Plant, Cell and Environment*, vol. 22, no. 1, pp. 61-70.

McCarty, CA & Taylor, HR 2001, 'The Genetics of Cataract', *Investigative Opthalmology and Visual Science*, vol. 42, no. 8, pp. 1677-8.

McConnell, JC & Jin, JJ 2008, 'Stratospheric ozone chemistry', *Atmosphere-Ocean*, vol. 46, no. 1, pp. 69-92.

McKenzie, RL 1991, 'Application of a simple model to calculate latitudinal and hemispheric differences in ultraviolet radiation', *Weather and Climate*, vol. 11, pp. 3-14.

McKenzie, R, Connor, B & Bodeker, G 1999, 'Increased summertime UV radiation in New Zealand in response to ozone loss', *Science*, vol. 285, pp. 1709-11.

McKenzie, R, Smale, S & Kotkamp, M 2004, 'Relationship between UVB and erythemally weighted radiation', *Photochemical and Photobiological Sciences*, vol. 3, pp. 252-6.

Mendeva, BD, Gogosheva, TN, Petkov, BH & Krastev, DG 2005, 'The total ozone and UV solar radiation oer Stara Zagora, Bulgaria', *Advances in Space Research*, vol. 35, no. 8, pp. 1366-8.

Meredith, P & Riesz, J 2004, 'Radiative relaxation quantum yields for synthetic eumelanin', *Photochemistry and Photobiology*, vol. 74, no. 2, pp. 211-6.

Milne, E, Corti, DR, English, D, Cross, D & Johnston, R 1999, 'The use of observational methods for monitoring sun-protection activities in schools', *Health Education Research*, vol. 14, no. 2, pp. 167-75.

Mims II, FM & Frederick, JE 1994, 'Cumulus cloud and UV-B', *Nature*, vol. 371, p. 291.

Moehrle, M & Garbe, C 2000, 'Personal UV Dosimetry by *Bacillus subtilis* Spore Films', *Dermatology*, vol. 200, pp. 1-5.

Montzka, SA, Butler, JH, Elkins, JW, Thompson, TM, Clarke, AE & Lock, LT 1999, 'Present and future trends in the atmospheric burden of ozone-depleting halogens', *Nature*, vol. 398, pp. 690-4.

Moore, DF & Zhou, W 1994, 'Photodegradation of sulfamethoxazole: a chemical system capable of monitoring seasonal changes in UVB intensity', *Photochemistry and Photobiology*, vol. 59, no. 5, pp. 497-502.

Nichol, S, Wood, S, Bodeker, G & Conner, B 2001, 'The 2000 antarctic ozone hole', *Water and Atmosphere*, vol. 9, no. 2 (published online). Hosted by the National Institute of Water and Atmospheric Research, New Zealand. Viewed Jan 2009 at http://www.niwa.cri.nz/__data/assets/pdf_file/0004/55633/antarctic.pdf.

NOAA (National Oceanic and Atmospheric Administration) n.d., *Meteorological Conditions & Ozone in the Polar Stratosphere* (published online). Hosted by the NOAA Central Library - National Oceanographic Data Center. Viewed March 2009 at http://www.lib.noaa.gov/researchtools/subjectguides/wind/windandsea2.html.

Norval, M., Cullen, A.P., de Gruijl, F.R., Longstreth, J., Takizawa, Y., Lucas, R.M., Noonan, F.P. & van de Leun, J.C. 2007, 'The effects on human health from

stratospheric ozone depletion and its interaction with climat change', *Photochemical and Photobiolocical Sciences*, vol. 6, pp. 232-51.

Orellana, C 2002, 'Ozone depletion linked to increasing skin cancer in Chile', *Lancet Oncology*, vol. 3, no. 3, p. 132.

Oriowo, OM, Cullen, AP & Sivak, JG 2002, 'Impairment of eye lens cell physiology and optics by broadband ultraviolet A-ultraviolet B radiation', *Photochemistry and Photobiology*, vol. 76, no. 3, pp. 361-7.

Ortiz de Galisteo, P, Toledano, C, Cachorro, V, Rodríguez, E & de Frutos, A 2008, 'Analysis of aerosol optical depth evaluation in polar regions and associated uncertainties', *Advances in Science and Research*, vol. 2, pp. 5-8.

Pacifico, A & Leone, G 2007, 'Role of *p53* and *CDKN2A* inactivation in human squamous cell carcinomas', *Journal of Biomedicine and Biotechnology*, vol. 2007, pp. 1-5.

Parisi, AV & Kimlin, MG 2004, 'Personal Solar UV Exposure Measurements Employing Modified Polysulphone with an Extended Dynamic Range', *Photochemistry and Photobiology*, vol. 79, no. 5, pp. 411-5.

Parisi, AV, Kimlin, MG, Wong, JCF & Wilson, M 2000, 'Personal exposure distribution of solar erythemal ultraviolet radiation in tree shade over summer', *Physics in Medicine and biology*, vol. 45, no. 2, pp. 349-56.

Parisi, AV & Wong, JCF 1999, 'Usage of a dosimeter spectrum evaluator for different environments', *Protection against the hazards of UVR* (published online). Hosted by Internet Photochemistry and Photobiology at http://www.photobiology.com/UVR98/.

Parisi, AV, Wong, JCF & Moore, GI 1997, 'Assessment of the exposure to biologically effective UV radiation using a dosimetric technique to evaluate the solar spectrum', *Physics in Medicine and biology*, vol. 42, pp. 77-88.

Petersen, JL & Small, GD 2001, 'A gene required for the novel activation of a class II DNA photolyase in *Chlamydomonas*', *Nucleic Acids Research*, vol. 29, no. 21, pp. 4472-81.

Piacentini, RD, Cede, A & Barcena, H 2003, 'Extreme solar total and UV irradiances due to cloud effects measured near the summer solstice at a high-altitude desertic plateau Puna of Atacama (Argentina)', *Journal of Atmospheric and Solar-Terrestrial Physics*, vol. 65, no. 6, pp. 727-31.

Pickett, JE 1994, 'Effect of stratospheric ozone depletion on terrestrial ultraviolet radiation: a review and analysis in relation to polymer degradation', *Polymer Degradation and Stability*, vol. 43, no. 3, pp. 353-62.

Quintern, LE, Horneck, G, Eschweiler, U & Bücker, H 1992, 'A biofilm used as ultraviolet-dosimeter', *Photochemistry and Photobiology*, vol. 55, no. 3, pp. 389-95.

Quintern, LE, Puskeppeleit, M, Rainer, P, Weber, S, El Naggar, S & Eschweiler, U 1994, 'Continuous dosimetry of the biologically harmful UV-radiation in Antarctica with the biofilm technique', *Journal of Photochemistry & Photobiology B: Biology*, vol. 22, pp. 59-66.

Rabo, JS, Usman, HS & Kolo, UM 2000, 'Studies on ocular squamous cell carcinoma among horses in Borno State, Nigeria', *African Journal of Biomedical Research*, vol. 3, no. 2, pp. 129-30.

Rahn, RO 1997, 'Potassium iodide as a chemical actinometer of 254 nm radiation: use of iodate as an electron scavenger', *Photochemistry and Photobiology*, vol. 66, pp. 450-5.

Rahn, R & Lee, MA 1998, 'Iodouracil as a Personal Dosimeter for Solar UVB', Photochemistry and Photobiology, vol. 68, no. 2, pp. 173-8.

Rahn, RO, Stefan, MI, Bolton, JR, Goron, E., Shaw, P-S, Lykke, KR 2003, 'Quantum uield of the iodide-iodate chemical actinometer: dependence on wavelength and concentration', *Photochemistry and Photobiology*, vol. 78, no. 2, pp. 146-52.

Rettburg, P & Cockell, CS 2004, 'Biological UV dosimetry using the DLR-biofilm', *Photochemical and Photobiological Sciences*, vol. 3, pp. 781-7.

Rontó, G, Bérces, A, Gróf, P, Fekete, A, Kerékgyártó, T, Gáspár, S & Stick, C 2000, 'Monitoring of environmental UV radiation by biological dosimeters', *Advances in Space Research*, vol. 26, no. 12, pp. 2021-8.

Rosenthal, I & Bercovici, T 1976, 'A chemical actinometer for measurements of U.V. radiation intensity in the atmosphere', *Atmospheric Environment*, vol. 10, pp. 1139-40.

Rousseaux, MC, Ballaré, CL, Giordano, CV, Scopal, AL, Zima, AM, Szwarcberg-Bracchitta, M, Bracchitta, M, Searles, PS, Caldwell, MM & Diaz, SB 1999, 'Ozone depletion and UVB radiation: Impact on plant DNA damage in southern South America', *Proceedings of the National Academy of Sciences of the United States of America*, vol. 96, no. 26, pp. 15310-5.

Roza, L, de Gruijl, FR, Henegouwen, JB, Guikers, K, Van Weelden, H, Van der Schans, GP & Baan, RA 1991, 'Detection of photorepair of UV-induced thymine dimers in human epidermis by immunofluorescence microscopy', *Journal of Investigative Dermatology*, vol. 96, no. 6, pp. 903-7.

Sabburg, J, Parisi, AV & Wong, J 2001, 'Effect of cloud on UVA and exposure to humans', *Photochemistry and Photobiology*, vol. 74, no. 3, pp. 412-6.

Sabziparvar, AA, de F. Forster, PM & Shine, KP 1998, 'Changes in ultraviolet radiation due to stratospheric and tropospheric ozone changes since preindustrial times', *Journal of Geophysical Research-Atmospheres*, vol. 103, no. D20, pp. 26107-13.

Schmucki, DA & Phiipona, R 2002, 'UV radiation in the Alps: the altitude effect', in JR Slusser, JR Herman & W Gao (eds.), *Proceedings of SPIE, Ultraviolet Ground- and Space-based measurements, Models, and Effects*, vol. 4482, pp. 234-9, The International Society of Optical Engineering, San Diego.

Schreder, JG, Blumthaler, M & Huber, M 1999, 'Design of an input optic for solar UV-measurements', *Protection Against the Hazards of UVR* (published online).

Hosted by Internet Photochemistry and Photobiology. Viewed Feb 2009 at http://www.photobiology.com/UVR98/schreder/index.htm.

Seckmeyer, G, Mayer, B, Bernhard, G, McKenzie, RL, Johnston, PV, Kotkamp, M, Booth, CR, Lucas, T, Mestechikina, T, Roy, CR, Gies, HP & Tomlinson, D 1995, 'Geographical differences in the UV measured by intercompared spectroradiometers', *Geophysical Research Letters*, vol. 22, pp. 1889-92.

Seckmeyer, G, Pissulla, D, Glandorf, M, Henriques, D, Johnsen, B, Webb, A, Siani, A-M, Bais, A, Kjeldstad, B, Brogniez, C, Lenoble, J, Gardiner, B, Kirsch, P, Koskela, T, Kaurola, J, Uhlmann, B, Slaper, H, den Outer, P, Janouch, M, Werle, P, Gröbner, J, Mayer, B, de la Casiniere, A, Simic, S & Carvalho, F 2008, 'Variability of UV irradiance in Europe', *Photochemistry & Photobiology*, vol. 84, no. 1, pp. 172-9.

Setlow, RB 1974, 'The wavelengths in sunlight effective in producing skin cancer: a theoretical analysis', *Proceedings of the National Academy of Sciences of the United States of America*, vol. 71, no. 9, pp. 3363-6.

Shaw, JS & Stroup, RL 1995, *Should We Worry About Ozone*, National Center for Policy Analysis Report No. 191, Property and Environmental Research Center, Dallas.

Sherbet, GV 2003, *Genetic Recombination in Cancer*, Academic Press, London.

Sherman, DM 2002, *Tending Animals in the Global Village: A Guide to International Veterinary Medicine*, Lippincott Williams Wilkins, Baltimore.

Sliney, DH 2005, 'Exposure Geometry and Spectral Environment Determine Photobiological Effects on the Human Eye', *Photochemistry and Photobiology*, vol. 81, pp. 483-9.

Smith, SH, Goldschmidt, MH & McManus, PM 2002, 'A comparative review of melanocytic neoplasms', *Veterinary Pathology*, vol. 39, pp. 651-78

Stulberg, DL, Crandell, B & Fawcett, RS 2004, 'Diagnosis and treatment of basal cell and squamous cell carcinomas', *American Family Physician*, vol. 70, no. 8, pp. 1481-8.

Sturman, A & Tapper, N 1996, *The Weather and Climate of Australia and New Zealand*, Oxford University Press, Melbourne.

Swanson, LN 2006, 'OTC Dermatological Agents', chapter 30 *II F* in L Shargel, AH Mutnick, PF Souney & LN Swanson (eds.), *Comprehensive Pharmacy Review*, 6th edn, Lippincott Williams & Wilkins, Baltimore.

Sydenham, MM, Collins, MJ & Hirst, LW 1996, 'The development and application of a polysulphone contact lense dosimeter', *XII International Congress of Eye Research - Experimental Eye Research*, The International Society for Eye Research, Ridgefield, New Jersey.

Tardif, R 2001, *Ineractions between aerosols and fog*, Project ATOC 5600: Physics and Chemistry of Clouds and Aerosols, Program in Atmospheric and Oceanic Sciences, University of Colorado, Boulder (published online). Hosted by the National Center for Atmospheric Research, Research Applications Laboratory, Boulder. Viewed Feb 2009 at http://www.rap.ucar.edu/staff/tardif/Documents/CUprojects/ATOC5600/.

Tate, TJ, Diffey, BL & Davis, A 1980, 'An ultraviolet radiation dosimeter based on the photosensitising drug, nalidixic acid', *Photochemistry and Photobiology*, vol. 31, no. 1, pp. 27-30.

Terenetskaya, I 2003, 'Solar UV-B dosimetry in situ with 'D-dosimeter': effect of ozone depletion on the Vitamin D synthetic capacity of sunlight', *Agricultural and Forest Meteorology*, vol. 120, pp. 45-50.

Thacker, J 2001, 'Homologous Recombination Repair', in M Schwab (ed.), *Encyclopedic Reference of Cancer*, Springer-Verlag, New York.

Thylefors, B, Négrel, A-D, Pararajasegaram, R & Dadzie, KY 1995, 'Global Data on Blindness - An Update', *Bulletin of the World Health Organization*, vol. 73, no. 1, pp. 115-21.

Tian, X & Lei, Y 2007, 'Physiological responses of wheat seedlings to drought and UV-B radiation. Effect of exogenous sodium nitroprusside application', *Russan Journal of Plant Physiology*, vol. 54, no. 5, pp. 676-82.

Tobin, AK 2002, 'The Effects of Ultraviolet B Radiation on Crop Plants', chapter 10 in RS Ambasht & NK Ambasht (eds.), *Modern Trends in Applied Terrestrial Ecology*, Kluwer Academic Publishers, New York.

Tolba, MK 1992, 'Ozone depletion', chapter 2 in OA El-Kholy, E El-Hinnawi, MW Holdgate, DF McMichael & RE Munn (eds.), *The world environment 1972-1992: Two decades of challenge*, Chapman and Hall, New York.

van der Rhee, H.J., de Vries, E. & Coebergh, J.W. 2006, 'Does sunlight prevent cancer? A systematic review', *European Journal of Cancer*, vol. 42, pp. 2222-32.

van Rensen, JJS, Vredenberg, WJ & Rodrigues, GC 2007, 'Time sequence of the damage to the acceptor and donor sides of photosystem II by UV-B radiation as evaluated by chlorophyll *a* fluorescence', *Photosynthesis Research*, vol. 94, pp. 291-7.

Weihs, P, Webb, AR, Hutchinson, SJ & Middleton, GW 2000, 'Measurements of the diffuse UV sky radiance during broken cloud conditions', *Journal of Geophysical Research-Atmospheres*, vol. 105, no. 4, pp. 4937-44.

WHO (World Health Organization) 1979, *Environmental Health Criteria 14: Ultraviolet Radiation* (published online). Hosted by the International Programme on Chemical Safety, United Nations Environmental Programme (UNEP) / WHO / International Radiation Protection Association (IRPA), Geneva. Viewed Mar 2009 at http://www.inchem.org/documents/ehc/ehc/ehc014.htm.

WHO (World Health Organization) n.d., 'What are the effects of UV on the eye?' (published online). Hosted online by World Health Organization, Geneva. Viewed Jan 2009 at http://www.who.int/uv/faq/uvhealtfac/en/index3.html.

Wong, CSM, Strange, RC & Lear, JT 2003, 'Clinical Review: Basal cell carcinoma', *British Medical Journal*, vol. 327, pp. 794-8.

Wood, SR, Berwick, M, Ley, RD, Walter, RB, Setlow, RB & Timmins, GS 2006, 'UV causation of melanoma in *Xiphophorus* is dominated by melanin photosensitized oxidant production', *Procedings of the National Academy of Sciences of the United States of America*, vol. 103, no. 11, pp. 4111-5.

Wuttke, S, Seckmeyer, G & König-Langlo, G 1996, 'Measurements of spectral albedo at Neumayer, Antarctica', *Annales Geophysicae*, vol. 24, pp. 7-21.

Yadav, LDS 2005, *Organic Spectroscopy*, Kluwer Academic Publishers, Dordrecht.

Yang, G, Rajadurai, A & Tsao, H 2005, 'Recurrent patterns of dual RB and p53 pathway inactivation in melanoma', *Journal of Investigative Dermatology*, vol. 125, pp. 1242-51.

Zhang, J-Y, Esrom, H & Boyd, IW 1999, 'UV intensity measurement of 308 nm excimer lamp using chemical actinometer', *Applied Surface Science*, vol. 138-9, pp. 315-9.

Appendices

Appendix A – Pilot study

The pilot study was a basic preliminary study to investigate the potential for PPO to be cast into thin film in an economical way, and for the film to provide a superior dynamic range, and to be fully characterised in terms of its optical properties. Preliminary casting experiments established chloroform as a suitable solvent for PPO powder and a series of casting experiments demonstrated that films of PPO could be efficiently manufactured with the casting equipment available at the University of Southern Queensland.

An uninterrupted broadband UV dose of 1 MJ m^{-2} was administered to a sample of PPO film. Slight signs of yellowing were evident after the exposure, but the film showed no signs of mechanical failure, and a clear response to the exposure could be measured photometrically indicating the potential of PPO film for large-dose measurements.

Preliminary exposures of PPO film samples to broadband UV irradiance administered by the fluorescent UV lamp showed consistent increases in optical absorbance corresponding to increasing UV dose, and indicated a monotonic response to UV exposure. Although the exposures were relatively short, sufficient data was accumulated to show that the response was nonlinear and similar in form to the response of polysulphone film.

Investigation of the spectral absorbance of PPO film and the effects of film thickness on the absorption spectra were investigated for films of 15 μm and 40 μm thicknesses as shown in figure A-1. The rapid rate of increasing absorbance at UVB wavelengths suggested a greater response to the UVB waveband. Thinner films resulted in a shift of the absorbance spectrum toward shorter wavelengths, and a substantial decrease in UV exposure sensitivity (figure A-1).

Appendix A – Pilot study

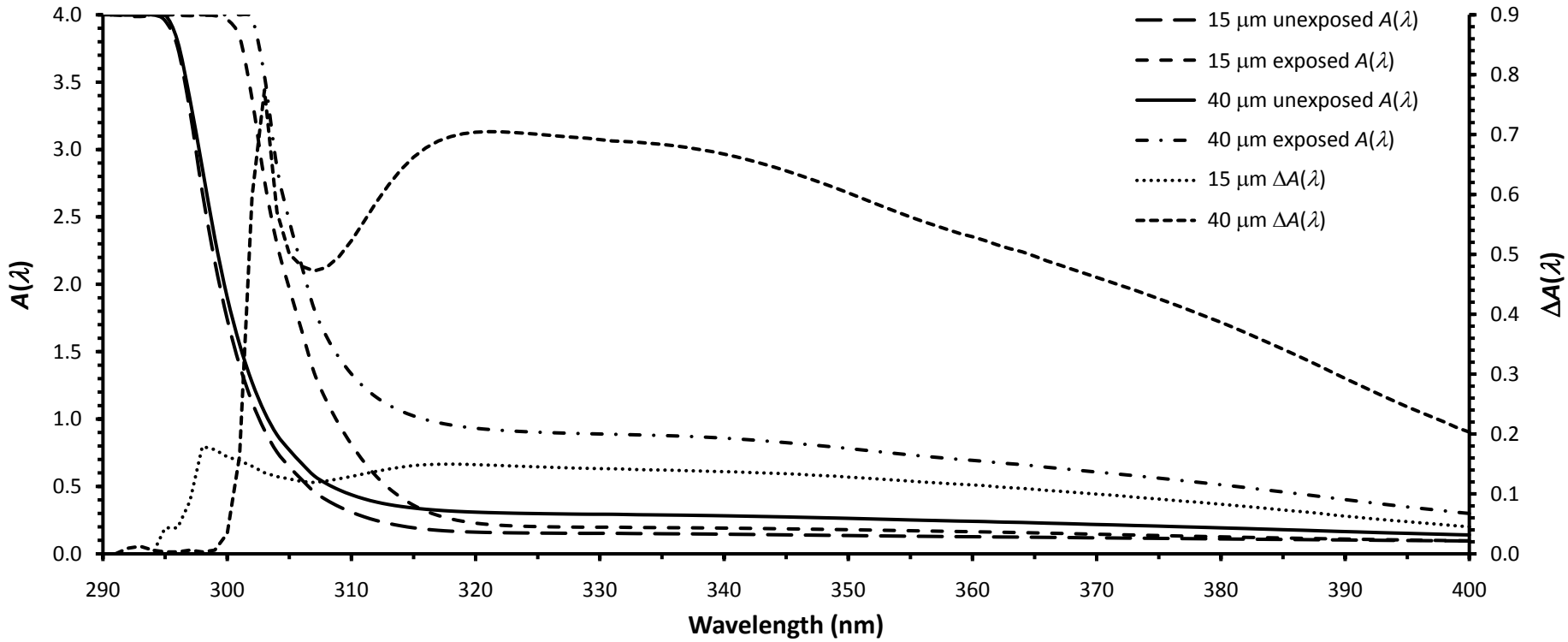

Figure A-1: Optical absorbance spectra $A(\lambda)$ of PPO film samples of 15 μm and 40 μm thicknesses before exposure and after an 8 hour broadband UV exposure (left axis), and the difference between the spectral absorbance $\Delta A(\lambda)$ of the films before and after exposure (right axis).

Appendix A – Pilot study

The greater spectral response of PPO film to the UVB waveband was confirmed by exposures of PPO film samples to the solar UV simulator conducted with, and without a UVB filter at the output aperture. A much larger response to the unfiltered output was observed, indicating that the PPO film samples were much more sensitive to the UVB portion of the spectrum than to the UVA.

This study has demonstrated the ability of PPO material to be cast into thin films by means of standard equipment, and confirms the larger broadband UV dynamic range of PPO film compared to the other materials reviewed. A monotonic response of the film to UV exposure appropriate for calibration was observed, and the study also prompts an investigation of the effect of film thickness on the response. Although the spectral response has yet to be determined, the difference in response due to UVB and UVA exposures is promising in terms of a UVB or biologically weighted actinometer. The pilot study has provided sufficiently strong evidence in the author's judgement to proceed with the development of PPO film actinometers.

Appendix B – Optical wedge interferometry

The phase difference $\Delta\phi$ between the radiation reflected from the upper and lower surfaces of the air wedge is $\Delta\phi = \frac{2y}{\lambda}2\pi$ where λ is the wavelength of the incident radiation (see figure B-1).

When radiation is incident upon a surface of refractive index, a phase reversal occurs. The effective phase difference is thus $\Delta\phi + \pi = \left(\frac{4y}{\pi} + 1\right)\pi$. Constructive interference occurs when $\Delta\phi = (2n+1)\pi \quad n = 0,1,2,...$ This occurs when $y = n\frac{\lambda}{2}$ and when $y = \left(n + \frac{1}{2}\right)\frac{\lambda}{2}$. The difference in the wedge thickness Δy between any two consecutive bright or dark fringes is therefore given by $\Delta y = \frac{\lambda}{2}$.

The mean distance d between consecutive bright or dark fringes was found by counting the number of bright fringes over the length of the glass plates and dividing by the length over which they were counted.

From figure B-1 it can be seen that $d = \frac{\Delta y}{\sin\theta} = \frac{\lambda}{2\sin\theta}$ where θ is the vertex angle of the wedge. Since θ is very small, $d = \frac{\lambda}{2\theta}$. The thickness T of the sliver of PPO film is then calculated by

$$T = L\sin\left(\frac{\lambda}{2d}\right) \text{ (m)}$$

where L is the distance from the vertex to the sliver of film that separates the glass plate at the opposite end.

Appendix B – Optical wedge interferometry

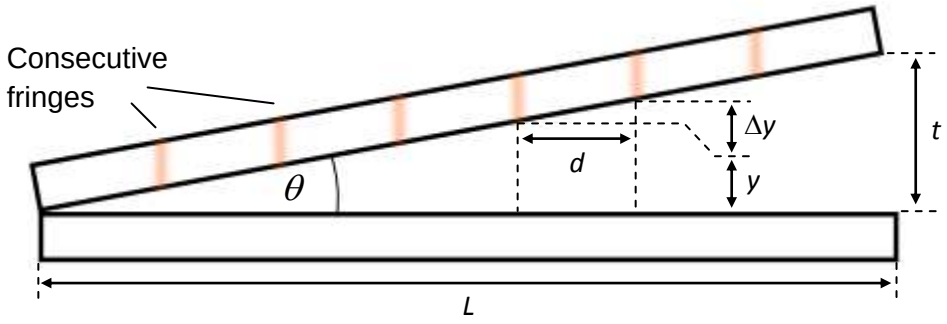

Figure B-1: Cross-sectional schematic of the optical wedge used to measure the thickness of PPO film samples. The vertical lines in the top glass plate represent interference fringes. All of the parameters required to calculate the film thickness are shown.

Appendix C – Paired *t*-tests for spectrophotometer beam effect on PPO film

Sample	Unexposed		Exposed	
	Set 1	Set 10	Set 1	Set 10
1	0.2278	0.2201	1.8079	1.8093
2	0.2286	0.2295	1.8098	1.8261
3	0.2276	0.2252	1.8146	1.8177
4	0.2246	0.2276	1.8449	1.8391
5	0.2280	0.2291	1.8412	1.8235
6	0.2302	0.2296	1.8432	1.8444
7	0.2269	0.2278	1.8288	1.8210
8	0.2289	0.2210	1.8485	1.8479
9	0.2283	0.2286	1.8447	1.8485
10	0.2273	0.2256	1.8183	1.8232
11	0.2246	0.2286	1.8181	1.8221
12	0.2292	0.2269	1.8165	1.8104
13	0.2296	0.2294	1.8307	1.8279
14	0.2245	0.2289	1.8047	1.8182
15	0.2281	0.2277	1.8355	1.8389
Statistics	μ_1 0.227613	μ_{10} 0.22704	μ_1 1.82716	μ_{10} 1.82788
	$\mu_{1\bar{x}}$ 0.000464	$\mu_{10\bar{x}}$ 0.000763	$\mu_{1\bar{x}}$ 0.003919	$\mu_{10\bar{x}}$ 0.003323
t	0.6218		0.3346	
$\mu_{\bar{x}}$	0.001		0.002	
SD	0.001796	0.002954	0.015179	0.012871
$\mu_{10} - \mu_1$	-0.00057		0.00072	
***p*-value**	0.27205		0.37145	

Appendix D – Analysis of variance test for temperature dependence

Sample	Temperature (°C)					
	1.5	10	30	40	50	20
1	1.84	1.77	1.85	1.77	1.81	1.76
2	1.85	1.84	1.85	1.82	1.85	1.85
3	1.88	1.89	1.87	1.84	1.87	1.85
4	1.89	1.89	1.89	1.85	1.87	1.86
5	1.92	1.90	1.89	1.88	1.87	1.87
6	1.95	1.90	1.91	1.89	1.90	1.87
7	1.95	1.90	2.01	1.92	2.05	1.87
8	2.05	2.02	2.05	1.93	2.06	1.97
9	2.07	2.02	2.06	1.98	2.08	2.03
10	2.10	2.09	2.08	2.05	2.12	2.06
$\bar{x}$	1.95	1.92	1.95	1.89	1.95	1.90
SD	0.09216	0.09581	0.0919	0.08184	0.116	0.09162

Source of Variation	Sum of Squares	d.f.	Mean Squares	F-ratio	*p*-value
Between	0.03894	5	0.003389	0.7452	0.593
Error	0.4912	54	0.0090966		
Total	0.5251	59			

Appendix E – PPO film artificial source broadband UV calibration equations

Film Thickness (μm)	Calibration equation (kJ m^{-2})	R^2
15	$H = 1469.3x^3 - 2020.3x^2 + 2124.2x$	0.9997
20	$H = 751.87x^3 - 908.53x^2 + 1318.7x$	0.9988
40	$H = 213.48x^3 - 21.531x^2 + 266.15x$	0.9971
50	$H = 208.44x^3 - 84.295x^2 + 182.15x$	0.9980
60	$H = 251.63x^3 - 259.33x^2 + 263.05x$	0.9968